Mireia Fontanet i Ambròs

Ph.D. Thesis

OPTIMAL IRRIGATION SCHEDULING COMBINING WATER CONTENT SENSORS AND REMOTE SENSING DATA

Supervisors:
Daniel Fernàndez Garcia
Francesc Ferrer Alegre

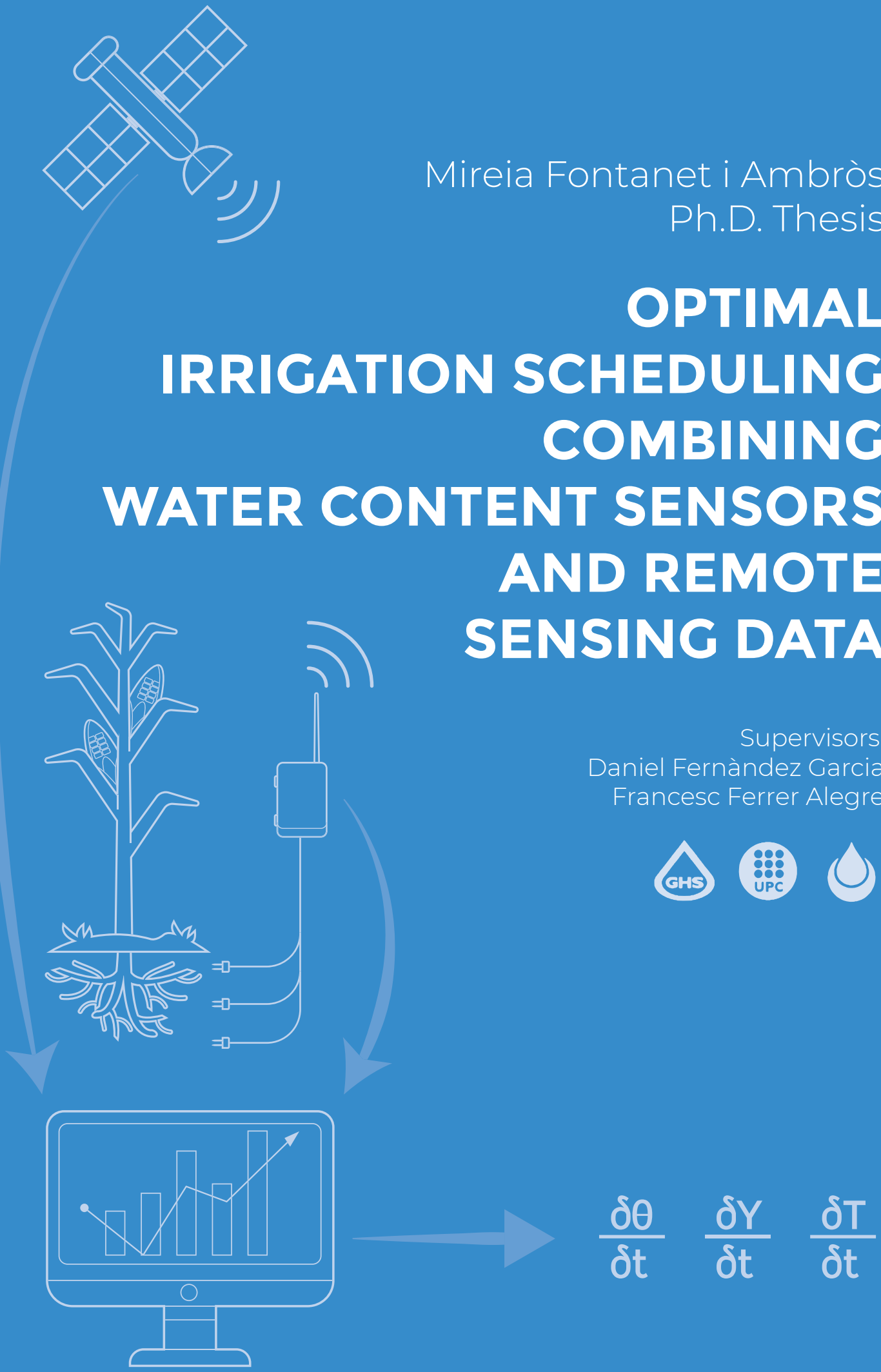

UNIVERSITAT POLITÈCNICA DE CATALUNYA

&

LABFERRER

OPTIMAL IRRIGATION SCHEDULING COMBINING WATER CONTENT SENSORS AND REMOTE SENSING DATA

by

Mireia Fontanet i Ambròs

Advised by Dr. Daniel Fernàndez Garcia and Dr. Francesc Ferrer Alegre

This thesis is submitted in the fulfilment of the requirements for the PhD degree to the doctoral school of the Universitat Politècnica de Catalunya

in the

Department of Civil and Environmental Engineering

Hydrogeology Group (UPC-CSIC)

October 2019

Grup d'**H**idrologia **S**ubterrània
UNIVERSITAT POLITÈCNICA DE CATALUNYA

UNIVERSITAT POLITÈCNICA DE CATALUNYA

Department of Civil and Environmental Engineering

&

LABFERRER

Abstract

by Mireia Fontanet i Ambròs

By 2025, the Food and Agriculture Organization (FAO) of the United Nations predicts that two-thirds of the world population will experience water stress conditions. In addition, it is expected that world population will increase significantly during the following years. Agriculture is the largest consumer of fresh water, estimated 75%. The optimization of its use is therefore crucial for future. The main objective of irrigation scheduling is to guarantee maximum crop yield while saving significant amounts of water.

The main difficulty to determine a correct and optimal irrigation scheduling strategy is due to complexity and variability of the Soil – Plant – Atmosphere (SPA) continuum. In each field site, this continuous SPA has different patterns as a consequence of environmental conditions, crop, soil hydraulic properties and soil tillage. Several tools and methodologies are employed nowadays to monitor an improve irrigation scheduling. However, they all have advantages and limitations, or, each one is used without considering the information provided by the others, simplifying the system and avoiding information.

This thesis aims to improve irrigation scheduling by combining different tools available at the present time. This combination aims to answer different kind of questions when irrigation scheduling in a field site must be defined. For this, each tool has been used and supported by others. In addition, this thesis will discuss when and how these tools might be employed.

Firstly, we compare different tools and methodologies used to measure water content in an agriculture field. Specifically, we compared gravimetric measurements and water content sensors measurements with DISPATCH algorithm data. This algorithm is one of several algorithms who estimates soil surface water content using remote sensing data. The main goal was determining if remote sensing data can improve water content data measured by sensors. We found that DISPATCH algorithm is capable of correctly estimating soil water content when water content fluctuations are produced by general rainfall events, but not

when fluctuations are produced by local irrigation. Thus, at present, and considering our field conditions, DISPATCH is no capable to improve water content sensors measurements.

Secondly, we present a methodology where a simulation-optimization problem is solved in order to find an optimal irrigation scheduling strategy. This strategy might guarantee the maximum economic net margin. This methodology has been applied in a real field. The optimal irrigation scheduling of this field is compared with the traditional irrigation scheduling method, based water requirements. Results show that even though the traditional method supplies the volume of water evapotranspired, this methodology of scheduling irrigation is not enough to avoid crop water stress, compromising final crop yield. In this case, optimal irrigation strategy improves the final net margin in comparison the traditional method. In order to emphasize the importance of soil characterization for irrigation scheduling, the methodology was applied to another soil type. We demonstrate that depending on soil properties, optimal irrigation scheduling is different.

Thirdly, considering the information reported before, we improved the irrigation scheduling in a field site where irrigation was applied with the same criteria. In this part of the thesis we employed NDVI remote sensing data, water content sensors and simulation models to determine the optimal irrigation. The improvement is based on management zones delineation with NDVI data. In this case, water content sensors are used to define if each management zone presents different water content patterns and to verify that when the field is divided into different management zones there is a gain in terms of water content uniformity. Finally, an optimal irrigation scheduling calendar is proposed to allow the consultants to take within-season irrigation decisions. Results show that management zones are dynamic during the growing season and the optimal irrigation scheduling might also be dynamic. In addition, we found that the uniform irrigation applied in the entire field, without considering the possible differences in soil properties, produced waterlogging in two management zones, therefore, transpiration decreases in comparison to the others management zones. Simulations show that optimal irrigation scheduling proposed can save water and to increase transpiration in all zones, solving the waterlogging problem which affects this field site.

This thesis has been conducted in two different field sites; the first one presented is called Foradada field; the second one is called Raïmat field. Both of them are located in the NE of Catalunya, Spain. Cultivated crop was *Zea mays L.* (maize) Crop cultivated was maize and the irrigation water was applied by a solid sprinkle system.

UNIVERSITAT POLITÈCNICA DE CATALUNYA

Departament d'Enginyeria Civil i Ambiental

&

LABFERRER

Resum

per Mireia Fontanet i Ambròs

El 2025 la "Food and Agriculture Organization" (FAO) de les Nacions Unides prediu que dues terceres parts de la població mundial patirà condicions d'estrés hídric. A més a més, s'espera que la població mundial augmenti els propers anys. L'agricultura, que és el sector que produeix l'aliment necessàri per alimentar la població mundial, és el consumidor principal d'aigua dolça, concretament un 75%. Considerant aquest context, existeix una necessitat important d'optimitzar l'aigua de reg en un futur proper. La programació del reg és l'encarregada de determinar el moment i la quantitat d'aigua que s'ha d'aplicar. El seu objectiu principal és garantir un rendiment màxim del cultiu i a la vegada estalviar aigua.

La dificultat principal per determinar l'estratègia de programació de reg correcta i òptima és degut a la complexitat i variabilitat del continu Sòl – Planta – Atmòsfera (SPA). En cada parcel·la de cultiu, el continu SPA té un comportament diferent degut a les condicions ambientals, de cultiu, propietats hidràuliques del sòl i maneig del mateix. Diverses eines i metodologies són emprades avui en dia per monitoritzar i determinar la programació del reg. Malgrat l'àmplia variabilitat de possibilitats, totes elles tenen avantatges i limitacions, o sovint, cada una d'elles és fa servir sense considerar la informació que poden proporcionar les altres, simplificant el sistema i obviant informació.

Aquesta tesis vol millorar la programació del reg combinant diferents eines i metodologies que estan disponibles avui en dia. La combinació té com a objectiu satisfer necessitats diferents en el moment que la programación del reg ha de ser definida, destacant les avantatges i minimitzant les limitacions de cada metodologia i eina, així com l'efecte de l'escala.

Primerament, hem comparat diferents eines i metodologies per mesurar el contingut d'aigua al sòl en una parcel·la de cultiu. Concretament, s'han comparat mesures gravimètriques i de contingut d'aigua de sensors amb mesures de l'algorisme DISPATCH. Aquest algorisme és un de varis algorismes que estimen el contingut d'aigua superficial del sòl emprant dades de teledetecció. L'objectiu principal era determinar si les dades de

teledetecció poden millorar les dades de contingut d'aigua mesurades pels sensors. Vam detectar que l'algorisme DISPATCH és capaç d'estimar correctament el contingut d'aigua al sòl quan els increments d'aigua són produïts per precipitacions generals, m'entres que quan els increments d'aigua al sòl són produïts per el reg local, el DISPATCH no els detecta. Per tant, ara per ara i considerant les condicions de camp, el DISPATCH no és capaç de millorar les mesures dels sensors de contingut d'aigua al sòl.

Després, presentem una metodologia on es soluciona un problema de simulació-optimització per a determinar una estratègia de programació de reg òptim. Aquesta estratègia ha de garantir un rendiment econòmic net màxim. S'ha aplicat en una parcel·la de cultiu real. L'estratègia de programació de reg òptim ha estat comparat amb el mètode tradicional de programació de reg, que està basat amb el càlcul de les necessitats hídriques. Encara que el mètode tradicional reemplaça per complet l'aigua evapotranspirada, els resultats mostren que la manera de repartir l'aigua no evita l'estres hídric del cultiu, disminuint el rendiment. En aquest cas, la programació del reg òptim millora el rendiment econòmic net. Per tal d'emfatitzar la importància de la caracterització hidràulica del sòl, aquesta metodologia s'aplica en un altre tipus de sòl. Els resultats mostren que depenent el tipus de sol, la programació del reg ha de ser diferent.

Finalment, considerant la informació descrita prèviament, s'ha millorat la programació del reg en una parcel·la de cultiu on el reg s'havia aplicat uniformement en tota la seva extensió. En aquesta part de la tesis, es fan servir dades de teledetecció de NDVI, dades de sensors de contingut d'aigua al sòl i models de simulació per a determinar el reg òptim. La millora està basada en la delineació de zones maneig amb les dades de NDVI. En aquest cas, els sensors s'han emprat per a determinar si casa zona de maneig representa diferents patrons de contingut d'aigua i per a validar si quan la parcel·la és dividida en zones de maneig, la variabilitat disminueix. Finalment, es proposa un calendari de programació de reg òptim per a poder prendre decisions en la campanya de reg. Els resultat mostren que les zones de maneig són dinàmiques així com el reg òptim. A més a més, es va detectar que l'aplicació d'un reg unifrome en tota la parcel·la, produeix saturació del sòl en algunes de les zones de maneig, per tant, la transpiració disminueix. Les simulacions mostren que el reg òptim proposat és capaç d'estalviar aigua i a més a més augmentar la transpiració en totes les zones, solucionant el problema de saturació del sòl que afecta aquesta parcel·la.

Aquesta tesis s'ha portat a terme en dues parcel·les diferents de cultiu; la primera és anomenada parcel·la de Foradada; i la segon s'anomenada parcel·la de Raïmat. Totes dues es troben al nord est de Catalunya. El cultiu en tots dos casos és blat de moro i el reg és aplicat mitjançant aspersors.

Contents

List of Figures

List of Tables

De mica en mica
s'omple la pica

Chapter 1

Introduction

1.1. General theoretical concepts

1.1.1. Soil - Plant – Atmosphere continuum

The Soil – Plant – Atmosphere (SPA) continuum (Philip, 1966) (Fig.1.1) is a concept who simplifies the great complexity showed by plants and their interaction with soil and atmosphere. It is a conceptual model that helps analysed water movement through the plant from soil as a source to atmosphere as a sink, considering the characteristics of the structure of the plant, the soil properties and atmospheric demand. At every specific case, continuum SPA has different features because the three elements who compose SPA continuum (soil, plant and atmosphere) offer a wide range of combinations, and they usually do not never present the same properties. Thus, their interactions are different in each case.

Before SPA continuum was formally defined, Huber (1928) and Van den Honert (1948) proposed a parallel between Ohm's law and water movement through SPA continuum. In this way, SPA continuum was compared to an electric circuit with several resistance connected between them (Fig.1.1). Each resistance represents elements of SPA continuum.

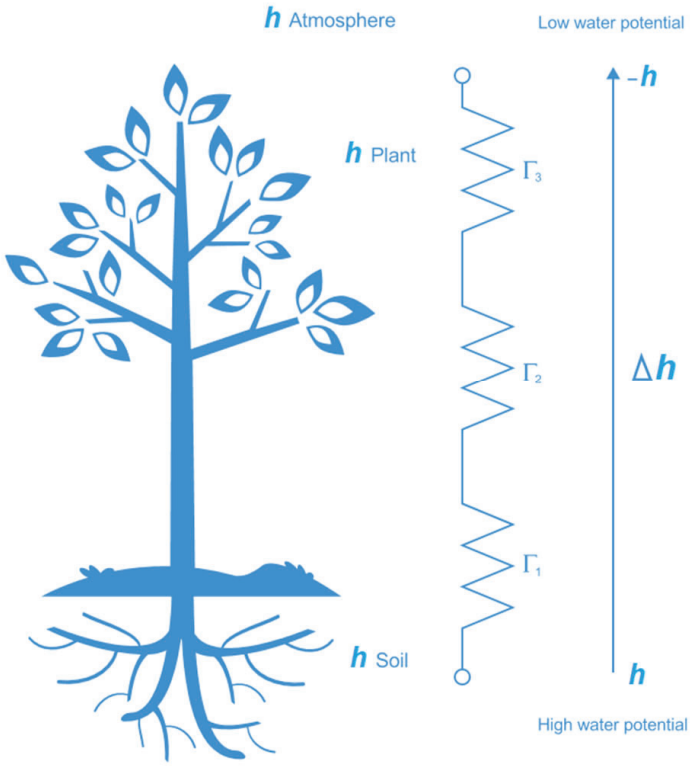

Figure 1.1 Continuum SPA example where pressure head goes from high to low pressure head values. Each element is represented as a electric resistance connected between them.

Water flux goes from the soil to roots, through xylem, through mesophyll cells and cell walls, and finally transpires into sub-stomatal cavities. In this way, the water flux is transported through the SPA continuum is with a pressure head gradient (Δh) between soil and atmosphere (Nobel, 1983) (Fig.1.1). Pressure head or water potential is the potential energy of water per unit volume relative to pure water under reference conditions. It quantifies the tendency of water to move from one area (soil) to another (atmosphere).

Considering the general idea about how SPA continuum works, in this thesis, the focus is specifically on one of the components of the SPA continuum, the soil, which is considered as the vadose zone. It plays a role as the source of water content and it works as a reservoir for all the other components. Thus, the water movement and processes in which water content is involved have a direct effect on SPA continuum.

1.1.2. Vadose Zone

The vadose zone or the unsaturated soil is the portion of the subsurface above the groundwater table (Radcliffe and Simunek, 2010). In this portion of the soil exists three-phase system composed of solids (soil), liquid (water and dissolved solutes) and gases (combination of gases).

The solid matrix is characterized by complicated geometries formed by particles with different size and shapes. Soil texture refers to the size distribution to composed a soil. According with United States Department of Agriculture (USDA), particles with diameter smaller than 0.002 mm are clay size, 0.002-0.05 mm are silt size and 0.05-2 mm are sand size.

Different soil textural classes are defined when percentages of sand, silt and clay are analysed. Thus, a textural class is determined based on solid particle size. Nowadays, several soil textural classes classification are available, but the most used is the USDA soil textural classification. This classification scheme allows for soils having different proportions of sand, silt and clay to be in the same textural class, depending on the lower and upper limits of the different classes. Even though a textural class can be determined, within the same class there is certain textural variability and soil properties change.

Soil structure is another important feature to define and usually is not considered. It modifies porosity and pores size distribution. Therefore, spaces that water can fill are also affected.

The interaction between water flux and soil depends on soil texture and soil structure. Unfortunately, these features usually present high spatial variability making difficult the characterization.

Two different types of curves are able to describe how water moves through a specific soil. On the one hand, Soil Water Retention Curve (SWRC) relates water content (θ) with pressure head (h), and on the other hand, Hydraulic Conductivity Curve (HCC) associates water content or pressure head with hydraulic conductivity (K). Both curves are characteristics of each soil and their hydraulic properties are different. Therefore, an accurate soil characterization provides powerful information about the interaction between soil and water movement.

Figure 1.2 shows two different examples (Clay soil and a Sandy Loam soil) of SWRC and HCC. The purpose of this figure is show how two different soils with different texture present different SWRC and HCC shapes. As a consequence, the water movement is different in each one. For instance, given a water potential value, Clay soil has greater water retention capacity than the Sandy Loam. But Clay soil hydraulic conductivity is lower, therefore, water moves slowly than Clay soil.

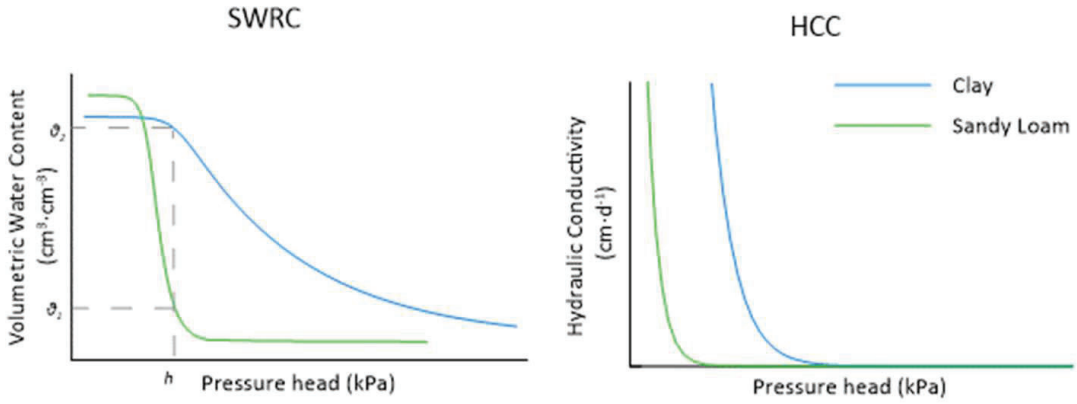

Figure 1.2. Soil water Retention Curve (SWRC) and Hydraulic Conductivity Curve (HCC) from a typical Clay soil and a Sandy Loam soil.

Considering that soil hydraulic properties govern water movement through the soil, it can be assumed that processes where water content is involved, such as, drainage, infiltration, run off… are also influenced.

1.1.3. Irrigation scheduling

Irrigation scheduling is the processes used by agricultures and stakeholders to apply water in the soil with a correct frequency and duration time. The main goal of irrigation scheduling

is to guarantee that crop is under water content optimal conditions applying the minimum volume of water and at the same time avoiding soil salinization. It has been explained in the previous sections that water interaction between soil and plants is complex. Therefore, the accurate determination of an optimized irrigation schedule is a time-consuming and nonintuitive process.

Firstly, when an irrigation is scheduled, the amount of water to be applied must be determined (Campbell, 1982). When water infiltrates, the wetting front pattern is redistributed through the root zone. Secondly, if the volume of water applied exceeds the soil retention capacity, part of this water is drained below the root zone. Also, water is evaporated from the top soil profile and roots take up the necessary water for phenological functions. In another words, there is a water consumption. It is when water content at the root zone reaches a minimum where a crop could experience non-optimal (stress) conditions. At this point, irrigation must be triggered and refill the root zone. These processes are represented by Fig.1.3.

Note that irrigation scheduling is a periodic process where soil water content can be delimitated employing different soil parameters or thresholds. These thresholds can be expressed in terms of θ or h. All of them are explained in the next section.

1.1.4. Water content dynamics for irrigation scheduling

One of the important soil parameters, who defines the maximum volume of water that a soil can storage, is the Porosity or the water content Saturation point (θ_s) (Zhang et al., 2018). Thus, soil can be considered as a reservoir with a maximum capacity defined by θ_s.

Although θ_s provide information about the maximum volume of water that a soil can storage, the most important soil parameters in terms of irrigation scheduling is Field Capacity point (θ_{fc}). It is considered that at this water content value is the most optimal conditions for crop water uptake. Gardener, (1960) defined θ_{fc} as the water content below which the hydraulic conductivity is sufficiently small that redistribution of moisture in the soil profile due to hydraulic gradients can be neglected. The processes, where water content is involved, between θ_s and θ_{fc} is drainage. When irrigation is applied, if water content value is over θ_{fc} and gets closer to θ_s this volume of water is drained and is not consumed by plants (Fig.1.3). Several methodologies have been developed to measure or define θ_{fc}. For instance, some researchers defines θ_{fc} using soil hydraulic conductivity curve (Campbell, 1982; Gardener, 1960). An arbitrary matric potential value of -33 kPa for all soils was defined as a θ_{fc} (Colman, 1947; Richards, 1944). In this case, it has seen that depending on soil hydraulic properties this arbitrary method does not represent θ_{fc}. For this reason,

Lehmann et al. (2008) proposed a formula based on van Genuchten, (1980) soil hydraulic parameters. Another option to define θ_{fc} is using dynamics water content values, where water content shows an inflection point when drainage is cessed (Zotarelli et al., 2010) (Fig.1.4). Finally, Twarakavi et al. (2009) and van Lier and Wendroth, (2016) employed numerical modelling to define θ_{fc}.

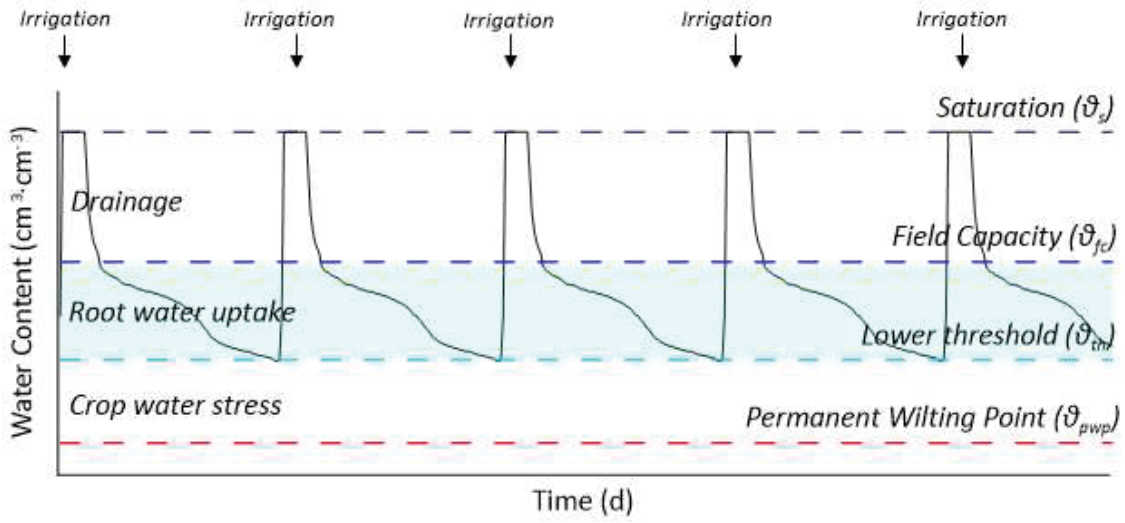

Figure 1.3. Water content dynamics when irrigation is applied. Water content comfort zone is represented in light blue. Soil saturation, Field Capacity, Lower threshold, Permanent Wilting Point are plotted. Drainage, root water uptake and crop water stress processes are located within the corresponen water content dynamics fringe.

The Permanent Wilting Point (θ_{pwp}) represents pressure head conditions in which restricts the water absorption by the plants, which will die if there is no replacement of the water in the soil (de Oliveira et al., 2015). Thus, when an irrigation is scheduled, water contents should never approach θ_{pwp}. Otherwise, crop water stress and crop yield reduce are related with it. In general, the permanent wilting point is also determined in the laboratory, by the retention curve method. In this method, the θ_{pwp} of the wilting point is represented by the balance moisture with tension of 1500 kPa.

Available Water (AW) is defined by the water available for plants uptake, which is the difference between θ_{fc} and θ_{pwp} (Zotarelli et al., 2010). AW can be expressed in relative terms (Eq.1.1), making comparable AW values between different sites. As the same case as threshold parameters, AW can be calculated with θ or h units.

$$AW\ [-] = \frac{\theta - \theta_{pwp}}{\theta_{fc} - \theta_{pwp}}, \tag{1.1}$$

Although AW represents the water that is theoretically available until θ_{pwp}, crop water uptake is reduced well before θ_{pwp} is reached. As the soil water content decreases, water becomes more strongly bound to the soil matrix and is more difficult to extract. When the soil water content drops below a Lower threshold value (θ_{th}), soil water can no longer be transported quickly enough towards the roots to respond to the transpiration demand and the crop begins to experience stress (Fig.1.3). The fraction of AW that a crop can extract from the root zone without suffering water stress is the Readily Available Water (RAW) (Allen et al., 1998, hereafter "FAO56") (represented in light blue in Fig.1.3). As the same case as AW, it can be expressed as relative terms (Eq.1.2) or AW fraction (Eq.1.3).

$$RAW\ [-] = \frac{\theta - \theta_{th}}{\theta_{fc} - \theta_{th}}, \tag{1.2}$$

$$RAW\ [-] = p \cdot AW, \tag{1.3}$$

Where p is average fraction of AW that can be depleted from the root zone before water content stress occurs [0 - 1]. p values can be found tabulated in FAO56 (Allen et al., 1998, hereafter "FAO56").

Note that all these soil parameters depend on soil hydraulic properties and soil type. Thus, when the full and refill points determined for the specific field and the water content monitoring method is selected, one is ready to start monitoring soil-water and irrigation scheduling (Campbell, 1982). Measurements of water content should be made as frequent as possible because all soil processes can be described better.

Several methodologies can be used to monitor water content dynamics, but the most used is installing water content sensors. Advances in water content sensors have made them easier to use and the cost of energy has made these sensors a more variable option. In addition, they are able to provide water content measurements at high temporal resolution. However, water content sensors represent a punctual point in the entire field. That is why that soil spatial variability complicates frequently the decision for sensors location and installation, and how a global water content values of the entire field are provided. Thus, before installing water content sensors a different field zone must be identified.

1.1.5. Use a model for irrigation scheduling

Applying new technologies to irrigation water management leads to improvements in the productivity and sustainability of agricultural systems (Burt et al., 1996; Vidal et al., 2001). Simulation models linked to decision support systems for the management of irrigated areas constitute powerful tools to achieve these goals (Hall, 1999; Playán et al., 2000;

Walker, 1999). In the last decades, the development of such models has been boosted by developments in computer science. They have become much more efficient, making their application to problems increasingly widespread (Simunek and Sejna, 2014).

As the same case as all simulation models, vadose zone simulation models need specific input parameters. In this case are defined, for instance, by environmental conditions, irrigation applied, crop and soil hydraulic parameters. Then, an unsaturated flow equation, such as Richard's equation (Richards, 1931) is solved providing the output with different variables (transpiration, drainage, water content dynamics…). In this way, irrigation scheduling can be assessed or a general point of view of the SPA continuum can be obtained.

The precision and accuracy of data introduced in the model (input data) is crucial to do not compromise results obtained (output data). For instance, there are some methodologies and equipment that can provide accurate soil hydraulic parameters (Schelle et al., 2013). If they are used in a simulation model and it is assumed that they are representative of the soil studied, the output simulations is going to be more realistic than soil hydraulic properties from different data bases (Saxton and Rawls, 2006; Schaap et al., 2001).

Although, simulation models can represent vadose zone, in reality, they are just an approximation and a simplification of the system. Even though input data employed is representative of the system studied, field measurements are needed in order to compare simulated data with measured data. It is when the model is calibrated minimizing its uncertainty. Measurements from sensors installed at the field site are the most methodology widely employed. As it has been commented in the previous section, they are able to provide measurements at high temporal resolution monitoring different crop-soil processes. Thus, sensors measurements or any kind of field measurements are needed in order to trust in simulation models results.

At this point, simulation models are capable to simulate "what-if" scenarios and it is considered that they have predictive capability. In this way, several hypothetical irrigation scheduling strategies can be simulated in order to assess each one. Also, these scenarios can help to understand how an irrigation strategy modifies water content patter through the root zone or which one is the most favorable for optimal crop conditions. Another purpose of simulation models and their "what-if" scenarios is found new alternatives or solutions to mitigate or solve possible problems detected in the field.

1.1.6. Spatial variability in an agriculture field

In conventional agriculture each field is considered as a uniform unit, by purpose ignoring the heterogeneity across the field, thereby decision-making is based on an estimation of

average conditions (Haghverdi et al., 2015). Unfortunately, an agriculture field soil properties, soil organic matter content, profile depth and another properties can vary significantly even within the same field (Koestel et al., 2013).

The motivation for site-specific crop management was first addressed by researchers during the late 80s and early 90s (Arslan and Colvin, 2002). Specifically, site-specific crop management is the management of agriculture crops at a spatial scale smaller than the whole field by considering local variability to cost-effectively maximize crop production and the efficient use of agrichemicals and irrigation to minimize detrimental environmental impacts (Martínez-Casasnovas et al., 2018). Thus, the concept of Management Zone (MZ) is introduced, which is a sub-region of a field that is relatively homogeneous with respect to soil-landscape attributes (Haghverdi et al., 2015).

A field can be zoned based on a single soil-crop attribute or combining different attributes from different source of information. Remote sensing is especially attractive technique because it is noninvasive and relatively inexpensive (Schepers et al., 2004). In addition, a difference in contrast to sensors, remote sensing provides continuous attribute maps allowing delineate MZs.

Remote sensing is able to measure different kinds of data; (i) crop cover variables, in which Normalized Difference Vegetation Index (NDVI), Leaf Area Index (LAI) and Land Surface Temperature (LST) can be measured. These variables can indicate the existence of crop development differences within the field. They can be related with irrigation scheduling problems assuming that crop is not under optimal water content conditions. In this way, when MZs are delineated, irrigation scheduling can be readjusted considering crop cover data. (ii) Water content, in which different algorithms are employed based on crop cover data. The main goal of these algorithm is to estimate water content for irrigation scheduling, but they need field validation and they only provide water content data fot the first 5 cm of soil, instead of the entire root zone.

1.2. Motivation and objectives

At present, there is not a unique methodology to determinate an optimal irrigation scheduling in a determinate field. Most of the researchers use a single methodology to monitor one parameter in the SPA continuum, resulting in incomplete information for the entire process. In addition, most of the times, soil is not considered or their water content processes are mostly simplified. That is why that in this thesis aims to improve irrigation

scheduling by integrating all the elements of SPA continuum, but with special emphasis with soil, because its status effects the rest of the elements.

The main objective of this thesis is defining how to improve irrigation scheduling combining three different methodologies; (i) water content sensors, (ii) remote sensing data, (iii) simulation models (Fig.1.5). Each methodology aims to supply a different gap when irrigation scheduling in a field site must be defined, highlighting the advantages and avoiding limitations of each one and the scale effect.

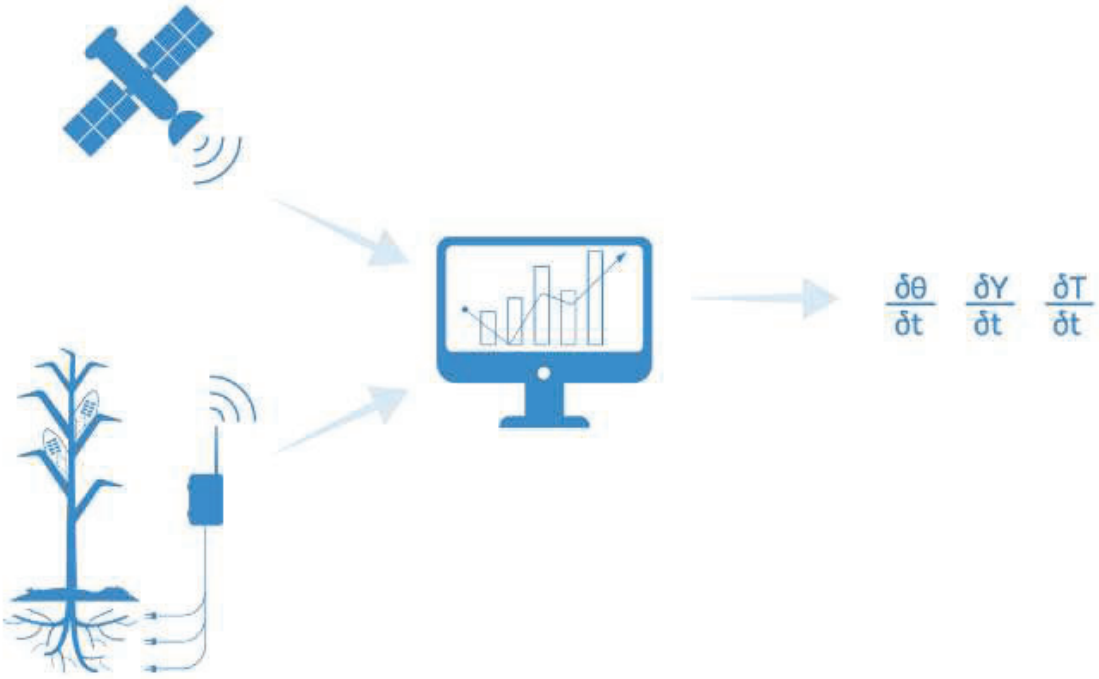

Figure 1.4. Remote sensing, water content sensors and model simulation combination data combination.

To accomplish this broad objective, specific targets are identified:

- Even though water content sensors provide water content measurements in a specific location for the entire field and the fact of some new emerging remote sensing algorithms are able to estimate water content, it is necessary to stablish if any remote sensing algorithm that estimates water content at field scale, are capable to improve water content sensors data.
- To present a methodology for optimizing irrigation scheduling in order to provide maximum economic net margin employing a simulation model. The methodology must have predictive capability when hypothetical irrigation scheduling strategies are simulated, and at the same time, it must be scaled to another field with different soil hydraulic properties, environmental conditions and crops.

- To define if joining crop cover remote sensing data and water content can validate the delineation of MZs during the growing season.
- To define if field management zones have a dynamic water content pattern during the growing season.
- To propose an optimal irrigation scheduling strategy calendar for each management zone to allow the irrigation consultant to take within-season irrigation decisions.

1.3. Thesis outline

Considering this introductory and first chapter, the resulting document is structured in five chapters. Even though each chapter is focused on answer different questions, all of them are related in order to supply information about irrigation scheduling.

Chapter 2 compares different methodologies to measure water content in an irrigation field. Specifically, gravimetric measurements and water content sensor measurements are compared with DISPATCH algorithm. This algorithm downscales Soil Moisture Ocean salinity (SMOS) satellite water content data from low to high spatial resolution. Downscaling process is based on Moderate Resolution Imaging Spectroradiometer (MODIS) LST and NDVI data. Water content sensors are the most feasible methodology when water content must be monitored to manage irrigation at field scale.

Chapter 3 presents a methodology which determines the optimal irrigation scheduling strategy for specific field. This methodology solves a simulation-optimization problem constrained by several irrigation control parameters that modifies an irrigation scheduling strategy in each case. In this way, the irrigation is optimized and economic net margin maximized. The methodology has been applied in a real field site and in a theoretical soil type. Moreover, the methodology has been compared with the traditional irrigation method, based on water requirements. Results shows that depending on soil hydraulic properties irrigation must be scheduled differently. In addition, results also show that this methodology provides a greater net margin than the traditional method.

Chapter 4 presents how to improve irrigation scheduling considering field spatial variability. Water content sensors, remote sensing data and simulation models are combined in this chapter. All of them, provide different kind of information which needs to be complemented by the others. Firstly, field spatial variability was assessed with NDVI remote sensing data and different management zones were delineated. Secondly, water content sensors provided information about spatial variability and they validated the

management zone distribution. Finally, the methodology presented in chapter 3 was applied to propose an alternative irrigation scheduling strategy. In this chapter, it has been demonstrated that management zones can have a dynamic pattern and irrigation scheduling could be readjusted depending on it.

Finally, Chapter 5 presents a summary of the conclusions drawn during the course of the thesis.

Chapter 2

The value of satellite remote sensing water content data and the DISPATCH algorithm in irrigation fields

Fontanet, M., Fernàndez-Garcia, D., and Ferrer, F.: The value of satellite remote sensing soil moisture data and the DISPATCH algorithm in irrigation fields, Hydrol. Earth Syst. Sci., 22, 5889-5900, https://doi.org/10.5194/hess-22-5889-2018, 2018.

2.1. Introduction

Water content measurements taken over different spatial and temporal scales are increasingly required in a wide range of environmental applications, which include crop yield forecasting (Holzman et al., 2014), irrigation planning (Vellidis et al., 2016), early warnings for floods and droughts (Koriche and Rientjes, 2016), and weather forecasting (Dillon et al., 2016). This is mostly due to the fact that water content controls the water and energy exchanges between key environmental compartments (atmosphere and earth) and hydrological processes, such as precipitation, evaporation, infiltration and runoff (Ochsner, 2013; Robock et al., 2000).

There are several applications in which water content measurements have been shown to provide relevant information (Robock et al., 2000). For example, in environmental applications, water content is typically used for defining the water stress occurring in natural and human systems (Irmak et al., 2000) or for quantifying nitrate leaching and drainage quality (Clothier and Green, 1994). Here, we highlight that water content measurements from the root zone yields important information for field irrigation scheduling, determining to a great extent the duration and frequency of irrigation needed for plant growth as a function of water availability (Blonquist et al., 2006; Campbell, 1982; Jones, 2004).

Water content is highly variable in space and time, mainly as a result of the spatial variability in soil properties (Hawley, 1983), topography (Burt and Butcher, 1985), land uses (Fu, 1994), vegetation (Le Roux et al., 1995) and atmospheric conditions (Koster and Suarez, 2001). As a result, water content data exhibits a strong scale effect that can substantially affect the reliability of predictions, depending on the method of measurement used. For this reason, it is important to understand how to measure water content for irrigation scheduling.

Nowadays, available techniques for measuring or estimating water content can provide data either at a small or at a large scale. Gravimetric measurements (Gardner, 1986) estimate water content by the difference between the natural and the dry weight of a given soil sample. They are used as a reference value of water content for sensor calibration (Starr and Paltineanu, 2002) or water content validation studies (Bosch et al., 2006; Cosh et al., 2006). The main disadvantage of this method is that these measurements are time-consuming; users have to go to the field to collect soil samples and place them in the oven for a long time. Water content sensors such as time domain reflectometry sensors (Clarke

Topp and Reynolds, 1998; Schaap et al., 2003; Topp et al., 1980) or capacitance sensors (Bogena et al., 2007; Dean et al., 1987) are capable of measuring water content continuously using a data logger, thereby enabling the final user to save time. Water content sensors are especially useful for studying processes at a small scale, but suffer from the typical low number of in situ sensors that provide an incomplete picture of a large area (Western et al., 1998). Nevertheless, the use of soil moisture sensors is a common practice for guiding irrigation scheduling in cropping field systems (Fares and Polyakov, 2006; Thompson et al., 2007; Vellidis et al., 2008).

Remote sensing can estimate water content continuously over large areas (Jackson et al., 1996). In this case, water content estimations refer to the near-surface water content (NSSM), which represents the first 5 cm (or less) of the top soil profile. In recent years, remote sensing techniques have improved and diversified their estimation, making them an interesting tool for monitoring NSSM and other variables such as the Normalized Difference Vegetation Index (NDVI) and the land surface temperature (LST). Different satellites exist that are capable of estimating NSSM: the Soil Moisture Active Passive (SMAP) satellite, the Advanced Scatterometer (ASCAT) remote sensing instrument on board the Meteorological Operational (METOP) satellite, the Advanced Microwave Scanning Radiometer 2 (AMSR2) instrument on board the Global Change Observation Mission 1-Water (GCOM-W1) satellite, and the Soil Moisture and Ocean Salinity (SMOS) satellite launched in November 2009 (Kerr et al., 2001). The SMOS satellite has global coverage and a revisit period of 3 days at the Equator, giving two water content estimations, the first one taken during the ascending overpass at 06:00 LST (local solar time) and the second one during the descending overpass at 18:00 LST. The SMOS satellite is a passive 2-D interferometer operating at L-band frequency (1.4 GHz) (Kerr et al., 2010). The spatial resolution ranges from 35 to 55 km, depending on the incident angle. Its goal is to retrieve NSSM with a target accuracy of a 0.04 m3 m−3 (Kerr et al., 2012). Since SMOS NSSM values have been validated on a regular basis since the beginning of its mission (Bitar et al., 2012; Delwart et al., 2008), they are considered suitable for hydro-climate applications (Lievens et al., 2015; Wanders et al., 2014).

The relatively large variability of water content compared to the low resolution of SMOS-NSSM data hinders the direct application of this method to irrigation scheduling. However, the need for estimating NSSM with a resolution higher than 35–55 km using remote sensing has increased for different reasons: (1) data are freely available, (2) a field installation of water content sensors is not necessary, and (3) no specific maintenance is needed. For these reasons, in the last few years, different algorithms have been developed to downscale remote sensing water content data to tens or hundreds of meters.

Chauhan et al. (2003) developed a Polynomial fitting method which estimates soil moisture at 1 km resolution (Carlson, 2007; Wang and Qu, 2009). This method links water content data with surface temperature, vegetation index and albedo. It does not require in situ measurements but cannot be used under cloud coverage conditions. The improvements in the detection method reported by Narayan et al. (2006) downscales water content at 100 m resolution. This is an optimal resolution for agricultural applications, but the method is highly dependent on the accuracy of its input data. The same problem is attributed to the Baseline algorithm for the SMAP satellite (Das and Mohanty, 2006), which downscales water content at 9 km resolution. These algorithms have to be validated using in situ measurements. For this purpose, most studies use water content sensors installed at the top soil profile, i.e., the first 5 cm of soil (Albergel et al., 2011; Cosh et al., 2004; Jackson et al., 2010), while others use gravimetric soil moisture measurements (Merlin et al., 2012) or the combination of both methodologies (Robock et al., 2000). Satellite water content has recently been used to provide irrigation detection signals (Lawston et al., 2017), quantify the amount of water applied (Brocca et al., 2018; Zaussinger et al., 2018) and estimate the water use (Zaussinger et al., 2018). All these deal with relatively homogeneous and extensive irrigation surface coverages (several kilometers).

Other satellites, such as Sentinel-1, can estimate NSSM at 1 km resolution (Bauer-Marschallinger et al., 2018; Hornacek et al., 2012; Mattia et al., 2015; Paloscia et al., 2013). Sentinel-1 provides two kinds of products, the first one is the Single Look Complex (SLC) algorithm and the second one is the Ground Range Detected (GRD) algorithm. The latter can be used for solving a wide range of problems related to Earth surface monitoring, such as water content, but it is not a direct measurement and therefore data processing is needed. In this case, the GRD product is converted into radar backscatter coefficients and then into decibels to estimate water content. Usually, these conversions are cumbersome because these kinds of measurements have surface roughness and vegetation influence that affect the signal (Garkusha et al., 2017; Wagner et al., 2010).

The DISPATCH method (DISaggagregation based on Physical And Theoretical CHange) (Merlin et al., 2012, 2008) is an algorithm that downscales SMOS NSSM data from 40 km (low resolution) to 1 km resolution (high resolution). This algorithm uses Terra and Aqua satellite data to estimate NDVI and LST twice a day using the Moderate Resolution Imaging Spectroradiometer (MODIS) sensor. These estimations have a resolution of 1 km and can be conducted only if there is no cloud cover. This downscaling process provides the final user with the possibility of estimating NSSM using remote sensing techniques at high resolution. DISPATCH successfully reveals spatial heterogeneities such as rivers, large irrigation areas and floods (Escorihuela and Quintana-Seguí, 2016; Merlin et al., 2015;

Molero et al., 2016) and it has also been validated (Malbéteau et al., 2015; Merlin et al., 2012; Molero et al., 2016) in fairly large and homogeneous irrigation areas, but it has not been applied in complex settings with spatially changing hydrologic conditions such as those representing a local irrigation field.

In this work, we evaluate the value of remote sensing in agricultural irrigation scheduling by comparing in situ water content data obtained from gravimetric and water content sensors, with soil moisture data determined by downscaling remote sensing information with the DISPATCH algorithm.

2.1.1. Study area

The study area shown in Fig. 2.1 is located in the village of Foradada (1.015º N, 41.866º W), in the Segarra–Garrigues (SG) system (Lleida, Catalonia). The SG system is an important irrigation development project currently being carried out in the province of Lleida, Catalonia, which involves converting most of the current dry-land fields into irrigated fields. Its construction enables 1000 new hectares with a long agricultural tradition to be irrigated. To achieve this, an 85 km long channel was constructed to supply water for irrigation. At present, approximately 16 000 irrigators are potential beneficiaries of these installations. However, most farmers have not yet installed this irrigation system, which means that the SG systems can still be regarded as dry land.

The Urgell area is located in the west of the SG system. This area has totally different water content conditions, especially during the summer season when the majority of fields are currently irrigated. This gives rise to two clearly distinguishable wet and dry water content conditions. Figure 2.1 shows the Foradada field, which represents 25 ha of a commercial field irrigated by a solid set sprinkler irrigation system distributed across 18 different irrigation sectors. The soil texture, in a single point, is 28% Clay, 58.4% Silt and 13.6% Sand. Every year two different crops are grown, the first one during the winter and spring seasons, when wet conditions are maintained by precipitation, and the second one during the summer and autumn seasons, when wet conditions are maintained by sprinkler irrigation. The Foradada field is thus one of the few irrigated fields located within the SG system. Consequently, this field has soil moisture conditions similar to those in the surrounding area during the winter and spring season, but completely different conditions during the summer and autumn seasons. This makes this site unique for assessing remote sensing in a distinct isolated irrigation field.

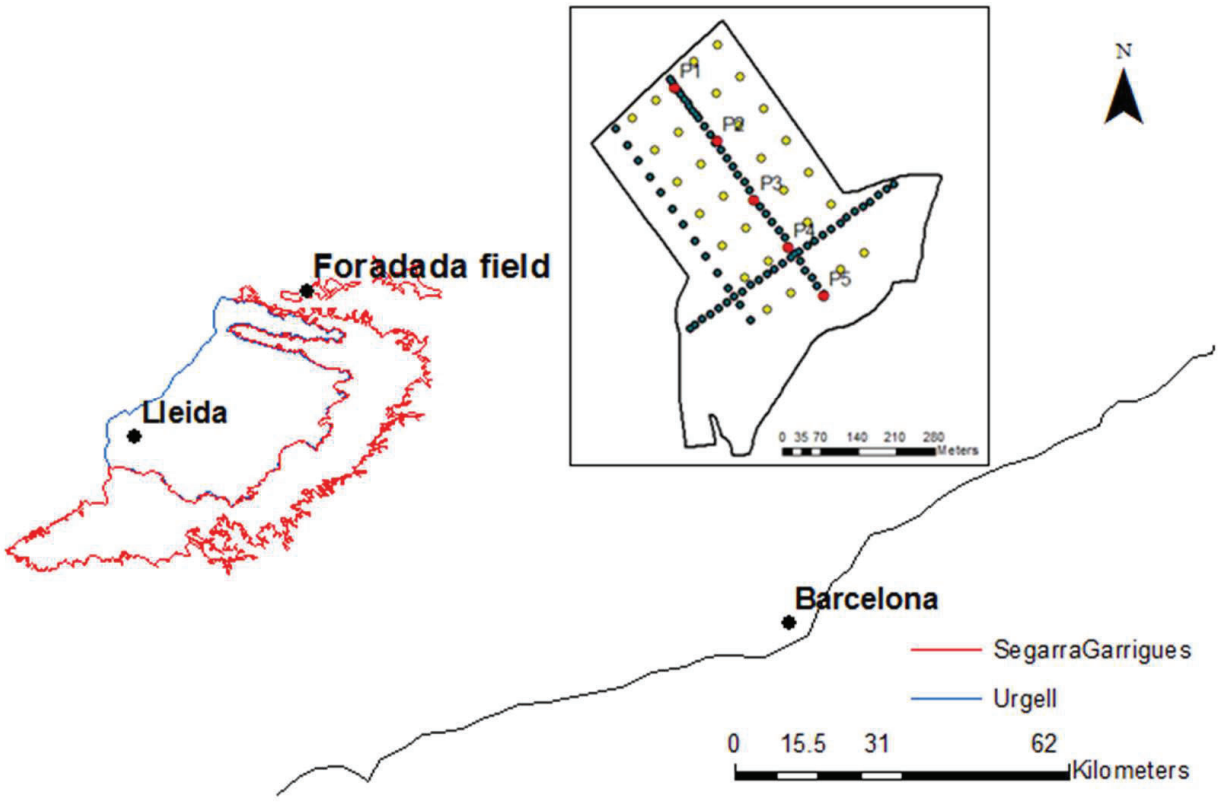

Figure 2.1. Location of the Foradada field site within the Segarra-Garriga irrigation system and distribution of soil moisture measurement points. Gravimetric measurement points are arranged with cross section points in green and support points in yellow. The location of EC-5 sensors are represented in red.

2.2. Materials and methods

2.2.1. In situ soil moisture measurements

A total of nine intensive and strategic field campaigns were conducted in the study area during 2016: DOY42, DOY85, DOY102, DOY187, DOY194, DOY200, DOY215, DOY221 and DOY224. During each field campaign, disturbed soil samples were collected from the top soil profile (0–5 cm depth) for measuring gravimetric water content data. A total of 101 measurement points, depicted in Fig. 2.1, were defined around the field. They are divided into two different kinds of points: (1) cross section points – 75 points defined to represent the spatial variability of soil moisture in different cross sections (in these cross sections, points are separated by 9, 16 and 35 m); (2) support points – 26 points defined to complement information measured from cross sections, thereby adding and supporting information about the spatial variability across the field. Each soil sample is analyzed using the gravimetric method for measuring gravimetric water content, which is transformed to volumetric soil moisture content using bulk density measurements (Letelier, 1982). Daily

averages of gravimetric measurements and their standard deviations were computed to represent the soil moisture associated with the entire field site.

Water content was also measured using capacitive EC-5 sensors (METER Group, Pullman, WA, USA), previously calibrated in the laboratory (Star and Paltineanu, 2002). As Fig. 2.1 shows, a total of five control points were installed across one of the three gravimetric cross sections. Each control point represents a different irrigation sector of the field. Water content sensors were installed at 5 cm depth, taking into account the measured volume of these sensors. Their accuracy is ±0.03 cm^3 cm^{-3} (Campbell and Devices, 1986). They were connected to an EM50G data logger (METER Group, Pullman, WA, USA) that registers soil moisture every 5 min.

2.2.2. DISPATCH soil moisture measurements

In this section we briefly describe the DISPATCH algorithm. Further details can be found in Merlin et al. (2013) and references therein. The DISPATCH algorithm aims to downscale NSSM data obtained from SMOS at 40 km resolution to 1 km resolution. The method assumes that NSSM is a linear function of the soil evaporative efficiency (SEE), which can be estimated at high resolution (1 km) from the acquisition of two products obtained from MODIS, i.e., LST and NDVI datasets. This MODIS-derived SEE is further considered as a proxy for the $NSSM$ variability within the SMOS pixel. The estimation of SEE is assumed to be approximately constant during the day given clear sky conditions. The downscaling relationship is given by Eq. (2.1):

$$\theta_{HR} = \theta_{SMOS} + \theta'_{HR}(\theta_{SMOS}) \cdot (SEE_{HR} - SEE_{SMOS}), \quad (2.1)$$

where θ_{SMOS} is the low-resolution SMOS soil moisture data, SEE_{HR} is the MODIS-derived SEE at a high resolution (1 km), SEE_{SMOS} is the average of SEE_{HR} within the SMOS pixel at a low resolution (40 km), and $\theta'_{HR}(\theta_{SMOS})$ is the partial derivative of water content with respect to the soil evaporative efficiency at high resolution evaluated at the SEE_{SMOS} value. This partial derivative is typically estimated by using the linear soil evaporative efficiency model of Budyko, (1961) and Manabe (1969), which is defined in Eq. (2.2):

$$\theta_{HR} = SEE_{HR} \cdot \theta_p, \quad (2.2)$$

where θ_{HR} represents the water content of the top soil layer (0–5 cm) at high resolution, and θ_p is an empirical parameter that depends on soil properties and atmospheric conditions. The soil evaporation efficiency at high-resolution SEE_{HR} is estimated as a linear function of the soil temperature at high resolution ($T_{s,HR}$) (Eq.2.3):

$$SEE_{HR} = \frac{T_{s,max} - T_{s,HR}}{T_{s,max} - T_{s,min}}, \tag{2.3}$$

The soil temperature at high resolution is estimated by partitioning the MODIS surface temperature data (LST) into the soil and the vegetation component according to the trapezoid method of Moran et al. (1994). This also requires an estimation of the fractional vegetation cover, which is calculated from the NDVI data. $T_{s,min}$ and $T_{s,max}$ are the soil temperature end-members (Merlin et al., 2012).

In this work, the DISPATCH algorithm has been applied during the period from DOY36 to DOY298 of 2016 to estimate *NSSM* at 1 km resolution in the Foradada field site. DISPATCH provides a daily NSSM pixel map (regular grid). The Foradada field site is entirely included in one pixel. In this pixel, 51.5 % of the total area corresponds to irrigated area. The remaining portion of the pixel corresponds to dry land (shown in Fig. 2.2).

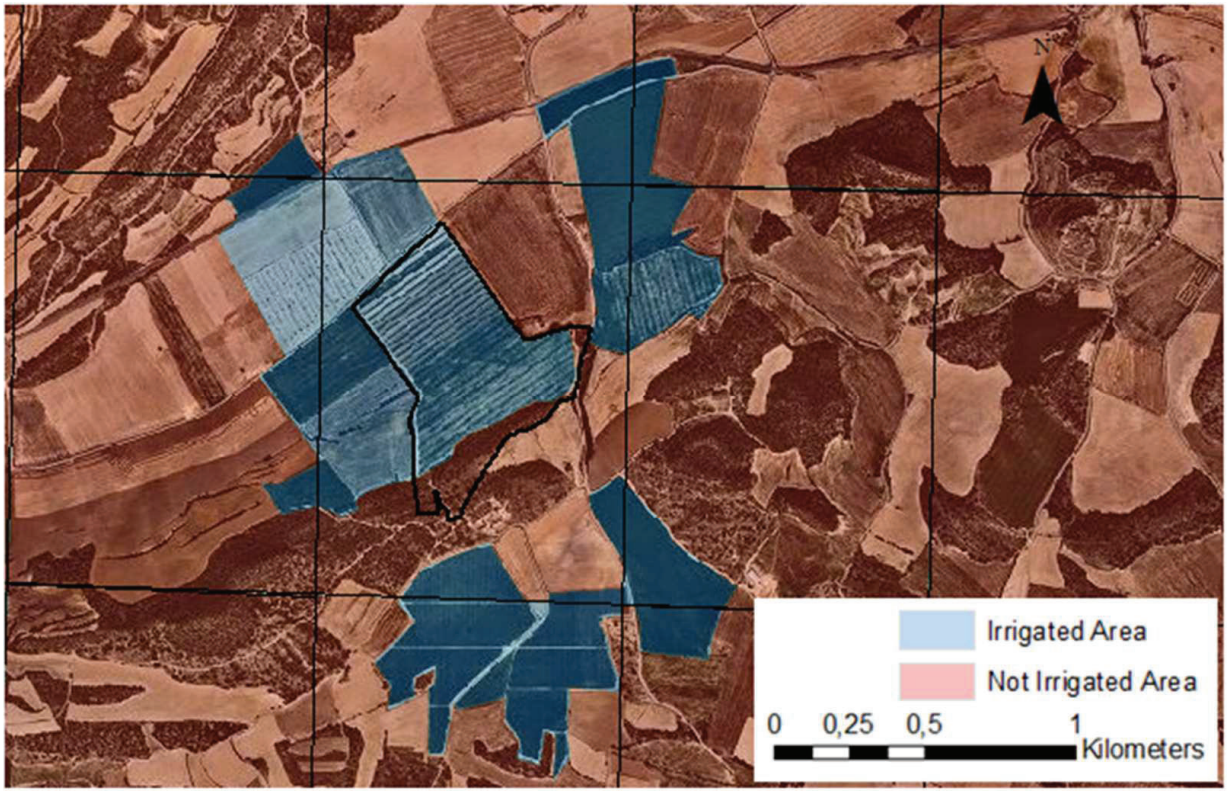

Figure 2.2. The DISPATCH grid representing the Foradada field, outlined in dark blue, irrigated fields in light blue, and dry land in light red.

2.2.3. Image spatial resolution and spatial variability

The information contained in a satellite image is characterized here by two properties: the spatial resolution and the spatial variability of the image attributes. The spatial resolution

of a satellite image is the ground area represented by each pixel, i.e., the raster cell size. It is essentially the representative support volume chosen to describe the variations of the attributes of interest at the ground surface. This is typically determined based on the type of satellite sensor. The spatial variability refers to the variations of the attributes presented in the image at the ground surface, e.g., patterns of spatial continuity, size of objects in the scene, and so on. In random field theory and geostatistics, the spatial variability is mainly characterized by the covariance function or by its equivalent, the semivariogram, which is defined by (Journel and Huijbregts, 1978) (Eq.2.4):

$$\gamma(\boldsymbol{h}) = \frac{1}{2} E\{[Z(\boldsymbol{x}+\boldsymbol{h}) - Z(\boldsymbol{x})]^2\}, \tag{2.4}$$

where $Z(\boldsymbol{x})$ is the random variable at the x position, and $E\{\cdot\}$ is the expectation operator. Essentially, the semivariogram is a function that measures the variability between pairs of variables separated by a distance $\boldsymbol{h}$. Very often, the correlation between two variables separated by a certain distance disappears when $|\boldsymbol{h}|$ becomes too large. At this instant, $\gamma(\boldsymbol{h})$ approaches a constant value. The distance beyond which $\gamma(\boldsymbol{h})$ can be considered to be a constant value is known as the range, which represents the transition of the variable to the state of negligible correlation. Thus, the range can ultimately be seen as the size of independent objects in the image. If the pixel size is smaller than 10 times the minimum range (in the absence of the nugget effect), then neighboring pixels will be alike, containing essentially the same level of information (Journel and Huijbregts, 1978). This will be a critical point in the discussion of the results later on. We note that the spatial resolution and the spatial variability are two related concepts. Several authors note that a rational choice of the spatial resolution for remote sensing should be based on the relationship between spatial resolution and spatial dependence (Atkinson and Curran, 1997; Curran, 1988). However, since this is not the usual procedure, the spatial resolution can be inappropriate in some cases or provide unnecessary data in others (Atkinson and Curran, 1997; Woodcock and Strahler, 1987).

2.3. Results

2.3.1. General observations

One of the main advantages of our experiment is that remote sensing soil moisture data is evaluated during two different hydrologic periods of the same year in a given agriculture field site. The first period represents crop growth with soil wet conditions caused by natural rainfall events (without irrigation). This period occurs during the winter and spring season,

i.e., from February to June. The following period occurs during the dry season with artificially created wet soil conditions caused by sprinkler irrigation operating to satisfy crop water requirements during the summer and autumn season, from June to October. In contrast to the rainfall events, sprinkler irrigation creates a local artificial rainfall event using several rotating sprinkler heads. The comparisons of these two hydrologic periods allow us to evaluate the effect of local sprinkler irrigation on remote sensing soil moisture estimations.

Figure 2.3 compares gravimetric and water content sensor measurements with the DISPATCH water content estimates obtained from remote sensing data during the first period of time (without irrigation). We note that the comparison here is not between the point gravimetric measurements (with a support volume of few centimeters) and the satellite information (1 km in resolution). Instead, we compare the average of these point measurements over the entire field site (very well distributed with more than 100 measurement points) with the satellite information. The average of the water content is representative of the entire irrigated area associated with the Foradada field site. Consequently, these two variables have similar support scale and are therefore comparable. Error bars in the gravimetric measurements represent the standard deviation of all the measurements obtained in 1 day. In addition, the area between the light and dark green lines in this figure displays the difference between the daily minimum and maximum values of water content data obtained from the five EC-5 sensors. We note that the average of the gravimetric water content data always lies within this region. This supports the use of this information to complement water content data on days where no gravimetric sampling is available. The error bars associated with DISPATCH data refer to the standard deviation obtained with two daily SMOS estimations and four MODIS data (two at) 06:00 LST and two more at 18:00 LST). To better appreciate tendencies, the same information is also presented as normalized relative water content, i.e., $(\theta-\theta_{min})/(\theta_{max}-\theta_{min})$, where θ_{min} and θ_{max} are the minimum and maximum values of the soil moisture time series data obtained with the EC-5 sensors. Results show that DISPATCH estimates can properly detect the relative increase in water content estimates caused by rainfall events. Note for instance that all methods produce a similar relative increase in water content signal after the occurrence of a strong rainfall event. In absolute terms, we see that DISPATCH slightly underestimates the true value of water content but this could be attributed to small differences between the support volume of the field site and the spatial resolution of the satellite image.

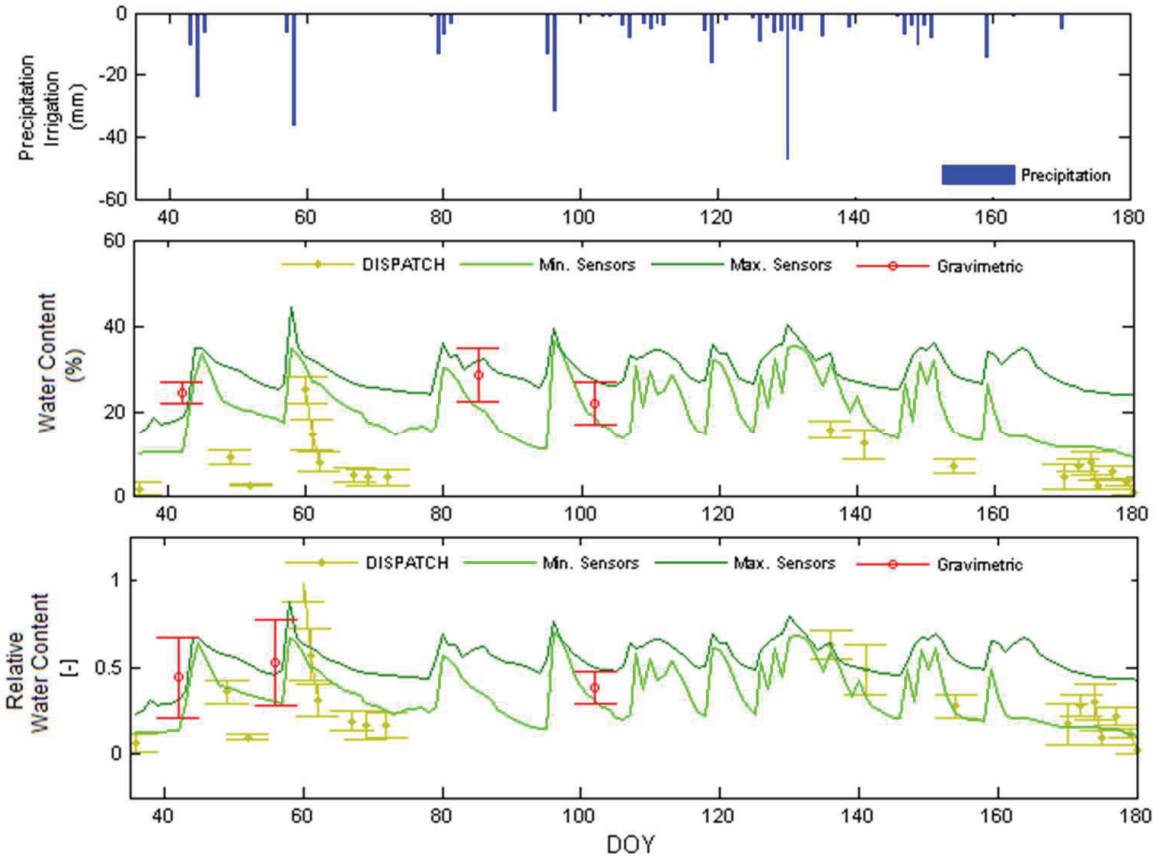

Figure 2.3. Comparison of average gravimetric water content measurements (red) with the DISPATCH soil moisture estimations (yellow) and the daily maximum and minimum water content sensor measurements (green) during the first hydrologic period (soil wet conditions caused by rainfall events only).

A similar analysis is shown in Fig. 2.4, which compares gravimetric and sensor water content measurements with DISPATCH water content estimations during the second period (wet soil conditions maintained by sprinkler irrigation). In contrast to our previous results, it can be seen that the DISPATCH dataset is essentially not sensitive to sprinkler irrigation even though there is a proper response to sporadic small rainfall events. Likewise, the relative increase in water content measurements also shows that sprinkler irrigation does not affect the DISPATCH estimation. Thus, even though the DISPATCH estimations seem to properly respond to rainfall events during the first period, irrigation operating at the Foradada field scale remains undetected during the second period. The DISPATCH dataset is not sensitive to irrigation and merely indicates that soil dry conditions exist at a larger scale.

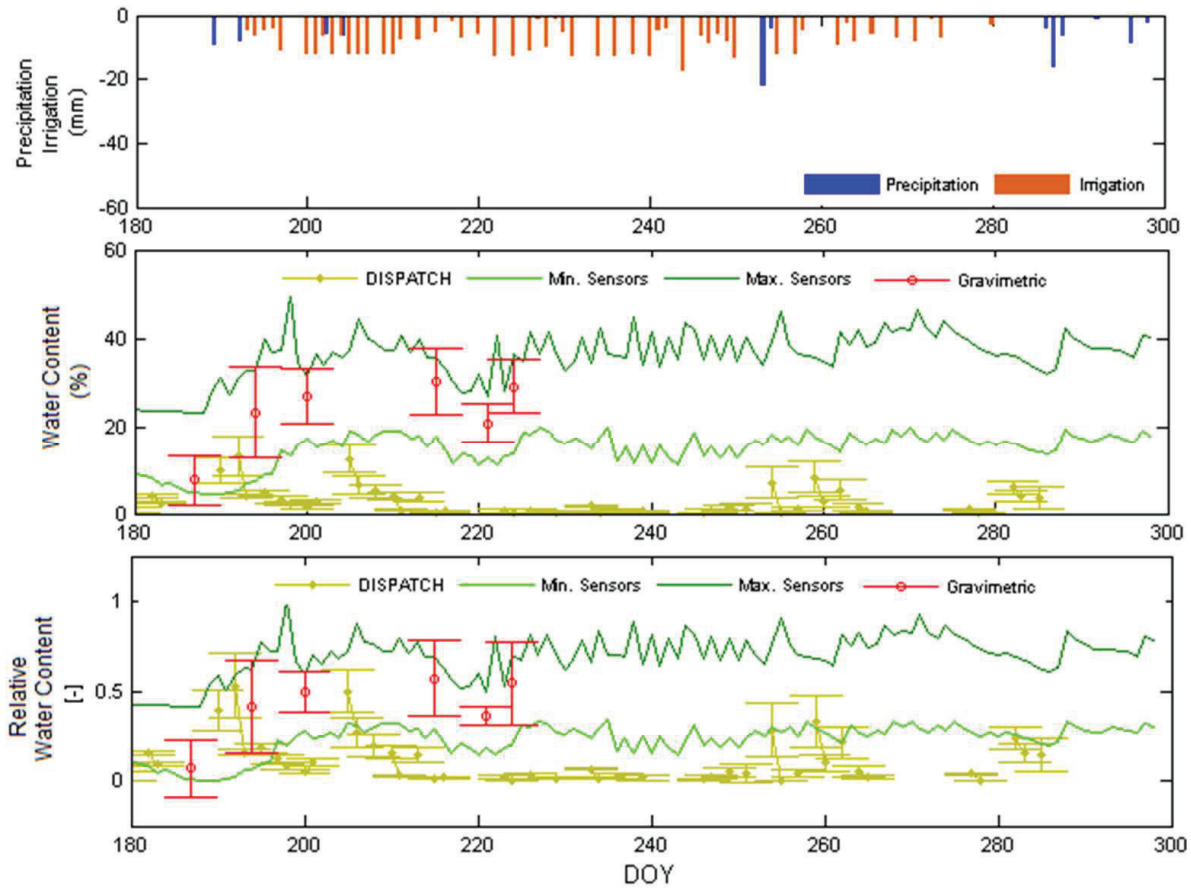

Figure 2.4. Comparison of average gravimetric water content measurements (red) with the DISPATCH soil moisture estimations (yellow) and the daily maximum and minimum water content sensor measurements (green) during the second hydrologic period (soil wet conditions caused by irrigation). The top figure shows the intensity of precipitation and irrigation.

This can also be seen from a different perspective by looking at the scatter plot between the average of the normalized relative water content data obtained with the EC-5 sensors and the corresponding DISPATCH measurement determined on the same day. Figure 5 shows the scatter plots obtained during rainfall events and irrigation period. We note that even though a clear tendency is seen during rainfall events (R^2 = 0.57), no correlation seems to exist during irrigation (R^2 = 0.04). We conclude then that the DISPATCH dataset provides representative estimates of water content at a lower resolution than expected.

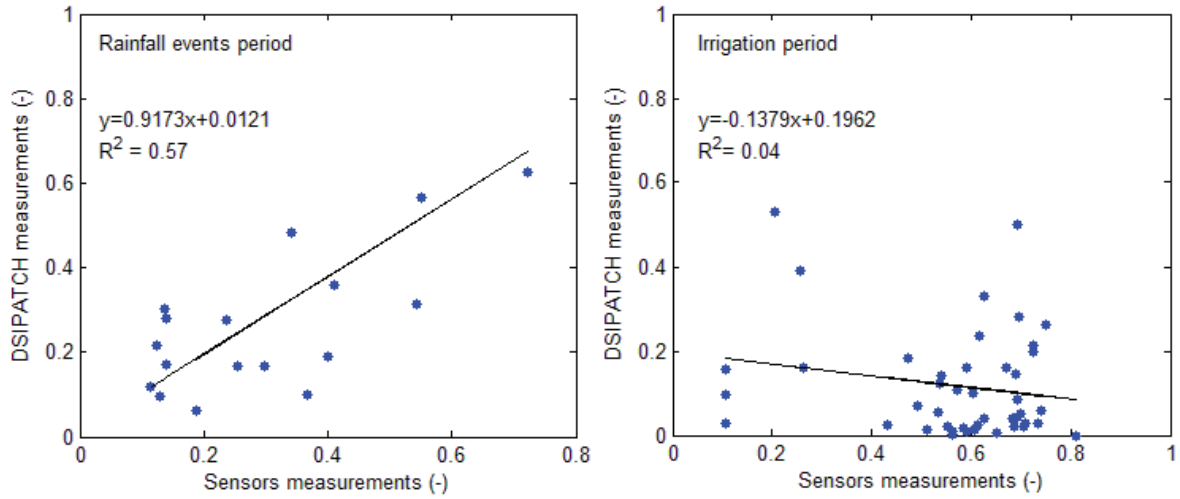

Figure 2.5. Scatter plot between the average of the normalized water content obtained with EC-5 sensors and the DISPATCH measurements obtained during both hydrologic scenarios, rainfall events and irrigation period.

2.4. Analysis and discussion

We seek to answer the important question of why the DISPATCH water content estimates obtained by downscaling satellite information from 40 to 1 km of resolution are not sensitive to sprinkler irrigation in this case. The following possible sources of discrepancies can be identified: (i) errors associated with the approximations used in the DISPATCH downscaling formulation, (ii) differences in the scale of observations, (iii) low quality of information associated with DISPATCH input variables, and (iv) poor relationship between irrigation fluctuations and DISPATCH input variables dynamics. We concentrate the analysis on (ii) and (iii). First, we note that the DISPATCH resolution of 1 km is similar to the characteristic scale of the irrigated area at the Foradada field site and therefore a better performance was expected. The extent of the irrigated area in the DISPATCH pixel size of interest is 51.5 % (see Fig. 2.2). Given that water content is a linear property, we contend that this cannot explain the negligible relative increase in water content obtained during irrigation. Then, we examine the semivariograms of the different input variables involved in the downscaling process, i.e., the NDVI and the LST properties provided by the MODIS sensor. The NDVI and LST semivariograms were respectively estimated from the MOD13A2 and MOD11A1 product data, which can be freely downloaded from the Google Earth Engine website (https://earthengine.google.com, last access: 15 January 2017). We selected daily representative images of April, June and August. The April image describes a general rainfall event in the region, the June image shows when local irrigation starts in the Foradada field, and finally the August image represents when the crop is well developed and frequent irrigation is needed. Experimental semivariograms have been fitted with a theoretical

model (spherical and exponential models for the LST and NDVI, respectively), which can be formally expressed as Eqs. (2.5) and (2.6):

$$\gamma_{LST} = c_{11} Sph\left(\frac{|\boldsymbol{h}|}{a_{11}}\right) + c_{12}\left[1 - cos\left(\frac{|\boldsymbol{h}|}{a_{12}}\pi\right)\right], \tag{2.5}$$

$$\gamma_{NDVI} = c_{21} Exp\left(\frac{|\boldsymbol{h}|}{a_{21}}\right) + c_{22} Exp\left(\frac{|\boldsymbol{h}|}{a_{22}}\right) + c_{23}\left[1 - cos\left(\frac{|\boldsymbol{h}|}{a_{23}}\pi\right)\right], \tag{2.6}$$

where c_{ij} are constant coefficients that represent the contribution of the different standard semivariogram models, and a_{ij} denotes the corresponding ranges of the different structures. The LST and NDVI experimental and theoretical semivariograms are shown in Fig. 2.6. The parameters adopted in the random function model are summarized in Tables 2.1 and 2.2. The analysis determines a nested structure with a positive linear combination between isotropic stationary semivariogram models and the hole effect model. Hole effect structures most often indicate a form of periodicity (Pyrcz and Deutsch, 2003). In our case, this periodicity reflects the presence of areas with different watering and crop growth conditions, i.e., in contrast to the dry-land conditions in the SG area, the Urgell area is based on irrigation.

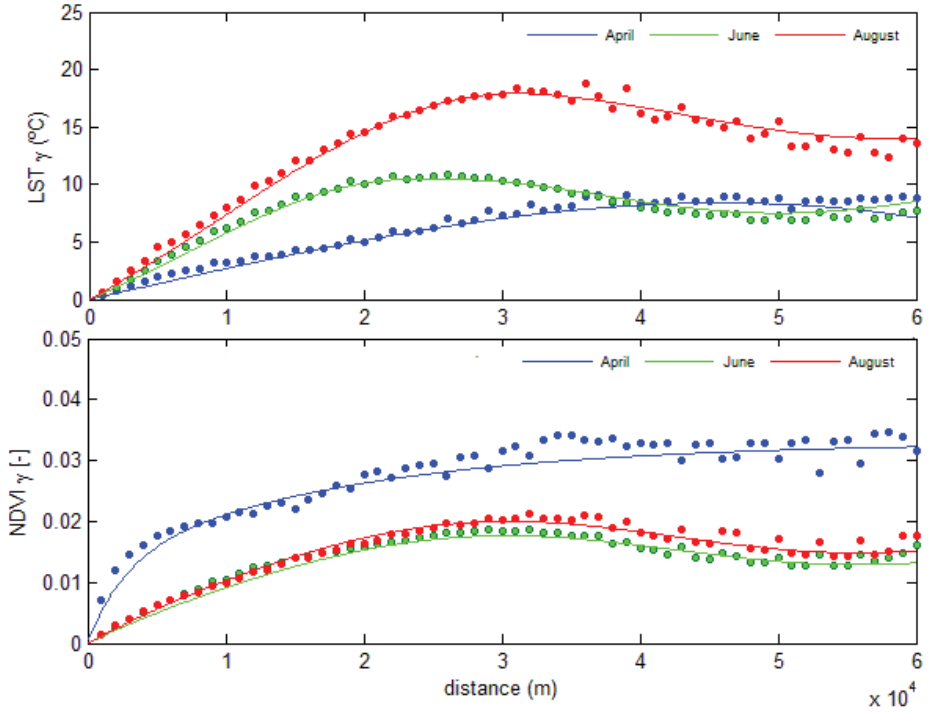

Figure 2.6. . LST and NDVI experimental and theoretical semivariograms associated with April (blue), June (green) and August (red).

The spatial variability of NDVI and LST vary with time according to changes in hydrologic conditions. In April, the semivariogram of NDVI displays more variability and less spatial continuity due to the differences in growth rate and crop type conditions existing at the regional scale during the wet season (controlled by rainfall events). On the other hand, the spatial dependence of LST is more significant in August. Importantly, results show that the scale of variability (range) associated with MODIS data during the dry season, when a controlled amount of water by irrigation is applied, ranges between 35 and 36 km for the NDVI and between 22 and 32 km for the LST. Recalling the discussion provided in section 2.2.3., this means that the size of independent objects in the NDVI and LST images is about 30 km and that insignificant spatial variations of NDVI and LST values are expected below 1/10 of this size. This suggests that the NDVI and LST products provided by MODIS cannot detect differences between neighboring pixels with a size of 1 km.

Table 2.1. Random function model parameters of LST semivariograms.

LST					
		Variogram		Hole effect	
Month	Model	Sill (c_{11})	Range (a_{11})	Sill (c_{12})	Range (a_{12})
April	Spheric	8.4	46000	-	-
June	Spheric	7.5	22000	1.5	25000
August	Spheric	14	32000	2	29000

Table 2.1. Random function model parameters of NDVI semivariograms.

NDVI							
		Variogram				Hole effect	
Month	Model	Sill (c_{21})	Range (a_{21})	Sill (c_{22})	Range (a_{22})	Sill (c_{23})	Range (a_{23})
April	Exponential	0.013	8000	0.02	55000	-	-
June	Exponential	0.013	35000	-	-	0.22	28000
August	Exponential	0.015	36000	-	-	0.21	28000

To further corroborate this point, Fig. 2.7 compares the temporal evolution of LST and NDVI obtained from two adjoining MODIS pixels: the Foradada pixel, where Foradada is located, and its northwest neighboring pixel. Note that the neighboring pixel corresponds to an area that is not irrigated. Data were downloaded using MOD13A2 and MOD11A1 products from the Google Earth Engine website, from DOY036 to DOY298. In general, based on DISPATCH suppositions, irrigation in an agriculture field site should produce a decrease in LST values as a consequence of uniform irrigation over the entire field site and an increase in NDVI due to well-developed crop growth conditions. However, Fig. 2.7 shows the same dynamics and similar values in both pixels even when irrigation is applied. Results show that the LST and NDVI information can detect neither the sprinkler irrigation nor the crop growth as a consequence of irrigation in this case. We finally note that these results suggest that the resolution of LST and NDVI is not appropriate in this case but can also express that these two variables are simply not sensitive to irrigation because they only provide information about the status of the crop and land surface. Further research is needed in this sense.

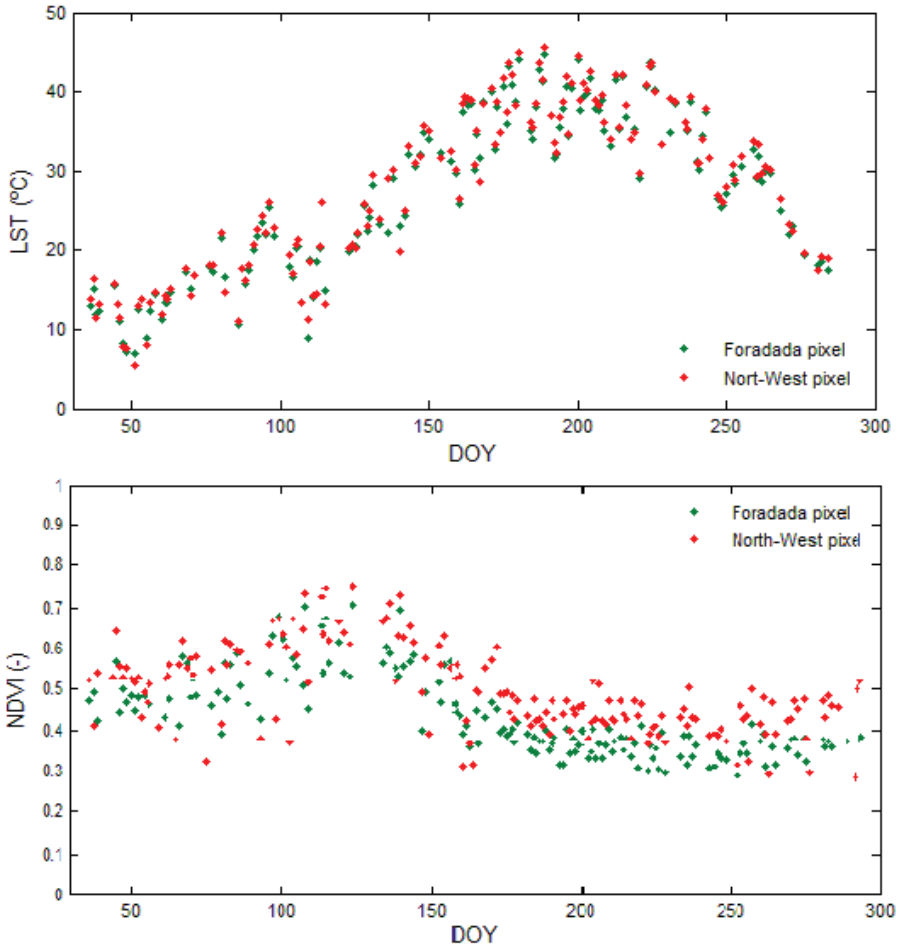

Figure 2.7. Temporal evolution of LST and NDVI obtained at the Foradada pixel and its neighboring northwest pixel situated 2 km away

2.5. Conclusion

We analyze the value of remote sensing and the DISPATCH downscaling algorithm for predicting water content variations in an irrigated field site of size close to image resolution. The DISPATCH algorithm based on the NDVI and LST data obtained from the MODIS satellite is used for downscaling the SMOS information and transforming the SMOS water content estimations from a resolution of 40 to 1 km. These estimates are then compared with average gravimetric and soil moisture sensor measurements taken all over the field site. Results have shown that in this case the downscaled water content estimations are capable of predicting the variations in soil moisture caused by rainfall events but fail to reproduce the temporal fluctuations in the average water content caused by local irrigation. To provide insight into this problem, we examine the spatial variability of the different input variables involved, i.e., the NDVI and LST. Results indicated that the size of individual objects in the NDVI and LST images is too large to be able to adequately represent the

variations of the average water content at the site. This effect is not significant during rainfall events because the typical spatial scale of rainfall events is much larger than the size of the irrigated field site.

From a different perspective, these results also suggest that irrigation scheduling based on satellite information coupled with the DISPATCH downscaling algorithm might be appropriate in regions of the world with extensive irrigation surface coverage, larger than approximately 10 km (e.g., Punjab basin). However, care should be taken when directly applying this method as its performance will strongly depend on the spatiotemporal variation of irrigation within the area. These variations can generate occasional areas with different hydrologic scenarios and behaviors leading to the failure of the soil moisture prediction method.

We thank our colleagues from "Root zone soil moisture Estimates at the daily and agricultural parcel scales for Crop irrigation management and water use impact" (REC project), who provided insight and expertise that greatly assisted the research.

Chapter 3

Combined simulation and optimization framework for irrigation scheduling in agriculture fields

Fontanet, M., Fernàndez-Garcia, D., Rodrigo, G., Ferrer, F., Villar, J.M.: Combined simulation and optimization framework for irrigation scheduling in agriculture fields. Vadose Zone Journal (VZJ) Manuscript Submitted.

3.1. Introduction

Agriculture is the largest consumer of freshwater and accounts for 75% of current human water use (Wallace, 2000). The Food and Agriculture Organization of the United Nations (FAO) predicts that if current consumption patterns continue at the present rate, two-thirds of the world's population could be living in water-stressed countries by 2025. As a result, water will become scarce not only in arid areas but also in regions where precipitation is abundant (Pereira et al., 2002). Within this context, optimal irrigation water strategies are crucial for saving water while guaranteeing maximum crop yields in the near future.

Irrigation scheduling is the process used by irrigation system managers to determine both the correct moment and the required amount of water to irrigate fields while maximizing crop yields with the minimum amount of water applied. Properly defining the moment of irrigation through water content (or pressure head) thresholds has been demonstrated to substantially increase the efficiency of agriculture fields (Dabach et al., 2013). However, irrigation water contains salts and fertilizers that often promotes soil salinization, which results in an increase in soil Electrical Conductivity (EC_e) and a reduction of crop productivity. Thus, optimal irrigation strategy should be design to avoid soil salinization (Gonçalves et al., 2007; Pereira et al., 2007).

Irrigation scheduling can modify water management strategies that control water governance (Budds and Hinojosa, 2012; Hanjra et al., 2012), irrigation system performance (Pitts et al., 1996; Sakthivadivel et al., 1993; Singh et al., 2006), water allocation (Dudley et al., 1971; Reca et al., 2001) and water accounting (Perry, 2011). Because of the importance of irrigation scheduling, a wide range of irrigation methodologies have been recently developed and used in the field to guarantee crop productivity and avoid soil salinization. We distinguish between methods based on water requirements, direct measurements of the plant water status or response to water stress, direct measurements of water content, and numerical modeling of flow and transport of salt concentrations in the vadose zone.

Water requirements determined from crop evapotranspiration calculations (ET_c) is the most widely used method for irrigation scheduling. ET_c is typically estimated as the product of two terms: the reference evapotranspiration (ET_0), generally defined for either clipped grass (Allen et al., 1998) or alfalfa (Wright and Jensen, 1978), and the specific crop coefficient (K_c), estimated from different tabulated information such as FAO56 Irrigation and Drainage Paper No. 56 (Allen et al., 1998). In this case, the daily or weekly volume of water evapotranspirated is estimated and used to schedule the irrigation in the next days or weeks (Pereira et al., 2009; Sun et al., 2006; Thompson et al., 2007). This method does

not provide the frequency and duration of irrigation (stakeholders do not know when to apply this volume of water) and requires accurate estimations of weather conditions.

Plant based methods include direct measurements of the plant water status as well as a number of plant processes that are known to depend on water deficits (Jones, 2004). Different types of measurements can be used to determine plant water and salt stress for irrigation scheduling. This includes photosynthetic capacity (de Lima et al., 2015; Flexas et al., 2004; Ribas-carbo et al., 2006), stomatal conductance (Flexas et al., 2004; Jones, 1999), leaf water potential (Alberola et al., 2008; Girona et al., 2006; Turner, 1990), and crop temperature (Bellvert et al., 2014; DeJonge et al., 2015; Kassie et al., 2018). In general, these methods only provide a direct measurement of the plant status without determining how much water is necessary. Moreover, these methods require sophisticated and calibrated devices (Jones, 2004).

Different sensors have been recently developed for the continuous measurement of water content, pressure head and EC with high precision and temporal resolution (Ferrarezi et al., 2015; Hanson et al., 1977). With these measurements it is possible to determine the Plant Available Water (PAW) (Denmead and Shaw, 1962) needed to estimate crop development and soil salinization for irrigation scheduling (Jones, 2004). These sensors are provided, for instance, by the METER and SENTEK Group, which assure an easy installation. The location and depth of the sensor may substantially affect the estimation of PAW, which strongly depends on soil heterogeneity and root distribution (see Chapter 2). Several authors have studied the optimal irrigation strategy in different field areas and crop types using sensors (Hoppula and Salo, 2007; Phene and Howell, 1984; Thompson et al., 2007). However, these results cannot be scaled to other crops and fields with different soil type and weather conditions.

Several algorithms for optimizing irrigation can be found in the literature. For instance, Soentoro et al. (2018) optimized irrigation by determining the cropping patterns and planting areas through linear programming. Ortega et al. (2004) and Martínez-Romero et al. (2017) proposed to determine irrigation by maximizing the gross margin through genetic algorithms. Finally, Noory et al. (2011) proposed a linear and a mixed-integer linear model for optimizing an irrigation water allocation and a multicrop planning problem that maximizes the total net benefit. None of these algorithms properly represent the water movement in the vadose zone.

Numerical models constitute an efficient tool for assessing irrigation scheduling (Linker et al., 2016; Ma et al., 2015). Among the different models available, HYDRUS (Šimůnek et al., 2016, 2008) is often used to simulate water fluxes, root water uptake, root growth, and

solute and head transport in the vadose zone. Several researchers have used HYDRUS for simulating water content, soil suction and EC to improve irrigation scheduling or to provide some information to stakeholder. For instance, Arbat et al. (2008) simulated soil suction with HYDRUS in order to demonstrate that this model is capable to assess irrigation scheduling in a given field site. Results cannot be directly extrapolated to other field conditions. Siyal and Skaggs, (2009) and Skaggs et al. (2010) simulated water content distribution patterns during drip irrigation. The water balance components were not analyzed in this study to ultimately define an optimal irrigation strategy. A different point of view was proposed by Twarakavi et al. (2009), who defined the field capacity point by simulating the drainage process with HYDRUS. These authors found that the field capacity point controls the irrigation schedule strategy but important variables such as the transpiration were not considered. The role of transpiration was latter on studied by Dabach et al. (2013), who analyzed different irrigations scheduling strategies through numerical simulations. However, in this case, irrigation scheduling was not chosen to maximize the net profit. From this, we see that it does not exist a scalable methodology to define an optimal irrigation scheduling strategy that links the water balance components with the crop yield and economical profit.

In this chapter, we present a combined simulation and optimization framework aimed at obtaining the irrigation scheduling parameters which maximizes crop yield with minimum applied water while guaranteeing maximum net profit without soil salinization. The methodology accounts also for the water movement in the unsaturated zone and can be easily exported to any field site, making it applicable to any kind of agricultural field, weather conditions, soils and crops. The chapter is organized as it follows. We first present the formulation of the optimization framework in section 3.2. Then, we applied the method to a specific field site in section 3.3. To do this, we set up a numerical model to simulate flow and transport through the vadose zone at the field site. The model is shown capable to simulate water content data recorded at different depths over one year. After this, we optimize the irrigation problem and we discuss the results in section 3.4. The optimal irrigation solution is compared against traditional methods in this section. Finally, in section 3.5, we used the proposed framework to analyze the impact of soil properties on irrigation scheduling.

3.2. Combined simulation – optimization framework

3.2.1. Optimization problem

A short-term irrigation optimization problem is formally presented here. The framework permits to find the optimal control settings of an irrigated field that maximize the net profit obtained in a short period of time T assuming minimum fluctuations and discounting in the water price. A short period of time refers for instance to the duration of a crop growing season. Let us consider that the schedule of irrigation depends on a vector of control variables $\mathbf{p}$ that characterize the irrigation rate $q_i(\mathbf{p}, t)$. The components of this vector can include for instance the pressure head threshold (h^*), which indicates the degree to which the soil can dry before irrigation is applied, and the duration of irrigation (τ) among others. The optimal irrigation scheduling strategy characterized by $\mathbf{p}$ (Eq. 3.1) is defined here as the one that is most productive and sustainable, which is mathematically formulated as the problem of finding the set of control variables $\mathbf{p}$ that maximizes the crop Net Margin (NM) cost Eq. (3.2) subject to operational and functional constraints. The NM cost is the revenue from crop production, i.e., the Gain Margin *(GM)* Eq. (3.3) subtracted by the cost of crop production during an operational time $t = T$. The cost of crop production consists of two main parts: capital costs and operation costs. Capital costs ($Capex$) Eq. (3.4) are the one-time expenses that usually incur during the purchase of land and equipment, i.e., expenses for bringing the irrigation field to an operable status. This includes the construction and installation of physical facilities such as the watering system, access roads, pipelines, drilling of wells and so on. Operation costs ($Opex$) Eq. (3.5) refers to the cost of specific activities incurred during the crop field lifecycle, which include equipment maintenance, product transport and overheads. From this, the optimization problem is mathematically formulated as

$$\mathbf{p}_{opt} = \max_{\mathbf{p}} NM(\mathbf{p}, T), \tag{3.1}$$

where,

$$NM(\mathbf{p}, T) = GM(\mathbf{p}, T) - Opex(\mathbf{p}, T) - Capex, \tag{3.2}$$

$$GM(\mathbf{p}, T) = Y_a(\mathbf{p}, T)\, C_y, \tag{3.3}$$

$$Capex = C_m + C_c\,, \tag{3.4}$$

$$Opex(\mathbf{p},T) = C_{Fix} + \int_0^T q_i(\mathbf{p},t')\,(C_{wVar} + C_e)\,dt', \tag{3.5}$$

The GM [€·ha^{-1}] is described here as the product between harvest price C_y [€·ha^{-1}] and the actual crop yield Y_a [t·ha^{-1}], C_{Fix} [€·ha^{-1}] is the water fixed cost, C_{wVar} [€·m^{-3}] is the water variable cost, C_e [€·ha^{-1}] is the energy cost, C_m [€·ha^{-1}] is the irrigation system maintenance cost, and C_c [€·ha^{-1}] is the capital cost.

In practice, irrigation control settings must satisfy also some operational constraints. The constraints can include limitations on irrigation parameters as well as limitations on leaching water quality (solute concentrations). These features are incorporated into the optimization problem by constraining the solution to practical limitations and requirements, formally written as

$$\mathbf{p_1} \leq \mathbf{p} \leq \mathbf{p_2} \tag{3.6}$$

$$g(\boldsymbol{c}) \leq \boldsymbol{a} \tag{3.7}$$

The first set of constraints Eq. (3.6) refers to practical issues such as those determined from the water system capacity installed. Here, we only set an upper and a lower bound of $\mathbf{p}$ to represent this. The other constraints Eq. (3.7) refer to solute concentrations, which can be used to limit for instance soil salinization. Note though that this methodology is not affected by the removal or the modification of the constraints included.

Solving this optimization problem results in the selection of optimal irrigation parameters. The solution will identify the maximum profitable solution subject to sustainable and feasible constraints. However, the simulation of crop yields requires two simulation components, one that simulates the distribution of water in the vadose zone as a result of irrigation and environmental conditions, and another that relates soil water content and water availability with crop yields. These two components are discussed in the following sections.

3.2.2. Flow and transport model

The simulation of water availability requires a numerical model capable to predict the flow of water in the unsaturated zone. The unsaturated flow is typically described by Richards' equation (Richards, 1931) Eq. (3.8), which can be written as

$$\frac{\partial \theta}{\partial t} = \nabla \cdot [K(h)\nabla h + K(h)\nabla z] - S, \tag{3.8}$$

where θ [-] is the volumetric water content, h [-] is the water pressure head, t is time, S [T^{-1}] is the source-sink term (includes root water uptake), and K [LT^{-1}] is the unsaturated hydraulic conductivity. Solving this partial differential equation requires the knowledge of the Soil Water Retention Curve (SWRC), which is the relationship between the water content and the pressure head, and the Hydraulic Conductivity Curve (HCC), which is the relationship between the hydraulic conductivity and the pressure head. These curves are characteristic for different types of soils.

The solution of Richards' equation requires also the knowledge of initial and boundary conditions. For our purposes, the boundary condition specified at the soil surface plays an important role as it defines the amount of water infiltrated into the soil during irrigation. The water flux across the soil surface depends on both external conditions such as irrigation water rates $q_i(\mathbf{p}, t)$ and the water content conditions in the soil. The corresponding boundary condition should represent for instance that run-off occurs when an irrigation rate exceeds the infiltration capacity of the soil or the fact that evaporation cannot exceed the capacity of the soil to deliver enough water to the soil surface. Solving Eq. (3.8) subject to a system-dependent boundary condition that limits the surface flux by the following two conditions (Eqs. 3.9 and 3.10) is often used to incorporate these features (Feddes et al., 1974; Neuman et al., 1974),

$$\left|q(z_{top}, t)\right| \leq |X(t)|, \tag{3.9}$$

$$h_d \leq h \leq h_s, \tag{3.10}$$

here $q(z_{top}, t)$ is the water flux at the soil top surface, z_{top} is the z-coordinate of the soil top surface, $X(t)$ is the prescribed maximum potential rate of infiltration or evaporation given by meteorological conditions [LT^{-1}], and h_d and h_s refer to dry and saturated water pressure heads, respectively. During evaporation, $X(t) > 0$ and this value represents the maximum evaporation rate E_p.

The numerical model should also describe the water extraction by plant roots. In this context, the root water uptake $S(h, h_\Phi, z, t)$ Eq. (3.11) is typically determined by the product of the water and salinity stress function $\alpha(h, h_\Phi)$, the root density distribution function $\beta(z, t)$ in the vertical direction, and the potential transpiration $T_p(t)$,

$$S(h, h_{\Phi}, z, t) = \alpha\left(h, h_{\Phi,}\right) \beta(z, t)\, T_p(t), \tag{3.11}$$

where h_{Φ} is the osmotic pressure head. Several stress models can be found in the literature. Among them, the model presented by Feddes et al. (1978) and van Genuchten (1987) are the most widely used. Essentially, the latter model considers a smooth monotonic function with maximum root uptake at saturated conditions, while the other represents a piecewise linear function with maximum uptake within a pressure (saturation) interval. Importantly, only the formulation presented by Feddes considers a transpiration reduction near saturation. Assuming an isothermal system, the osmotic pressure head depends only on the solute concentrations of the chemical compounds in water, i.e., $h_{\Phi} = F(c_i)$. This relationship is often determined based on empirical relationships.

The simulation of solute concentrations is needed for two reasons: to evaluate constraints in concentrations (prevent soil salinization) and to estimate osmotic pressures. Solute transport in the unsaturated zone is typically described by the advection-dispersion equation Eq. (3.12), which is written as,

$$\frac{\partial(R\theta c_i)}{\partial t} = -\nabla \cdot (\boldsymbol{q} c_i) + \nabla \cdot (\theta \mathbf{D} \nabla c_i) + f_i, \quad i = 1, \ldots, N_s \tag{3.12}$$

where c_i is the solute concentration of the i-th chemical component, $\boldsymbol{q}$ is the Darcy flux, $\mathbf{D}$ is the hydrodynamic dispersion tensor, N_s is the number of chemical components considered, and f_i is the concentration source-sink term.

3.2.3. Soil – water – crop productivity relationship

An estimation of the crop yield is required to evaluate the revenue from crop production during optimization. Crop productivity models can be complex as they include the interaction between genetics, physiology and environmental conditions such as water content. To facilitate the estimation procedure, one often considers an empirical model that relates crop water needs to crop yields. The model presented by Stewart et al. (1977) Eq. (3.13) has been widely accepted and recommended by the Food and Agriculture Organization of the United Nations (FAO) (Doorenbos and Pruitt, 1975, hereafter FAO24). This model represents the seasonal pattern of crop water needs by different growing stages (four in the case of maize). The potential crop yield is penalized at each growth stage depending on the deficit of water, which is estimated by the relative discrepancy between potential (maximum) and actual evapotranspiration. The model determines that

$$Y_a = Y_p \prod_{\mathrm{k}=1}^{\mathrm{N_y}} \left(1 - K_{y_k}\left(1 - \left(\frac{ET_a}{ET_c}\right)_{\mathrm{k}}\right)\right) \tag{3.13}$$

where Y_p [t·ha^{-1}] is the potential crop Yield for the total growing season, k is the growing stage index, $\mathrm{N_y}$ is the number of growing stages, and K_{y_k} [-] is the crop yield response factor associated with the k-th growing stage. ET_a and ET_c are the actual and potential accumulated crop evapotranspiration in each growing stage k [mm]. Note that the crop is under stress conditions when $ET_a/ET_c < 1$.

At each growing stage, according to Allen et al. (1998) the potential evapotranspiration ET_c Eq. (3.14) is estimated by the crop coefficient K_c and the reference evapotranspiration ET_0. The latter can be calculated by the Penman-Monteith equation (Allen et al., 1998), which is a function of the input daily mean temperature, the wind speed, the relative humidity and the solar radiation.

$$ET_c = K_c\, ET_0\,, \tag{3.14}$$

The actual evapotranspiration is estimated from the simulation of flow in the vadose zone, which gives the evaporation at the soil surface and the water uptake by plant roots $S(h, h_\Phi, z, t)$. From this, the ET_a Eq. (3.15) of the k-th growing stage taking place in the time interval (t_k, t_{k+1}) can be determined by

$$ET_a = \int_{t_k}^{t_{k+1}} q\left(z_{top}, t'\right) I\left(q\left(z_{top}, t'\right) > 0\right) dt' + \int_{t_k}^{t_{k+1}} \int_{z_{top}-L_R}^{z_{top}} S(h, h_\Phi, z, t')\, dz\, dt' \tag{3.15}$$

where $I(q > 0)$ is an indicator function that is equal to one during evaporation ($q > 0$) and zero otherwise, z_{top} is the z-coordinate of the soil top surface, and L_R is the vertical length of the root zone.

3.3. Field application

3.3.1. Field site description

In this section we illustrate the applicability of the method in a real field setting. The study area considers the same commercial field exposed in chapter 2 (Foradada field) Fig.3.1. The irrigation method is fully covered with irrigation sprinkles, distributed with 23 different irrigation sectors. The irrigation rate is 6.5 L·m^{-2}·h^{-1}. Two sectors can be irrigated at the

same time during 24 h·d^{-1}. The soil texture can be classified as a Silty Clay Loam (USDA classification) with 28% Clay, 58.4% Silt and 13.6% Sand. Every year two different crops are grown: The first crop is usually canola and the growing season extends between winter and spring, during which wet conditions take place due to rainfall events. The second crop is always maize and takes place during the summer and autumn seasons, where wet conditions are maintained by applying periodic irrigation. Correct irrigation scheduling is needed to maximize productivity.

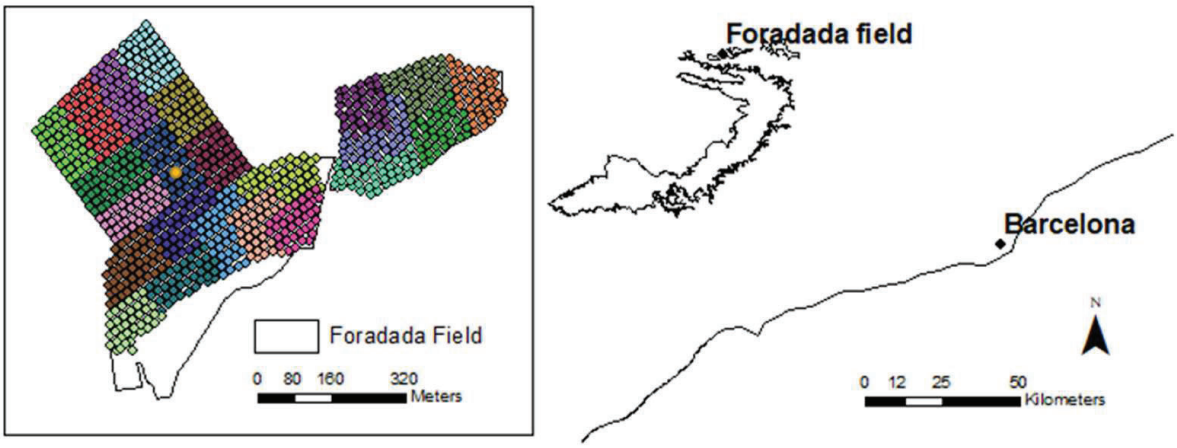

Figure 3.1. The Foradada field is located within the Aigües Segarra garrigues (ASG) canal. Solid irrigation sprinkle systems installed and distributed in 23 sectors are represented in different colors. Water content monitoring station and sampling is represented in yellow.

A field campaign was conducted to install water content sensors and collect undisturbed soil core samples. Two EC-5 soil moisture sensors (METER Group, Pullman, WA, USA) were installed at 10 and 20 cm depth in a representative location (Fig.3.1). Sensor data was collected every 5 minutes with an accuracy of ±0.03 cm3·cm^{-3} (Campbell and Devices, 1986). Two undisturbed soil samples were taken near the EC-5 sensors using a stainless-steel ring of 250 cm^3 capacity. These soil samples were used to measure the SWRC and HCC with high precision and over a wide range of pressures. This was achieved by combining the HYPROP, the WP4c, and the KSat devices (METER Group, Pullman, WA, USA). Whereas the HYPROP device is capable to measure SWRC and HCC, WP4c can complement SWRC in the dry region. The KSat system does the same for HCC. A comparison of approaches has been reported by Schelle et al. (2013). These authors demonstrated that this combined method shows less noise than the other traditional methods. The experimental data was fitted to the van Genuchten–Mualem SWRC model using the HYPROP Fit software (METER Group). Figure 3.2 shows SWRC and HCC measured by HYPROP, WP4c and KSat. Note that these devices provide SWRC and HCC with high resolution. SWRC describes a soil with a

quite high-water content retention capacity and a low air enter potential and slope. This is shown by the shape parameters α and n with values of 0.0678 and 1.186, respectively. HCC is characterized by a low K_s value with 12 cm·d^{-1}, indicating slow wetting front movement during irrigation.

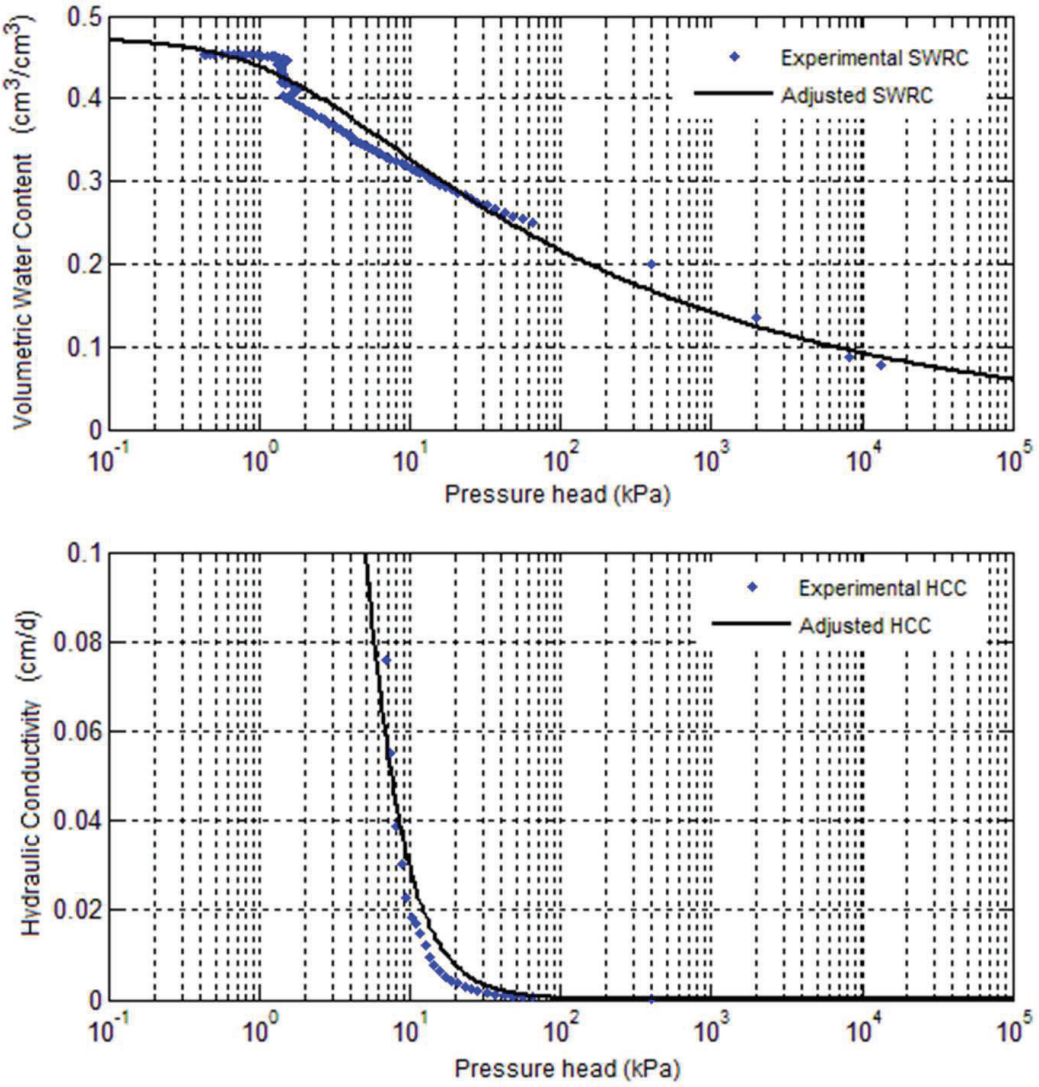

Figure 3.2. Soil Water retention Curve (SWRC) and Hydraulic Conductivity Curve (HCC) measured by HYPROP, WP4c and KSat systems and fitted by van Genuchten – Mualem model.

3.3.2. Model setup

We use the HYDRUS-1D software package (Šimůnek et al., 2016, 2008) for simulating the one-dimensional movement of water and solute transport in variably-saturated porous media at the field site. This code solves Richards' equation to simulate water flow in the unsaturated zone and the advection-dispersion equation to simulate solute transport using numerical methods based on the Galerkin finite element method. We consider a 60 cm

vertical soil profile representative of the Foradada field site. The domain was discretized into 101 segment elements. The column represents the movement of water through the soil profile associated with the water content sensors and core samples. A system-dependent boundary condition was imposed at the soil top surface according to Eqs. (3.9) and(3.10). Since the water table is far below, a free drainage boundary condition was imposed at the column bottom, i.e., $q = -K(h)$. Initial conditions were set to $\theta = 0.25$. A multiplicative model was used to represent the water and salinity stress function, i.e., $\alpha(h, h_\Phi) = \alpha(h)\alpha(h_\Phi)$, where $\alpha(h)$ and $\alpha(h_\Phi)$ are the water and salinity stress functions, respectively. The Feddes et al. (1978) Eq. (3.16) model is used to represent the water stress function,

$$\alpha(h) = \begin{cases} \dfrac{h - h_4}{h_3 - h_4} & h_3 > h > h_4 \\ 1 & h_2 \geq h \geq h_3 \\ \dfrac{h - h_1}{h_2 - h_1} & h_1 > h > h_2 \\ 0 & h \leq h_4 \; or \; h \geq h_1 \end{cases}, \tag{3.16}$$

which describes that the plant suffers water stress outside the pressure head range (h_2, h_3). The water stress reduction decreases linearly from those pressure points and gets to a minimum ($\alpha = 0$) below or above h_4 and h_1. The salinity stress function is defined using the threshold-slope salinity stress reduction function (Maas and Hoffman, 1977) Eq. (3.17),

$$\alpha(h_\Phi) = \begin{cases} 1, & a \leq h_\Phi \leq 0 \\ 1 + b\left(h_\phi - a\right), & a > h_\Phi > -\dfrac{1}{b} \\ 0, & h_\Phi \leq a - \dfrac{1}{b} \end{cases}, \tag{3.17}$$

Here, the salinity threshold value a quantifies the minimum osmotic head above which root water uptake occurs without reduction, and the slope b determines the fractional root water uptake decline per unit increase in salinity below the threshold. The parameters adopted to define these stress functions were chosen from the HYDRUS internal database and are summarized in Table 3.1. The transport model is simplified to simulate only one representative chemical component, i.e., Electrical Conductivity EC, which is assumed to behave as a conservative species (non-reactive). We neglect salt precipitation and dissolution processes. The osmotic pressure is assumed to be proportional to EC by the expression $EC = 1h_\phi$ (Simunek and Sejna, 2014).

Table 2.1. Water and salinity stress function parameters.

Feddes Function (water stress)			Mass and Hoffman (salinity stress)		
h_1	1.5	kPa	a	3.4	dS/m
h_2	3.0	kPa	b	6	-
h_3	32.5 – 600.0	kPa			
h_4	800.0	kPa			

An initial estimation of model properties (e.g., SWRC and HCC) was known from core sample measurements. The model parameters were then calibrated to reproduce the recorded soil moisture data obtained at the field site. The calibrated parameters were not significantly different from the initial estimation. Table 3.2 summarizes the measured and calibrated parameters. Parameters modified in the calibration process were α and n. The simulation considered 240 days, from February 9th 2017 to October 31st 2017. Two different crops growing at different periods of time were accounted for during the simulation; canola from February, 9th 2017 to May, 31st 2017, and maize from June, 1st 2017 to October, 31st 2017. Meteorological parameters were downloaded from the nearest available weather station to compute ET_0, which was then converted into daily ET_c values with the K_c coefficients shown in Table 3.3. The potential evaporation and transpiration values needed in the root water uptake model, Eqs (3.9) and (3.11), were calculated by partitioning ET_c into potential evaporation E_p and transpiration T_p based on the Canopy Cover (Raes et al., 2010), which determines that $ET_c = \alpha E_p + (1 - \alpha)T_p$, being α the soil cover fraction. Figure 3.4 compares simulation results with water content field measurements obtained at two different depths. Simulations are in good agreement with soil moisture data. Table 3.4 shows several goodness-of-fit statistics calculated for both depths.

Table 3.2. Foradada and Loamy Sand Soil hydraulic parameters used in simulations. θ_r, is the residual volumetric water content; θ_s, is the saturated volumetric water content; α, n and i the are shape parameters, and K_s is the saturated hydraulic conductivity.

Location	Soil	θ_r ($cm^3 \cdot cm^{-3}$)	θ_s ($cm^3 \cdot cm^{-3}$)	α ($1 \cdot h^{-1}$)	n (-)	K_s ($cm \cdot d^{-1}$)	i (-)
Foradada soil	Measured	0.012	0.473	0.0421	1.157	12	0.5
	Calibrated	0.012	0.473	0.0678	1.186	12	0.5
Theoretical soil	Loamy Sand	0.05	0.41	0.124	2.28	350	0.5

Table 3.3. Canola crop coefficient (K_{c1}), maize crop coefficients (K_{c2}) applied for ET_c, where Stage I represents the initial period; Stage II is crop development; Stage III mid-season; Stage IV is late season. Crop yield response factor (K_y) used for actual Yield estimations, where Stage I is vegetative period, Stage II is flowering period, Stage III the yield formation, and Stage IV ripening.

Stage	I	II	III	IV
K_{c1}	0.2	0.7	1.15	0.2
K_{c2}	0.3	0.3 – 1.1	1.1	1.10 – 0.55
K_y	0.35	1.05	0.4	0.2

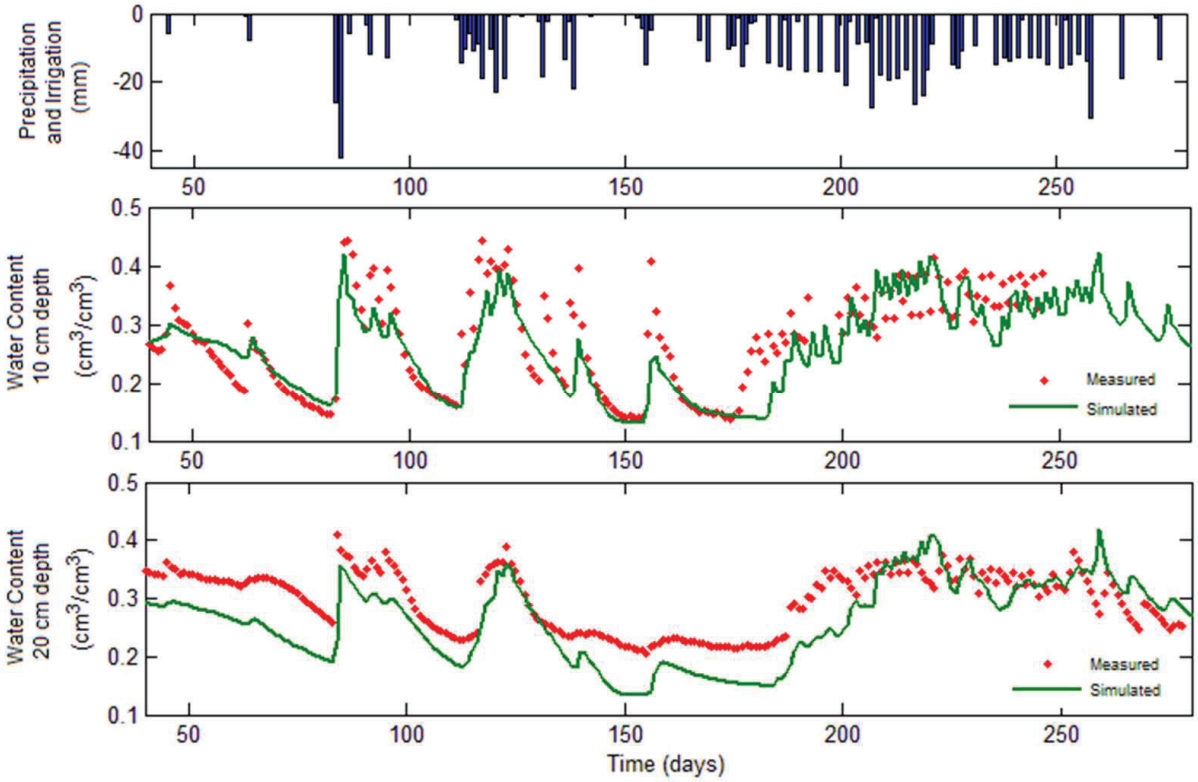

Figure 3.3. Comparison between daily soil moisture field measurements and the soil moisture output from the validation model at 10 and 20 cm depth.

Table 3.4. Statistical index calculated with observed and simulated water content values.

Observation Point	RMSE	Willomtt Index	R^2
θ 10 cm Depth	0.12	0.89	0.61
θ 20 cm Depth	0.08	0.96	0.60

3.3.3. Optimal irrigation scheduling problem setup

We applied the simulation-optimization framework presented in section 3.2 to the Foradada field site to estimate optimal irrigation scheduling parameters during a growing season with unfavorable weather conditions. The methods and parameters used here were directly adopted from the previous calibrated model. However, weather conditions were considered to represent the growing season with the highest ET_c values estimated between 2008 and 2017. The corresponding K_c coefficients are presented in Table 3.3. The year with more water demand was 2016. Rainfall events were neglected. Initial conditions were $\theta = 0.25$ and EC = 0.6 dS/m, which represents an average water content of the field site without salinity problems. Simulations considered the entire growing season of maize, from June 15th (sowing) to November 11th (harvesting). Data necessary to evaluate the crop net margin cost NM is summarized in Table 3.5, mostly provided by the Aigües Segarra Garrigues (ASG) company.

Table 3.5. Parameters necessary to apply Stewart and Net Margin (NM) equations. Y_p is the potential crop yield; C_y is the harvest price; C_m, is the maintenance cost; C_c, are the capital costs; C_{Fix}, is the fix water cost; C_{wVar}, is the variable water cost; C_e, is the energy cost; q_i, is the irrigation rate.

Parameter	Value		Reference
Y_p	19.5	t·ha^{-1}	Martínez-Romero et al. (2017)
C_y	171.8	€·t^{-1}	www.mapama.gob.es
C_m	No data available	€·ha^{-1}	-
C_c	No data available	€·ha^{-1}	-
C_{Fix}	115.35	€·ha^{-1}	Aigües Segarra Garrigues
C_{wVar}	0.1003	€·m^{-3}	Aigües Segarra Garrigues
C_e	No data available	€·m^{-3}	-
q_i	6.5	l·m^{-2}·h^{-1}	Aigües Segarra Garrigues

Two control irrigation parameters were used to characterize water irrigation rates, i.e., the pressure head threshold h^* observed at a control point and the duration of irrigation τ. The control point is located at the vertical midpoint of the maximum maize root length (20 cm below soil surface). The pressure head at the control point triggers irrigation when $h < h^*$ (when the soil is dry). At this moment, the model applies water at a constant irrigation rate q_i for an irrigation time τ. Since the watering capacity is fixed by the type of irrigation equipment installed, the irrigation rate is not considered to be a control parameter in this case (q_i is set constant to 6.5 L·m^{-2}·h^{-1}). Figure 3.4 presents an illustrative sketch of the

irrigation. The salt concentration in the irrigated water is assumed to have electrical conductivity values of 0.4 dS/m. The optimization is constraint to fulfill that $EC_e < 3.4$ dS/m (below this threshold maize is not under salinity stress).

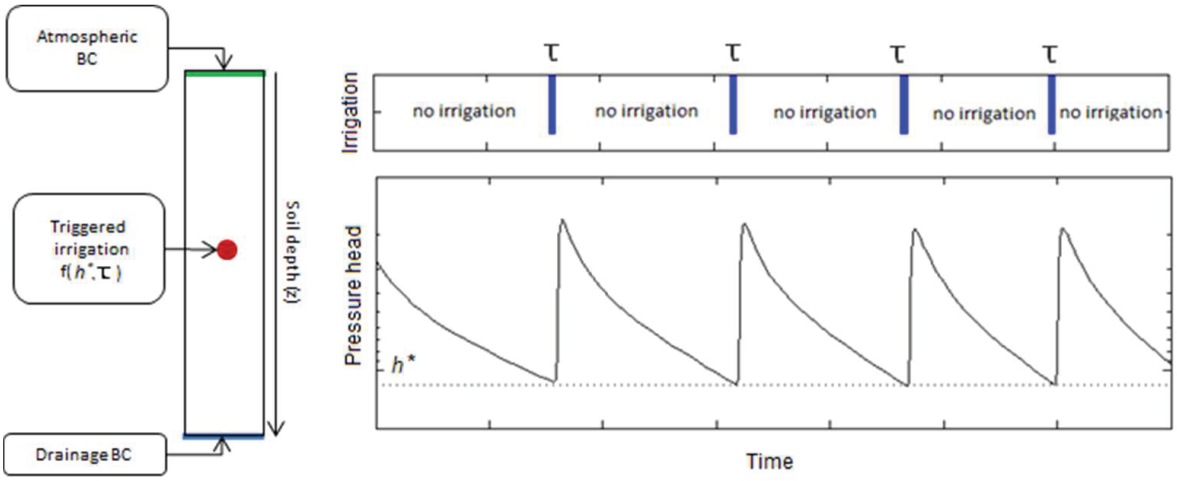

Figure 3.4. On the right, boundary conditions imposed in the model where triggered irrigation is a function of h^* and τ. On the left, a synthetic case about how the model triggers the irrigation, when h^* and τ are defined.

A large number of algorithms can be used to maximize the crop net margin cost function NM with constraints. Here, we chose to maximize NM over a given range by brute force, which simply consists in computing the function's value at each point of the parameter space to find the global maximum. This can be inefficient in practical applications but provides detail insights about irrigation scheduling as well as the full shape of the NM cost function, which is the objective here. To do this, the parameter space (τ, h^*) was discretized into a 4×10 regular mesh, where τ ranges between 1 and 4 hours and the threshold pressure head h^* varies between -100 KPa and -10 KPa.

In order to analyze the performance of the method, we compared the optimal irrigation results obtained with our proposed framework with those given by a traditional irrigation method. The traditional irrigation scheduling method is based on water requirements and consists in irrigating as much water as that evapotranspirated in the previous week. To this end, the farmer must devise an irrigation calendar. Thus, to reproduce the traditional method, the weekly ET_c value is calculated and this volume of water is applied over the next week. This amount of water is uniformly distributed over the next week. All other parameters are kept the same. The relative difference between the Net Margin obtained with the traditional method (NM_{trad}) and the optimal one is computed as follows (3.18)

$$\Delta_r NM = \frac{NM - NM_{trad}}{NM}, \tag{3.18}$$

3.4. Simulation – optimization results

In this section, we present the simulation-optimization results of the Foradada irrigation scheduling problem. Figure 3.5a shows a map of the net margin NM function obtained from all the irrigation strategies simulated as a function of h^* and τ. A clear NM maximum value of 2791 €·ha^{-1} can be seen in this figure for τ = 1 h and h^*= -40 kPa. This optimal irrigation strategy represents a short but moderately frequent irrigation, i.e., moderate h^* value, which results from balancing the gain margin GM with the operational expenses $Opex$. The corresponding maps of GM and $Opex$ are also depicted in Fig. 3.5b and Fig. 3.5c, respectively. The maximum gain requires a more frequent irrigation with τ = 1 h and h^*= -25 kPa (more irrigated water) but the operational expenses significantly increase in this region. Thus, even though this is the most productive strategy, $Opex$ penalizes economically GM and, consequently, NM decreases. Thus, although this irrigation strategy could be the most productive in crop yield terms, the required volume of water and expenses related can substantially affect the optimal irrigation strategy. On the contrary, $Opex$ is minimum when the frequency of irrigation is very small, implying that less water is used for irrigation. Figure 3.5d shows the relative difference between the traditional method and the optimal solution obtained with the proposed methodology. Results show that the proposed method can increase the net margin by 7%. We also note that the NM function can give smaller values than the traditional one when either irrigations strategies apply a large volume of water (increasing $Opex$) or when h^* is too small (decrease in GM). This situation is far away from the optimal irrigation strategy and thereby the simulation-optimization method seems mandatory in routine field applications.

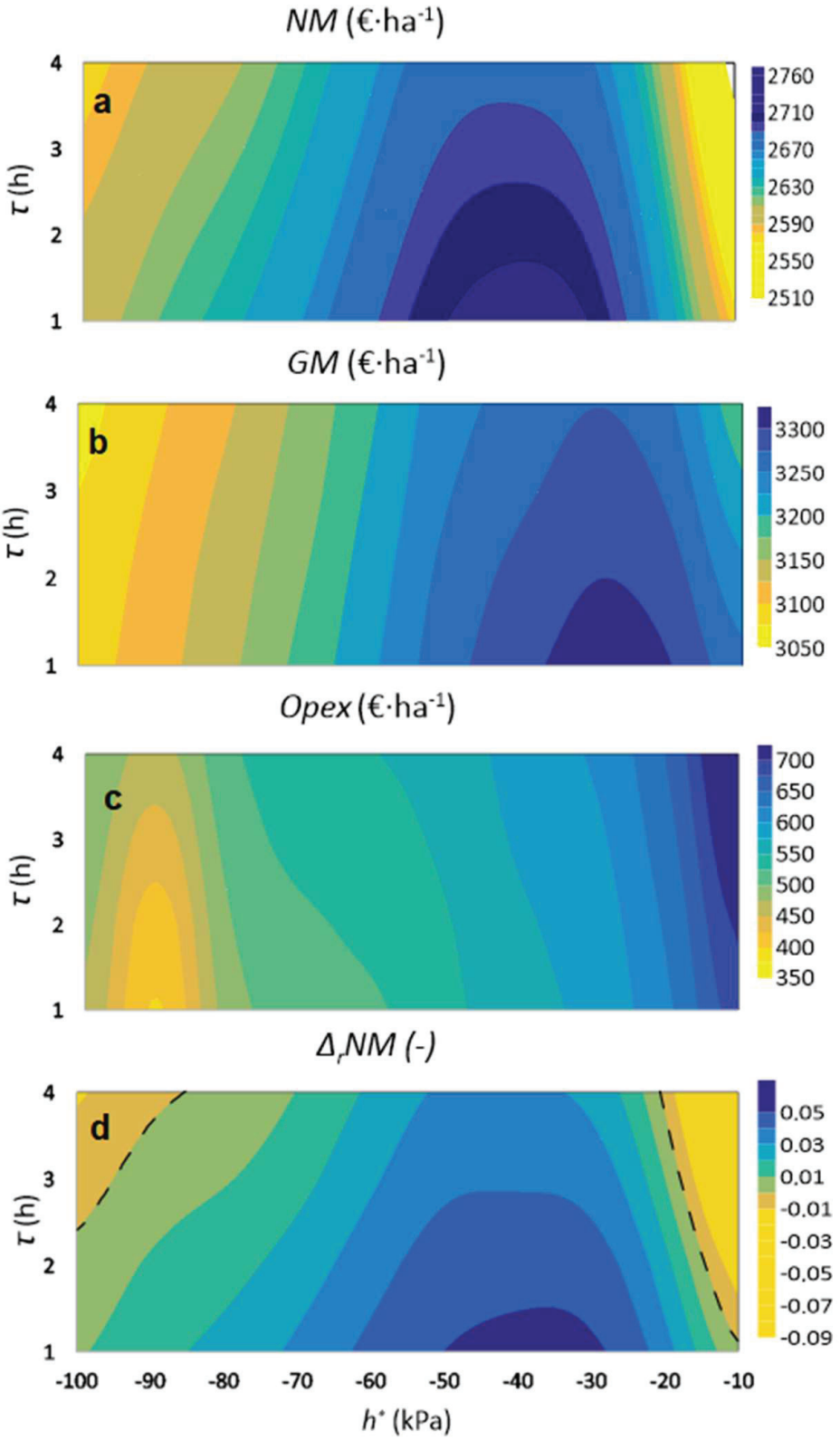

Figure 3.5 a) Net Margin (NM) Foradada soil results and objective functions elements, being b) GM, Gain Margin; c) $Opex$, Operational costs and d) $\Delta_r NM$, fractional difference between NM and NM_{trad}. Dash line in $\Delta_r NM$ map represents when the relative increment is zero.

A more profound understanding of the difference between the traditional irrigation scheme and the optimal irrigation method (τ = 1 h and h^* = -40 kPa) can be seen from Fig. 3.6, which compares the temporal evolution of the water content resulting from both methods at 4 different soil depths during the growing season. The optimal irrigation strategy applies water for 1 hour during several days and stops when h^* approaches -40 kPa. The traditional method applies water every day. The main difference is that the optimal solution provides a more uniform variation of the water content over the entire season, i.e., oscillates between 0.20 and 0.32 $cm^3 \cdot cm^{-3}$, compared with the traditional method, which fluctuates between 0.16 and 0.34. Moreover, the optimal method is capable to increase the water content globally in the root zone, in particular at 10 cm depth, whereas the traditional method stresses the system during periods with higher ET_c demand by letting the water content to decrease up to 0.16 $cm^3 \cdot cm^{-3}$. This water stress affects crop productivity because water content conditions are not optimal. We also note that when the volume of water applied is less than 5 $mm \cdot d^{-1}$, the wetting front does not arrive to the deeper soil parts, compromising root water uptake. This way, even though the traditional method applies the total volume of water evapotranspired during the growing season, this is not enough to maintain a more constant the water content during the growing season.

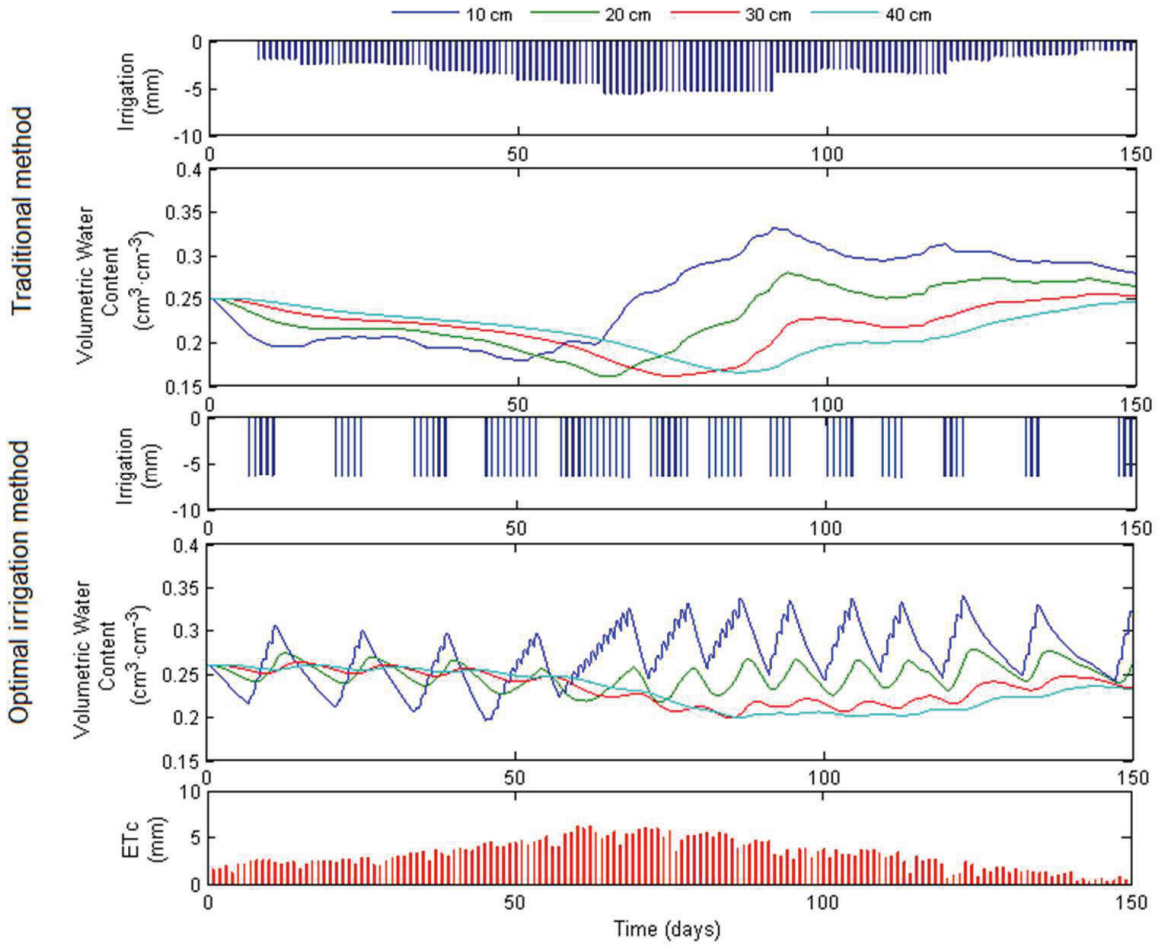

Figure 3.6. Irrigation scheduling from both strategies, where irrigation, volumetric water content dynamics at different depths and the potential evapotranspiration demand (ET_c) are plotted.

To better understand the results, Fig. 3.7 describes the impact that each irrigation strategy produces on T_a, E_a and soil EC_e. The optimal strategy is highlighted in these figures with a black circle. Figure 3.7a presents the simulated transpiration values obtained as a function of h^* and τ. Remarkably, the optimal irrigation strategy is not the one that produces more transpiration but lies within the plant water stress region, i.e., $\alpha(h^*)$ is smaller but close to 1. This means that the gain in crop productivity obtained for $\alpha = 1$ does not compensate the expenses associated with the increase in irrigated water. Results also show a decrease in transpiration when irrigation applies water during several hours. This is caused by the saturation of the top horizon of the soil (see Fig. 3.8).

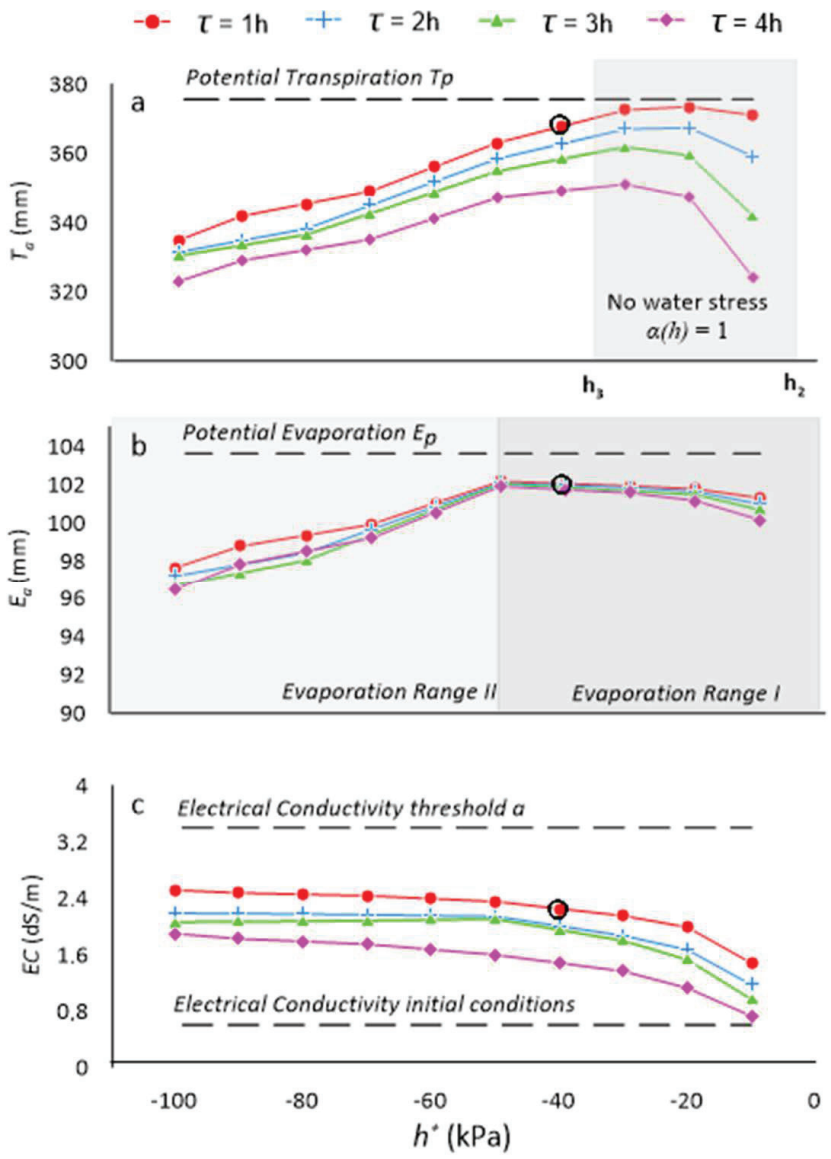

Figure 3.7. a) Actual Transpiration (T_a), b) actual Evapotranspiration (E_a) and c) Electrical Conductivity at the root zone (EC) resulting from Foradada soil showing all the irrigation strategies simulated. Circles show the strategy who provides maximum Net Margin (NM).

Figure 3.7b plots the corresponding evaporation values. According to Philip (1956) and Ritchie (1972), we distinguish between two evaporation regions: Range I represents an energy-limited evaporation process where the soil surface is wetted by irrigation and water evaporates from a thin soil surface layer; Range II represents a falling-rate evaporation process that occurs when water content flows from the soil layer below. Results show that the optimal irrigation strategy is energy-limited because the Foradada soil has a high-water content retention capacity.

Figure 3.7c presents the simulated EC_e values at the end of the season as a function of h^* and τ. They are the average from the four observation points inserted at different depths. Even though none of the irrigation strategies exhibit salinity stress (above threshold) an increase in EC is seen in all simulations. Consequently, salts are accumulated through the root zone presenting a maximum at the end of the season. This is more pronounced for small h^* values. This increase could significantly affect the crop productivity in the following seasons and reflects the importance of rainfall events in wet periods (spring and summer). This volume of water should be responsible for flushing out the salts accumulated during dry periods. Our simulated scenarios considered only dry conditions without rainfall events and thereby this flushing mechanism could not be seen.

Figure 3.8 displays the wetting front resulting from different irrigation events for 4 different irrigation strategies. One can observe that when water is applied over several hours (i.e., more that indicated by the optimal irrigation strategy), the top horizon of the soil becomes almost saturated and thereby water uptake is negligible in this region (pressure head overpasses the h_2 threshold). This prolonged saturation of the top soil horizon due to poor drainage inhibits crop productivity. This is in turn reflected by smaller T_a values in Fig. 3.7a.

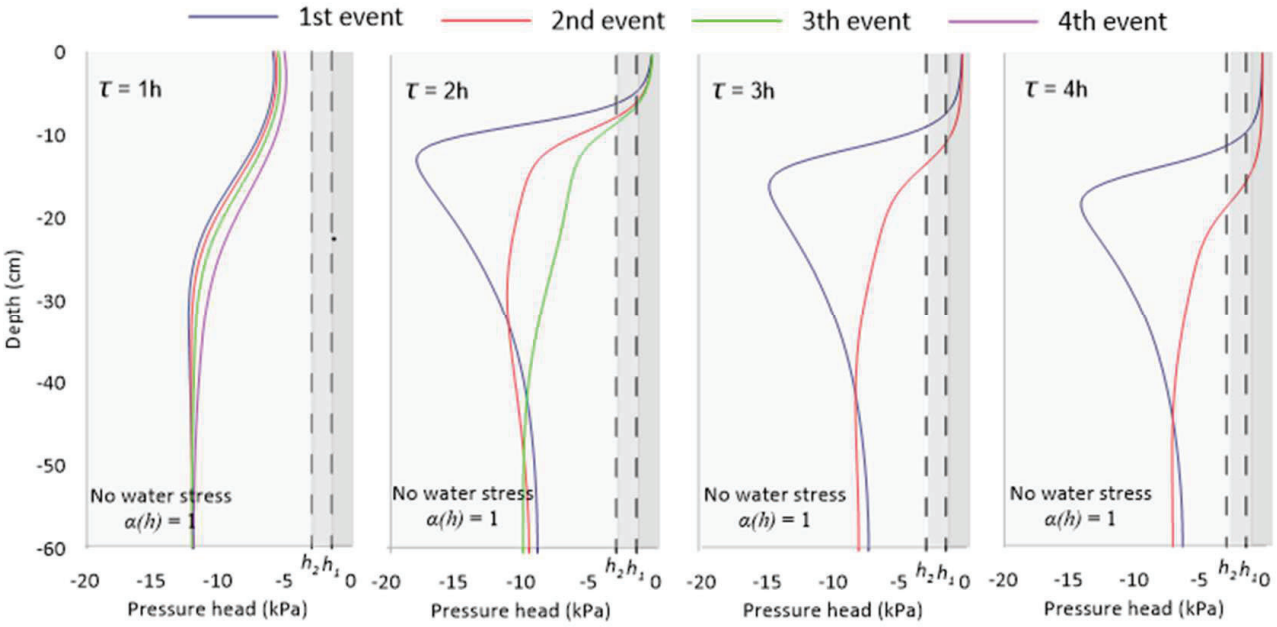

Figure 3.8. Wetting patterns when irrigation strategy is fixed at τ = 1, 2, 3, 4 h and h^* = 10 kPa. Some water stress function parameters (h_1 and h_2) are plotted indicating when transpiration decreases as a consequence of water logging.

3.4.1. Impact of soil hydraulic properties on the optimal irrigation strategy

In order to evaluate the impact that soil hydraulic properties have on the optimal irrigation strategy, we also solved the optimization-simulation problem considering a different soil type. The chosen soil hydraulic properties have been downloaded from the Rosetta database (Schaap et al., 2001) available from HYDRUS 1D. Table 2 shows the soil hydraulic parameters of a Loamy Sand soil. In this specific case, α and n parameters represent a soil with less soil moisture retention capacity than the Foradada soil, and K_s is substantially higher than the soil previously studied ($K_s = 350$ cm·d^{-1}). Taking these observations into account, a lower soil moisture retention with a faster wetting front movement is expected. Figure 3.9 shows the map of the NM, GM, and $Opex$ function depending on h^* and τ. The linear-like shape of these functions are strikingly different from those of Foradada, which exhibited a strong nonlinear behavior close to the optimal value. Consequently, results show that in this case h^* is mostly controlling NM and τ has little effect. An optimal irrigation strategy is found for τ = 1 h and h^*= -10 kPa. The maximum NM value is 2719 €·ha^{-1}, which is slightly smaller than that of the Foradada soil of 2719 €·ha^{-1}. This irrigation strategy represents a short but very frequent irrigation. We conclude then that the optimal irrigation strategy can drastically change from one soil type to another.

The physical process by which the NM function associated with a Loamy Sand soil is now mostly controlled by the pressure head threshold h^* and not τ can be seen from the dependence of T_a, E_a, and EC_e with h^* shown in Fig. 3.10. Note that in all cases these results are substantially different than those of the Foradada soil (Fig. 3.7). In this case, results indicate that the irrigation water can easily infiltrate and redistribute through the entire root zone, following a falling-rate evaporation process. In contrast to our previous results, a more permeable soil leads to an optimal irrigation strategy (black circle) that favors maximum transpiration rates with zero plant water stress. The optimal strategy also inhibits waterlogging and provides minimum salinization compared to other irrigation strategies obtained with different pressure head thresholds (Fig. 3.10c). Again, this can be explained by an effective percolation of water through the root zone, which gives good internal drainage.

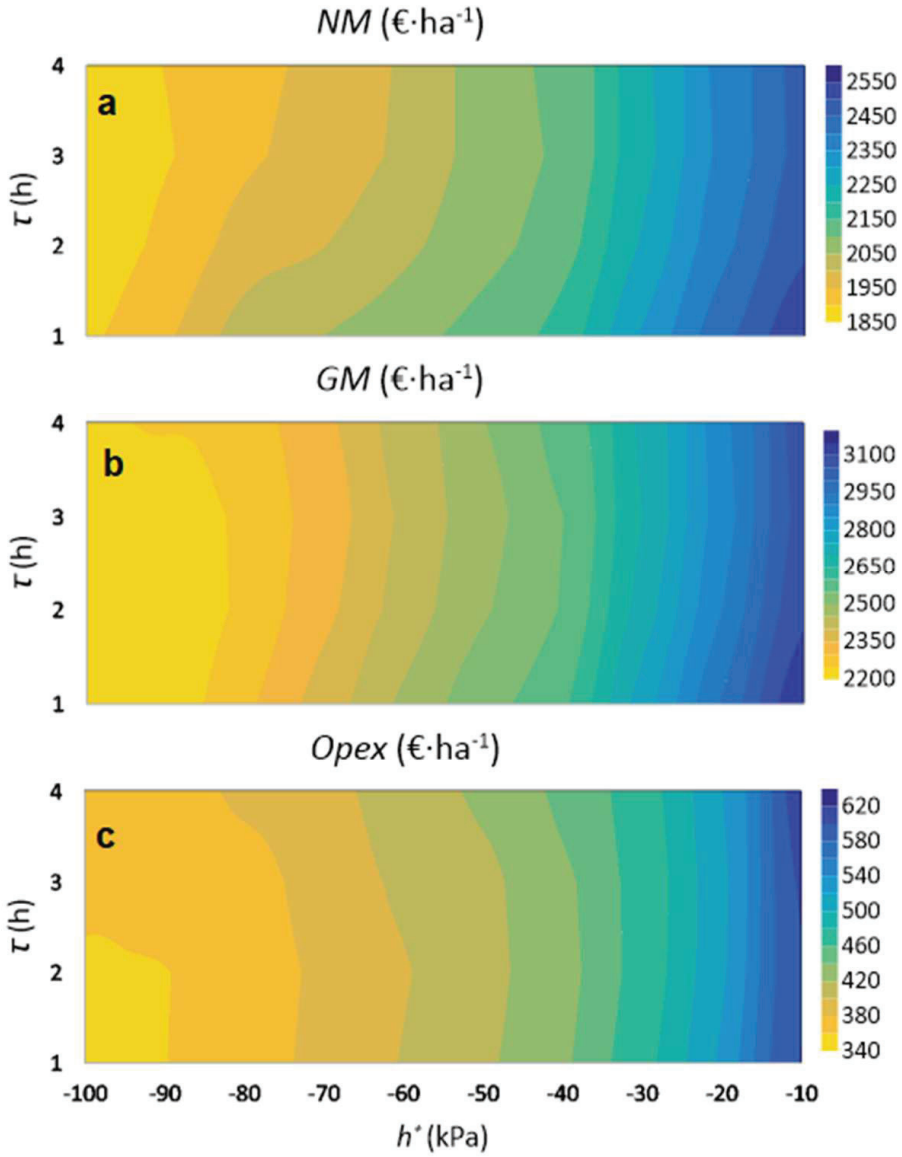

Figure 3.9. a) Net Margin (*NM*) Loamy sand soil results and objective functions elements, being b) *GM*, Gain Margin and c) *Opex*, Operational costs.

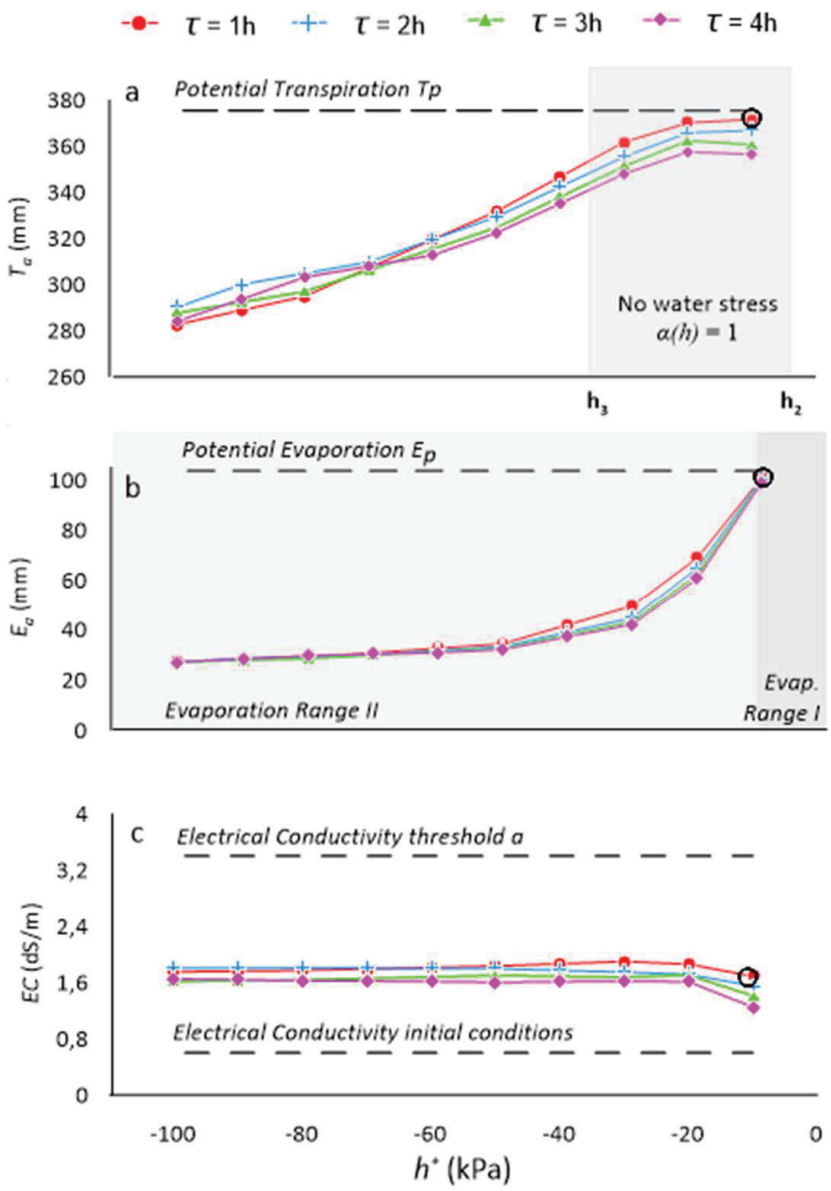

Figure 3.10. a) Actual Transpiration (T_a), b) actual Evapotranspiration (E_a) and c) Electrical Conductivity at the root zone (EC) resulting from Loamy Sand soil showing all the irrigation strategies simulated. Circles show the strategy who provides maximum Net Margin (NM).

3.5. Conclusions

Irrigation scheduling in agriculture is crucial for saving water while guaranteeing maximum crop yields in arid regions as well as in future areas affected by climate change and water scarcity. However, irrigation scheduling is typically conducted based on simple water requirement calculations without accounting for the strong link between water movement in the root zone, crop yields and irrigation expenses. In this work, we have presented a combined simulation and optimization framework aimed at estimating irrigation

parameters that maximize the crop net margin cost subject to operational and functional constraints. The simulation component couples the movement of water in a variably saturated porous media driven by irrigation with plant water uptake and crop yields. The optimization component assures maximum gain with minimum cost of crop production during a growing season.

An application of the method was presented in the Foradada irrigation field test site, where soil hydraulic parameters represented a soil with high water content capacity and slow wetting front percolation. The method was demonstrated to yield optimum irrigation parameters at the site (irrigation duration of 1 hour and a frequency determined by a pressure head threshold of -40 kPa). These parameters were substantially different from those estimated with traditional water requirement methods based on previous evapotranspiration values. Results have shown that even though the volume of water evapotranspired during the growing season is fully replaced by the traditional method, the way to schedule irrigation does not guarantee that water content values vary within an optimal water content fringe. Prolonged saturation of the top soil horizon is often shown to occur with the traditional method. On the contrary, the optimal irrigation scheduling solution prevents waterlogging and provides a more constant value of water content during the entire growing season within the root zone. As a result, the crop net margin cost exhibited an increase with respect to the traditional method by a factor of 7%. The optimal irrigation solution is also demonstrated to properly balance the crop gain margin and operational expenses. Results have shown that even though some strategies can be more productive, irrigation expenses counterbalance the economic benefit ultimately leading to a compromise between them. At this stage, we highlight the practical advantages of the method proposed compared to traditional water requirement methods: (i) agriculture stakeholders can obtain better crop gain margins to achieve the same crop productivity; and (ii) irrigation scheduling parameters can be known prior the start of the growing season. However, the method requires a more important soil characterization of the field site and the installation of sensors to measure (at least) pressure head potentials.

The impact of soil hydraulic properties has been also analyzed by assuming another soil type (Loamy Sand soil). Soil hydraulic parameters described a soil with less water retention capacity than the Foradada soil and easier wetting front percolation. Results have shown that the optimal solution strongly depends on the type of soil. In this case, the frequency of irrigation was much larger given by a pressure head threshold of -10 kPa.

We thank our colleagues from Aigües Segarra-Garrigues (ASG) company for sharing some of the data necessary to conduct this chapter.

Chapter 4

Dynamic management zones to improve irrigation scheduling

Fontanet, M., Scudiero, E., Skaggs, T., Fernàndez-Garcia, D., Rodrigo, G., Bellvert, J., Ferrer, F.: Dynamic management zones to improve irrigation scheduling. Agricultural Water Management Manuscript Submitted.

4.1. Introduction

Irrigation is the process where water is applied artificially to a specific field in order to supply water evaporated and/or taken up plants. In humid areas precipitation covers the largest fraction of this crop and atmosphere demand, but in dry regions precipitation is not enough to satisfy it and irrigation covers the evapotranspiration demand (Evans et al., 2013). In addition, it is generally expected that irrigated agriculture will have to be extended in the future in order to feed the world's growing population (Döll, 2002). Thus, water optimization without compromising crop yield will play a crucial role in the near future, where optimal irrigation scheduling is responsible for this.

One of the main difficulties for stakeholders to make decisions about irrigation scheduling involves field spatial variability. Irrigation is frequently applied with uniform criteria in the entire field, and water content patterns present differences as a consequence of soil hydraulic properties (Hawley, 1983), topography (Burt and Butcher, 1985) and vegetation (Le Roux et al., 1995). This spatial variability should be taken into consideration, since it significantly determines how the irrigation criteria should be managed differently, thereby guaranteeing optimal crop development and decreasing water use. In addition, processes involved in the Soil – Plant – Atmosphere (SPA) continuum under any kind of irrigation system are complex and difficult to characterize (Mailhol et al., 2011; Buckley, 2017).

With regard to this spatial variability, precision agriculture proposes to achieve the optimization of input use efficiency by site-specific application of nutrients and water on small, within-field management zones of more homogeneous soil properties and crop growth conditions (Zhang et al., 2002). In this framework, the concept of Management Zone (MZ) must be introduced. A MZ is a sub-region of a field that is relatively homogeneous with respect to soil-landscape attributes (Haghverdi et al., 2015). Thus, the presence of different MZs represents different patterns in the same field. Nowadays, different clustering methods such as *k*-mean, IDODATA and Gaussian Mixture are available for delineating MZs based on different data sources. In regard to the necessary data, Yield maps, topography, remote sensing data and soil apparent electrical conductivity are used to delineate MZs. However, remote sensing data is frequently used in agriculture because it is a noninvasive method and data can be downloaded without any cost (see chapter 2) .

Several researchers have defined MZs in a specific field, with the main goal of increasing crop yield and decreasing water use. Inman et al. (2008) and Schenatto et al. (2015) delineated MZs with NDVI data and different crop indices. Liu et al. (2018) delineated MZs based on yield and band vegetation indices maps. Scudiero et al. (2013) defined different MZs, but in this case using geospatial apparent soil electrical conductivity and bare soil

reflectance measurements. These data were correlated and linked with soil properties (salinity, texture, carbon content and bulk density). A similar study was presented by Reyes et al. (2019), in which MZs were defined with NDVI data and complemented with soil properties. Georgi et al. (2018) developed an algorithm to delineate MZs automatically, based on remote sensing data. However, one of the disadvantages of this algorithm is that it does not work properly on fields with unstable spatial patterns. All the studies sited above consider that MZ distribution is static and assume that these distributions have no dynamic pattern during the growing season. Thus, in fields where spatial variability has a dynamic pattern, it is necessary for MZ delineation to be improved, a measure which some researchers have indeed advocated (Evans et al., 2013; Haghverdi et al., 2015).

Water content sensors constitute an optimal tool for real-time monitoring of water content dynamics in the field. Although sensors are able to monitor water content at a single point, the study of spatial and temporal variations of soil water content and the interaction with crop can be analyzed if several sensors are installed across the field (Biswas and Si, 2011; Biswas, 2014; Yang et al., 2016; Huang et al., 2019). Furthermore, infiltration rates and water movement also have subsurface spatial variability when irrigation is applied (Nielsen, 1985; Wendroth et al., 1999). These measurements can provide us information about the reason for the existence of different MZs as well as complementing their delineation. Thus, variables that influence or correlate with soil hydraulic properties and soil water status and dynamics should be considered in the delineation of MZs (Reyes et al., 2019). In this way, it is known that water content dynamics is a consequence of soil properties that affect crop performance (Scudiero et al., 2018) and modify MZ patterns.

HYDRUS (Šimůnek et al., 2008, 2016) simulates water content, pressure head and solute transport in the vadose zone considering root water uptake and root growth. Any kind of simulation model requires field measurements, such as those from water content sensors, in order to validate and calibrate the model. However, HYDRUS is an optimal tool for simulating processes measured in the field and for the subsequent simulation of "what-if" scenarios. In addition, an analysis of all the outputs obtained at each simulation can be conducted afterwards in order to provide an overall view of the system simulated. In this way, it is possible to propose an alternative or to mitigate the existence of a hypothetical problem in a field. Several researchers have used HYDRUS to improve irrigation or to assess water content patterns through the soil profile change when different irrigation strategies are applied (Arbat et al., 2008, 2009; Siyal and Skaggs, 2009; Twarakavi et al., 2009a; Skaggs et al., 2010; Dabach et al., 2013). One of the main disadvantages of these studies is that the results cannot be scaled to soil and environmental conditions or another crop. Furthermore, while they all consider a homogeneous soil profile or with several materials in the depth

domain, they do not take into account spatial variability in the entire field with different memberships properties. This may be due to the fact that soil hydraulic properties cannot be measured in the entire field; thus, simulations represent a particular point at which soil parameters are measured. In chapter 3 is proposed a methodology where a simulation-optimization problem is solved and enables an optimal irrigation scheduling strategy to be determined. The improvement in comparison with the other studies is that this methodology can be scaled to any kind of field. Nevertheless, as in the case of these other studies, it does not consider the existence of MZs, since the simulation model represents a particular point. This may pose a problem if a field is divided into different MZs, because a global pattern of all variables, such as transpiration, must be provided in order to propose an irrigation alternative or to understand specific water processes in each MZ.

Note that several methodologies and technologies can be used in order to improve irrigation scheduling strategies, each of which may provide different kinds of information. However, if the aim is to obtained an overall view of the entire system, all of these methodologies and technologies should be employed together and all must be employed for different purposes. Thus, it is clear that if optimal crop performance and water use are to be guaranteed, the first step is to take field spatial variability into account. When the field spatial variability is identified and the MZs are delineated, water content sensors can provide substantial information about the specific water processes that affect or characterize each MZ. In another words, they can verify in real-time if the irrigation scheduling is not optimal and if differences in water content processes between MZs exist. Finally, the purpose of simulation models is to propose an alternative irrigation scheduling and to adjust it in accordance with MZ features.

In this study, we combine several methodologies with the main goal of improving irrigation scheduling. They are (i) crop cover remote sensing data form Sentinel 2 satellite; (ii) water content sensors; (iii) Hydrus 1-D simulations. All the methodologies have provided different kinds of information and have been used at different times for different purposes. None of them can be used separately because each one needs to be complemented by the others. However, this is not the only objective of this work, all of which are specified below:

- To determine if MZs have a dynamic pattern during the growing season.
- To validate MZ delineation with water content sensors and ground measurements.
- Considering that irrigation is applied with uniform criteria, to identify if each MZ corresponds to a different soil-water pattern affecting crop cover remote sensing data.

- To prove if Hydrus 1-D simulations are capable of representing similar soil-water conditions and if they can be used as "what-if" scenarios.
- To propose an optimal irrigation scheduling calendar at each MZ, to enable the consultant to make within-season irrigation scheduling decision-making.

4.2. Materials and methods

4.2.1. Study site

The research site was a 5.8-ha maize (*Zea mays* L.) field located in Raïmat, about 170 km west of Barcelona, Spain (Fig.4.1). The study region has a semi-arid climate. Summer temperatures average 24 ºC, with several days of the year above 40 ºC. Summer is the dry season, with seasonal rainfall of 45 mm.

Land use at the study site has changed over the years (Fig. 1 in the supporting information). Originally, the site was a forest where no tillage occurred. Approximately 30 years ago, the land was converted to a vineyard. The topography of the field was modified, with soil being added or removed in various sections, such that the site can now be regarded as having an anthropogenic soil. In 2017, one year before the current study, grapevines were removed and maize was grown at the site.

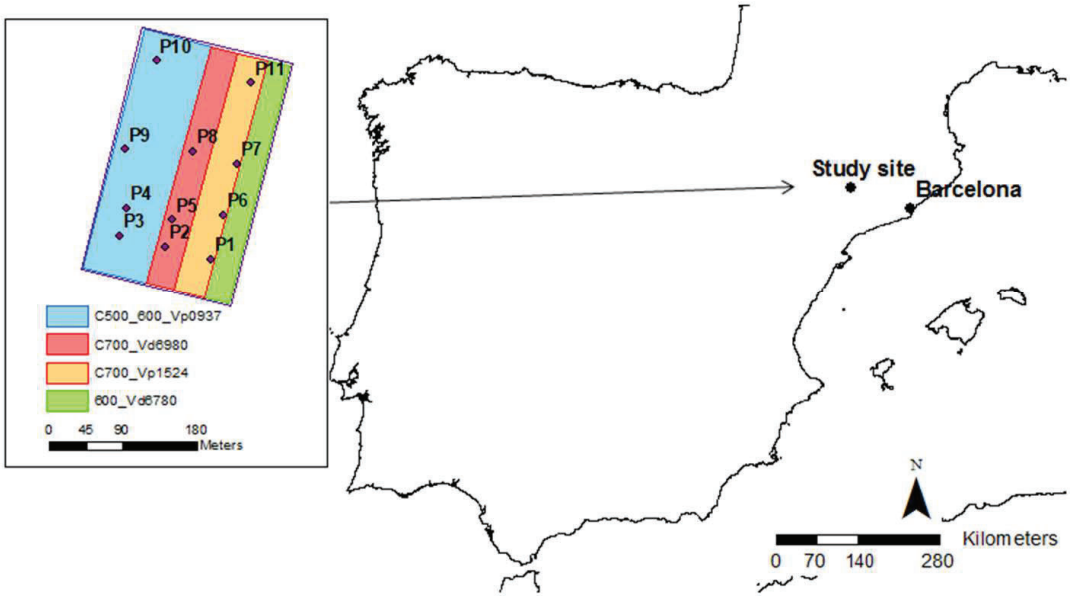

Figure 4.1 Study site general location, the soil moisture stations installed in the field and the four maize varieties distribution, where the blue area represents maize variety p0937 (a combination of 500 and 600 series), the red area is the variety d6980 (700 series), the yellow area is p1524 (700 series) and the green area is d6780 (600 series).

4.2.2. Sowing and irrigation

The field was sectioned into four plots that were each sowed with a different maize variety (Fig.4.1). The varieties were, from west to east: p0937 (DuPont Pioneer, Johnston, IA), d6980 (DEKALB Genetics Corporation, Dekalb, IL), p1524 (DuPont Pioneer), and d6780 (DEKALB). All plots were sown on May 3, 2018, with a sowing density of 90000 seeds·ha^{-1}. The seed companies indicated that the varieties planted on the west and east edges of the field (p0937 and d6780, respectively) grow slightly faster than those planted down the center (d6980 and p1524), although all varieties were anticipated to reach full maturity 125-165 days after sowing. Plants started to emerge on May 12, 2018. The site was harvested on September 22, 2018.

The field was irrigated with a Solid Set sprinkler system (Nelson Irrigation Corporation, Walla Walla, WA) having 15 x 15 m spacing. Water was delivered over 18 irrigation zones at a rate of 6.5 L·m^{-2}·h^{-1}. Total applied water during the season was 679 mm. Irrigation was applied uniformly over the field with scheduling and depths determined using a crop coefficient approach (FAO56). For most of the site, irrigation ended 115 days after sowing. But, in two 0.3-ha sections located at the north-east end of the site, irrigation was halted 74 days after sowing.

4.2.3. Soil, environment, and crop measurements

Field data was collected between May 2018 and September 2018. Water content, soil and crop parameters, environmental variables, and remote sensing NDVI data were measured. In May 2018, 33 capacitive EC-5 soil moisture sensors (METER Group, Pullman, WA, USA) with an accuracy of ± 0.03 cm^3·cm^{-3} (Campbell and Devices, 1986) were installed at 11 locations named P1, P2, …, and P11 (Fig.4.1). The sensors were installed at 15, 35, and 50-cm depths. Water content data were registered every 30 minutes using an EM5b data logger (METER Group).

At each station, three disturbed soil samples were collected at 0-5, 5-35 and 30-60 cm depth for organic matter (OM) and soil texture analyses. The Walkley-Black method was used to measure OM (Nelson and Sommers, 1996), whereas soil particle size distribution was measured according to the gravimetric method (Gee and Bauder, 1986).

Particles were categorized into the following size classes: clay (soil particle diameter, D < 0.002 mm), fine silt (0.002 < D < 0.02 mm), coarse silt (0.02 < D < 0.05 mm) and sand (0.05 < D < 2 mm). Undisturbed soil cores were also collected at the same locations and depths for measuring soil hydraulic properties. The soil water retention curve (SWRC) and unsaturated hydraulic conductivity curve (HCC) were determined using a combination of

three laboratory devices: Hyprop, WP4c, and KSat (METER Group). The van Genuchten model (van Genuchten, 1980) was fit to the measured curves using the RETC software (van Genuchten MTh, Leij FJ, 1991) to estimate saturated water content (θ_s), residual water content (θ_r), saturated hydraulic conductivity (K_s) and the shape parameters α and n. Principal Component Analysis (PCA) Abdi and Williams, (2013) and Martini et al. (2017) was used to investigate the relationships between soil texture, OM, bulk density, and hydraulic parameters. The PCA calculations were done with Statistica 12 (StatSoft Inc. Tulsa, OK, USA).

A weather station consisting of an ECRN-100 rain gauge (METER Group), a cup anemometer (Davis Instruments, Hayward, CA, USA), and PYR pyranometer and VP-4 relative humidity and temperature sensors (METER Group) was installed 150 m from the north-east corner of the field. The measured temperature, wind speed, relative humidity, and solar radiation were used to calculate daily reference evapotranspiration (ET_0) using the Penman Monteith equation as specified in FAO Irrigation and Drainage Paper No. 56 (Allen et al, 1998; hereafter "FAO56"). The estimated ET_0 was converted into daily water requirements or potential evapotranspiration (ET_c) using the maize crop coefficient (k_c) from FAO56. Maximum and minimum daily temperatures measurements were used to calculate growing degree days (GDD) according to FAO56 and to determinate reference maize growing stages (Ritchie et al., 1997).

Remote sensing data from Sentinel 2 were used to determine normalized difference vegetation index ($NDVI$) Eq. (4.1) (Rouse et al., 1974).

$$NDVI = \frac{(NIR - Red)}{(NIR + Red)} \tag{4.1}$$

where NIR and Red are measured reflectance values in the near-infrared and visible red regions, respectively. $NDVI$ was used to evaluate spatial variability in the field. Remote sensing data were downloaded with 10-m spatial resolution every 5 days unless there was cloud coverage. The first and last images downloaded were the 15th and 135th day after sowing. Remote sensing data were processed with the Sentinel application platform (SNAP) software (Zuhlke et al., 2015).

4.2.4. Management zones delineation

Sentinel 2 NDVI was used to characterize the spatial variability of crop vigor through the season. A k-means (also known as "fuzzy c-means") unsupervised clustering algorithm (Odeh et al., 2010) was used to classify the NDVI data into temporally dynamic MZs. The Grouping Analysis tool in ArcMap 10.4.1 (ESRI, Rdlands, CA) was used for the MZ

delineation. Anytime a new Sentinel 2 NDVI scene was available at the site, a new MZ scheme was delineated. Designs having 2 to 6 MZs were considered. The Calinski–Harabasz criterion (CHC) Eq. (4.2) (Harabasz et al., 1974) was used to evaluate the clusters and MZ delineations and select the optimum number of MZs. The CHC, also known as a pseudo F-statistic, measures the ratio of between-MZ differences and within-MZ similarity. It is formulated as:

$$\mathrm{CHC} = \frac{BMZSS/(MZn-1)}{WMZSS/(N-MZn)} \tag{4.2}$$

where N is the number of pixels, MZn is the number of considered zones, $BMZSS$ is the between-zones sum of squares, and $WMZSS$ is the within-zone sum of squares. Large CHC values indicate high within-MZ homogeneity and between-MZ heterogeneity.

The $NDVI$ averages and maximum and minimum values within each MZ were calculated for further comparison between different MZs. MZs were not defined for the beginning of the season (0-20 day after sowing) because plants had not yet germinated or were not big enough to influence $NDVI$, and for the end of the season (beyond 130 days after sowing) because in that period the crop is in a late phenological stage and not irrigated. Differences in soil properties across MZs over time were assessed using a Kruskal-Wallis (Kruskal and Wallis, 1952) rank test (i.e., a non-parametric analysis of variance), calculated with Statistica 12.

Additionally, we subdivided the site into four contiguous field: one for each maize variety. The CHC was calculated for each available $NDVI$ scene to compare a variety-based MZ approach to the dynamic $NDVI$-based MZ delineation.

4.2.5. Management zones available water

Soil-water status for the MZs was modeled as plant available water (AW) Eq. (4.3) (Liang et al., 2016; Vellidis et al., 2016; Zurweller et al., 2019):

$$AW^j(t) = \frac{1}{Z_\mathrm{T}} \sum_m \left(\frac{\theta^{j,m}(t) - \theta_{\mathrm{wp}}^{j,m}}{\theta_{\mathrm{fc}}^{j,m} - \theta_{\mathrm{wp}}^{j,m}} \right) \Delta z^m \tag{4.3}$$

where $AW^j(t)$ is the profile average available water at monitoring station j and time t, m indexes the measurement depths, Δz^m (cm) is the depth increment associated with the moisture sensor at depth m, $Z_\mathrm{T} = \sum \Delta z_m$ (cm) is the total soil profile depth, $\theta^{j,m}$ ($\mathrm{cm^3 \cdot cm^{-3}}$) is soil water content, $\theta_{\mathrm{wp}}^{j,m}$ ($\mathrm{cm^3 \cdot cm^{-3}}$) is the wilting point (water content at -1500 kPa),

and $\theta_{fc}^{j,m}$ ($cm^3 \cdot cm^{-3}$) is field capacity (determined using the method of Twarakavi et al., (2009)). The AW for each MZ was defined to be the average AW for all monitoring stations located within each MZ. Note that the MZ design changed over the growing season, so the MZ membership of some stations also changed. In addition to the CHC calculation on the $NDVI$ data, the spatiotemporal variability of AW was also used for in-season evaluation of the dynamic MZ-design. Following Fraisse et al., (2001), we calculated the daily weighted within-MZ AW variance Eq. (4.4),

$$S_{MZ_i}^2 = \frac{N_{S_i} N_t}{N_S N_t} \times \frac{1}{N_{S_i} N_t} \sum_{j,k} [AW^j(t_k) - \overline{AW_i}]^2 \quad (4.4)$$

where $S_{MZ_i}^2$ is the daily weighted AW variance within management zone i; j indexes the monitoring stations within management zone i; k indexes the measurement times during the current day; N_{S_i} is the number of stations in management zone i; $N_S(= 11)$ is the total number of stations in the field; $N_t(= 48)$ is the number of measurements per day (every 30 min), AW^j is defined by (3), and $\overline{AW_i}$ is the average profile AW across monitoring stations in management zone i and measurement times in the current day. The total within-zone variance is equal to the sum of the weighted within-zone variances, $S^2 = \sum_i S_{MZ_i}^2$. By comparing S^2 with the total daily field-wide AW variance, it is possible to determine how much was gained in terms of AW uniformity by dividing the field into MZs (Fraisse et al., 2001).

4.3. Results

4.3.1. Soil properties

Texture, OM contents and bulk density (ρ_b) values measured at each station are reported in Table 4.1. The soil texture classes (USDA system) of samples taken from the 11 stations were clay loam (42.4 % of samples), loam (42.4%), and silty clay loam (15.2%). Stations on the east side (P1, P6, P7, P11) of the field had, on average, lower sand and higher silt and clay contents than those on the west. Average OM contents ranged between 0.57 and 1.96 %, which is typical for agricultural soils in the region (Romanyà and Rovira, 2011). Fitted and measured parameters for the soil hydraulic properties measured at each station are reported in Table 4.2. Consistent with the spatial trend in soil texture noted previously, the SWRCs measured on the east side of the study site (stations P1, P6, P7, P11) had lower fitted n values than in the rest of the site. On the wet end of a retention curve, a lower n value

corresponds to a more gradual transition in water content as pressure head changes. Figure 4.2 SWRCs observed at stations on the west (P9) and east (P11) sides of the field.

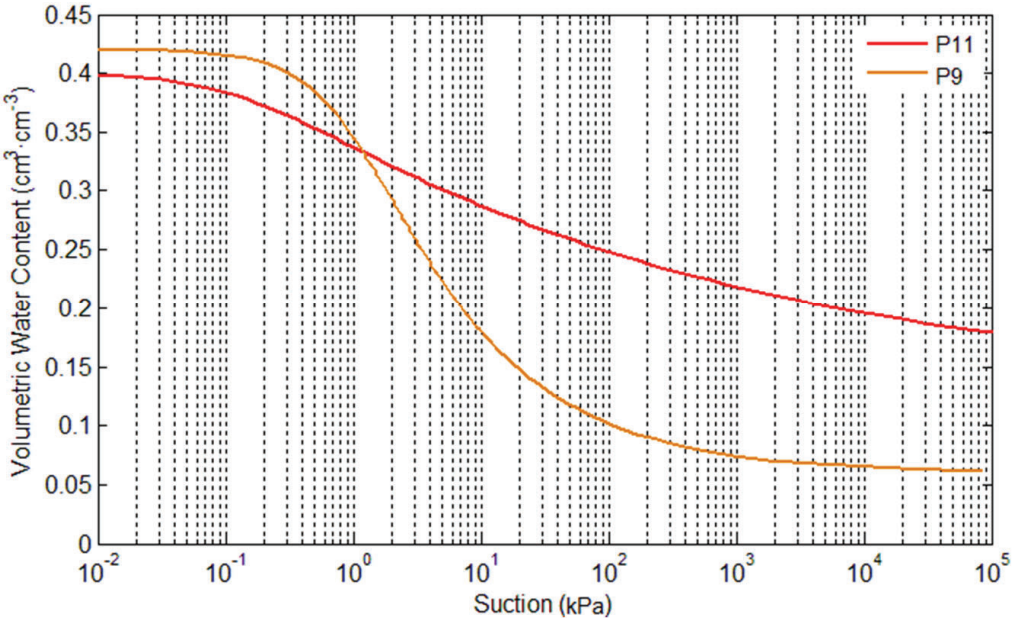

Figure 4.2. Soil water retention curves at 10 cm depth from two stations located on opposite edges of the filed. Station P9 is located on the west side and P11 on the east.

Table 4.1. Soil samples texture, Organic Matter (OM) and bulk density (ρ_b) averages at each station.

Station	Depth (cm)	D<0.002 mm Clay (%)	0.002<D<0.02 mm Fine Silt (%)	0.02<D<0.05 mm Coarse Silt (%)	0.05<D<2 mm Sand (%)	OM (%)	ρb (gr/cm3)
P1	0 - 5	36	27.3	13.8	22.9	1.18	1.66
	5 - 35	32	33.6	14.5	19.9	0.71	1.63
	35 - 60	26.5	28.1	9.7	35.7	0.5	1.68
P2	0 - 5	25.9	26.4	14.8	32.9	1.59	1.57
	5 - 35	25.2	26.1	15.1	33.6	1.1	1.58
	35 - 60	24.2	23.4	14.7	37.7	0.98	1.59
P3	0 - 5	36.5	32.1	14.5	16.9	0.7	1.54
	5 - 35	21.3	27.8	16.7	34.2	0.5	1.65
	35 - 60	24.4	31.8	8.3	35.9	0.65	1.60
P4	0 - 5	28.7	23.6	13.2	34.5	2.71	1.48
	5 - 35	28.5	28.9	11	31.6	1.02	1.59
	35 - 60	28.6	19.8	10.4	41.2	1.14	1.60
P5	0 - 5	22.5	26.3	15.6	35.6	0.57	1.56
	5 - 35	28.9	36.6	20.3	14.2	0.72	1.58
	35 - 60	21.8	28.9	7.3	42.0	0.42	1.56
P6	0 - 5	29.9	26.9	15.1	28.1	2.11	1.64
	5 - 35	29.3	25.7	14.9	30.1	0.85	1.67
	35 - 60	30.2	26	14.8	29.0	0.7	1.69
P7	0 - 5	28.1	36	17.1	18.8	3.14	1.65
	5 - 35	28	27.8	11.9	32.3	1.48	1.72
	35 - 60	27.2	24.3	14.3	34.2	1.27	1.69
P8	0 - 5	25.7	28.7	15.2	30.4	2.22	1.58
	5 - 35	27.7	26.1	14.7	31.5	1.5	1.64
	35 - 60	29.2	27.3	14.7	28.8	1.02	1.78
P9	0 - 5	23.7	26.1	14.8	35.4	2.48	1.53
	5 - 35	23.6	27.8	14.4	34.2	1.06	1.51
	35 - 60	23.5	27.7	14.8	34	0.99	1.51
P10	0 - 5	27.7	25.8	20.3	26.2	1.84	1.61
	5 - 35	28.3	29.5	19.2	26.0	0.72	1.62
	35 - 60	24.6	33.5	9.5	32.4	0.81	1.80
P11	0 - 5	29.4	35.9	14.9	19.8	0.73	1.63
	5 - 35	30.3	34.7	14.9	20.1	0.5	1.65
	35 - 60	26.1	30.5	16.4	27.0	0.5	1.64

Table 4.2. Soil hydraulic parameters from each station, where: θ_s is the saturated water content; θ_r is the residual water content; α and n are shape parameters; K_s is the saturated hydraulic conductivity; θ_{fc} is simulated field capacity; and θ_{wp} is wilting point.

Station	Depth	θ_s	θ_r	α	n	K_s	θ_{fc}	θ_{wp}
	(cm)	($cm^3 \cdot cm^{-3}$)	($cm^3 \cdot cm^{-3}$)	(cm^{-1})	(-)	($cm \cdot d^{-1}$)	($cm^3 \cdot cm^{-3}$)	($cm^3 \cdot cm^{-3}$)
P1	0 - 5	0.424	0.026	0.0169	1.140	2.05	0.345	0.196
	5 – 35	0.407	0.027	0.0150	1.141	2.52	0.351	0.190
	35 - 60	0.364	0.037	0.0115	1.232	1.00	0.350	0.110
P2	0 - 5	0.389	0.061	0.0126	1.364	2.95	0.270	0.103
	5 – 35	0.388	0.060	0.0130	1.358	2.94	0.265	0.104
	35 - 60	0.321	0.047	0.0242	1.354	1.53	0.290	0.124
P3	0 - 5	0.418	0.012	0.0103	1.313	4.42	0.330	0.085
	5 – 35	0.362	0.025	0.0101	1.329	5.63	0.273	0.070
	35 - 60	0.341	0.017	0.0083	1.345	11.47	0.261	0.066
P4	0 - 5	0.439	0.024	0.0658	1.301	5.70	0.340	0.187
	5 – 35	0.400	0.031	0.0143	1.290	4.60	0.300	0.192
	35 - 60	0.395	0.018	0.0424	1.315	4.90	0.315	0.181
P5	0 - 5	0.450	0.062	0.0099	1.497	6.88	0.340	0.070
	5 – 35	0.460	0.067	0.0094	1.402	1.94	0.340	0.080
	35 - 60	-	-	-	-	-	-	-
P6	0 - 5	0.420	0.030	0.0126	1.153	12.00	0.371	0.172
	5 – 35	0.430	0.050	0.0828	1.154	9.40	0.390	0.198
	35 - 60	0.421	0.010	0.0974	1.146	8.10	0.390	0.182
P7	0 - 5	0.375	0.024	0.0105	1.118	1.06	0.300	0.208
	5 – 35	0.349	0.026	0.0380	1.141	3.34	0.300	0.196
	35 - 60	0.361	0.049	0.0391	1.141	4.10	0.280	0.107
P8	0 - 5	0.402	0.040	0.0135	1.375	4.01	0.310	0.123
	5 – 35	0.379	0.030	0.0115	1.356	3.05	0.280	0.090
	35 - 60	0.328	0.020	0.0121	1.287	1.75	0.280	0.080
P9	0 - 5	0.420	0.060	0.0105	1.462	5.79	0.300	0.089
	5 – 35	0.430	0.060	0.0107	1.441	4.70	0.330	0.091
	35 - 60	0.430	0.060	0.0109	1.433	5.52	0.330	0.090
P10	0 - 5	0.389	0.073	0.0115	1.421	3.98	0.301	0.105
	5 – 35	0.387	0.072	0.0112	1.425	4.56	0.300	0.080
	35 - 60	0.320	0.058	0.0181	1.256	1.87	0.290	0.090
P11	0 - 5	0.400	0.012	0.0784	1.121	10.00	0.380	0.188
	5 – 35	0.451	0.018	0.0308	1.141	5.27	0.375	0.188
	35 - 60	0.420	0.014	0.0121	1.112	11.00	0.350	0.250

The principal component analysis (PCA) indicated that 8 principal components were needed to explain 95% of the variability in the soil dataset (Fig. S2; supplementary material). The first three components, PC1 (30.9%), PC2 (18.6%), and PC3 (15.9%), explained around two thirds of the variance in the soil dataset. Particularly, PC1 indicated that clay content clustered (was positively correlated) with θ_{wp}, θ_{fc}, and α. The PC1 also indicated that clay content was negatively correlated with sand content, θ_r, and n. Further detail about PC1, PC2, and PC3 are reported in Fig. S2 in the supplementary materials.

4.3.2. Remote sensing and dynamics management zones delineation

The site average, minimum, and maximum $NDVI$ values for each available Sentinel 2 scene are reported in Fig. 4.3a. The changes in average $NDVI$ generally corresponded to the evolution of ET_c at the site, consistent with reports for maize grown in Mediterranean climates in other studies (Segovia-Cardozo et al., 2019; Toureiro et al., 2017). Figure 4.3b shows that cumulative input water (irrigation and precipitation) (618 mm) exceeded by 10.2% the site-wide cumulative ET_c (561 mm). At the bottom of Fig. 4.4, reference growing stages for maize at the site are shown (Ritchie et al., 1997). Varieties at the site took 120 to 130 days to reach maturity. Thus, we considered the reference growing stages to be representative for all maize varieties grown at the site. $NDVI$ and ET_c were low during the early vegetative stages, had maximum values during the late vegetative stage (VT) through the beginning of the reproductive stages (R1-R6), then decreased after R6. The temporal changes of $NDVI$ at the site are comparable to those observed in other studies on maize (Viña et al., 2004). In the early vegetative stages (V0 to V5), the $NDVI$ range of each Sentinel 2 scene was narrow. In later vegetative stages and early reproductive stages, the $NDVI$ ranges were much larger, indicating considerable variability in crop status (greenness, health) at the site.

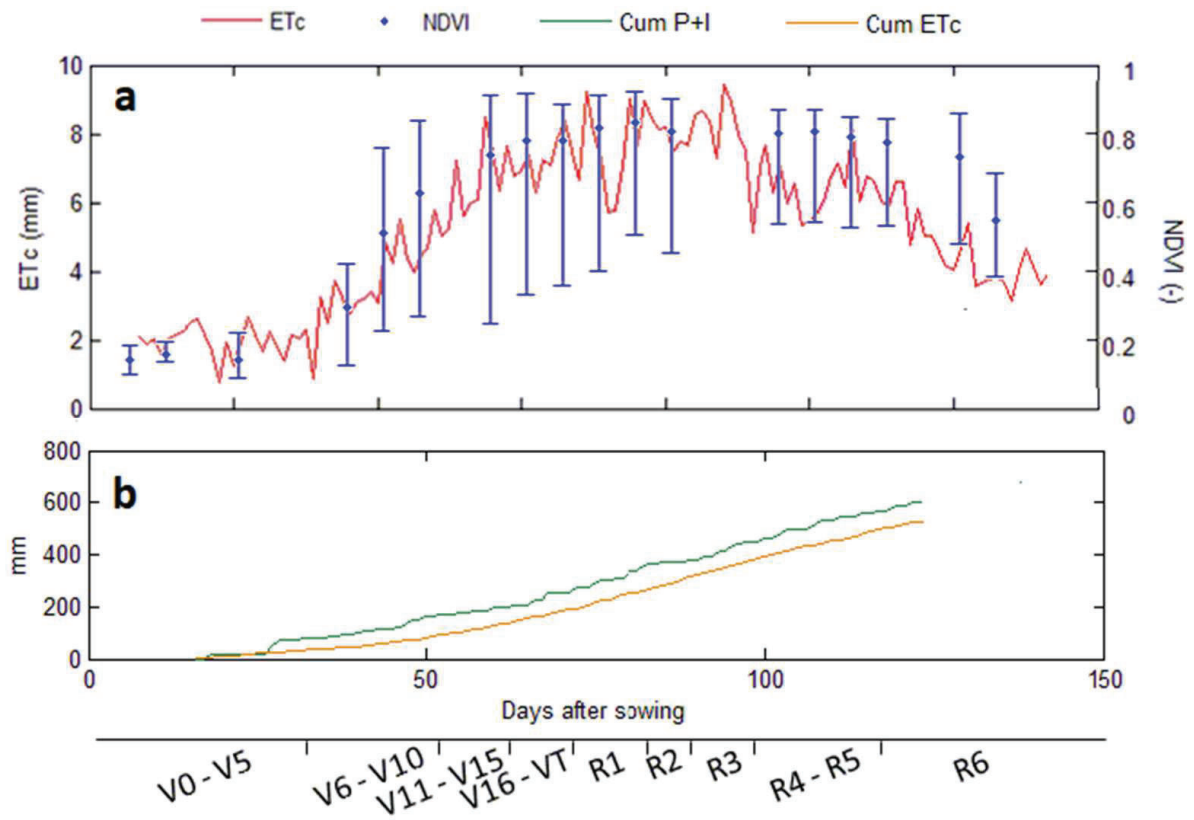

Figure 4.3. a) Maize growth stages, where V is vegetative stage and R represents reproductive stage; Normalized Difference Vegetation Index (NDVI) evolution, in blue; daily water requirements (ETc), in red; cumulative Precipitation and Irrigation (Cum P+I), in green and cumulative water requirements (Cum ETc), in orange.

Figure 4.4a shows the spatiotemporal changes of *NDVI* at the sites. Areas with high and low *NDVI* were observed at the site throughout the growing season. However, the *NDVI* spatial patterns changed over time, suggesting that homogeneous or static site-specific management may be inadequate to address crop needs over time at this site. Figure 4.4b shows the dynamic MZ delineation obtained with unsupervised clustering of the *NDVI* data. Through the growing season, the number of MZs, as well as their spatial distribution, changed. At the beginning of the season, until 50 days after sowing, the *CHC* indicated that three MZs were optimal for identifying homogeneous zones at the site. The MZ1 covered the north-west side of the site and had the highest *NDVI* values; the MZ2 had intermediate *NDVI* and spanned across the south of the site until the 45th day after sowing and after that over the south-west only. The MZ3 had lower *NDVI* values and was initially the north-eastern side of the site, then covered the entire western side of the field at 45 days after sowing. From the 50th day after sowing, the *CHC* indicated that four clusters were best at identifying areas with homogeneous *NDVI*. MZ1 and MZ2 covered similar extents than earlier in the season. The MZ4 identified an area of moderately low *NDVI* at the south-

eastern portion of the site, whereas MZ3 was characterized by the lowest $NDVI$ values, in the north-eastern side of the site. The spatial patterns of the four MZs change only slightly over time, until the 130th day after sowing, when the size of MZ3 increased remarkably while MZ4's extent decreased. The unsupervised $NDVI$ clustering was compared to dividing the site into four blocks, one for each maize variety. Figure 4.4c shows the CHC values for $NDVI$ clustering into dynamic MZ and into varietal blocks strategies through the growing season. The dynamic MZ-design strategy had larger CHC values for the entire growing season than the variety-block strategy, indicating that the dynamic MZs identified by unsupervised clustering had more homogeneous $NDVI$ than the varietal blocks.

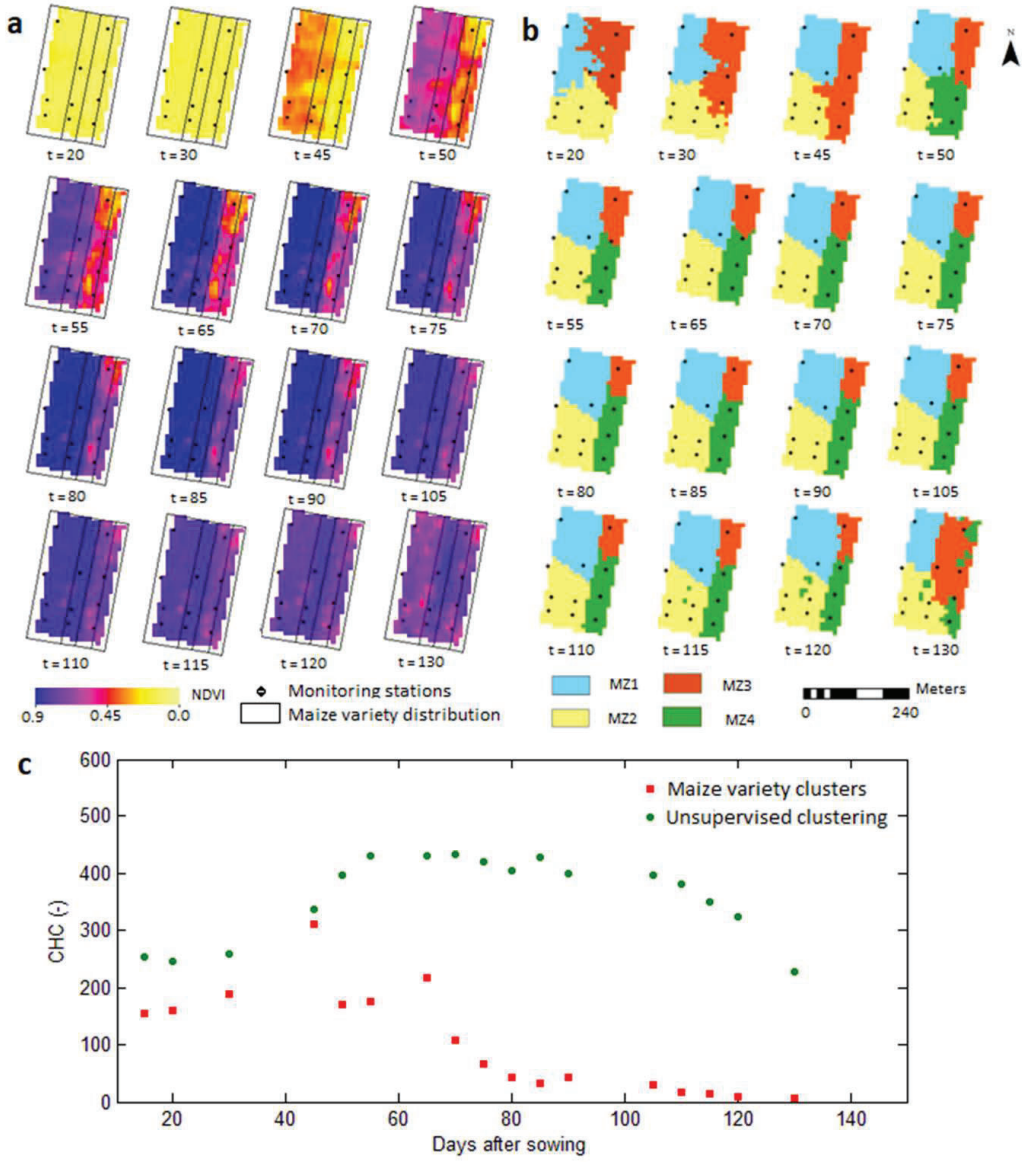

Figure 4.4. a) Normalized Difference Vegetation Index (NDVI) datasets measured by Sentinel 2 satellite through the growing season; b) dynamic management zone (MZ) delineation. The letter t indicates day after sowing; and c) Calinski-Harabaz criterion (CHC) for the NDVI grouped by maize variety (squares) and with the unsupervised fuzzy-k clustering (dots).

Figure 4.4a shows contrasting *NDVI* values between the eastern and western side of the field, especially visible along the boundary between the d6980 and p1524 varieties. The boundary between the d6980 and p1524 varieties seemed to be a big factor in the determination of the boundary between eastern (MZ1 and MZ2) and western (MZ3 and MZ4) zones from 55 to 120 days after sowing (Fig. 4.4b). Figure S1f in the supporting information shows the p1524 and d6780 varieties doing relatively poorly in July 2018. So in addition to different soil hydrualic properties on the east side of the field, crop genetics (e.g., pest resistance, germination rate between the varieties) and uneven management (e.g., mechanical sowing, fertilization, soil tillage) could have been contributing factors to the poor performance of the p1524 and d6780 varieties. Changes in MZ delineation over time led to some changes in MZ membership for certain soil-water monitoring stations (Table 4.3). These changes occurred frequently in the early vegetative stages (i.e., until 54 days after sowing). No MZ membership change occurred in the late vegetative and reproductive stages. The MZs were characterized by contrasting soil properties throughout the season. The MZ had significantly ($p<0.05$) different PC1 scores throughout the season according to the Kruskal Wallis test: MZ1 and MZ2 were characterized by low PC1 scores, whereas MZ3 and MZ4 were characterized by the highest PC1 scores (Fig. S2 in the supporting information).

Table 4.3. Periods where one or more stations change MZ membership.

Period (Day after sowing)	MZ1	MZ2	MZ3	MZ4
Period 1 (19-29)	P8, P9, P10	P1, P2, P3, P4, P5, P6	P7, P11	-
Period 2 (30-44)	P8, P9, P10	P1, P2, P3, P4, P5	P6, P7, P11	-
Period 3 (45-49)	P8, P10	P2, P3, P4, P5, P9	P1, P6, P7, P11	-
Period 4 (50-54)	P8, P10	P2, P3, P4, P9	P7, P11	P1, P5, P6
Period 5 (55-115)	P8, P10	P2, P3, P4, P5, P9	P11	P1, P6, P7

4.3.3. NDVI and applied water

Changes in *NDVI* and *AW* across MZs are depicted in Fig. 4.5a (MZ1), 4.5b (MZ2), 4.5c (MZ3), and 4.5d (MZ4). Through the growing season, *NDVI* in MZ1 and MZ2 was higher

than in MZ3 and MZ4. Furthermore, $NDVI$ was slightly higher in MZ1 than in MZ2. Average AW in MZ1 was close to 1 (i.e., water content was near θ_{fc}) throughout the entire growing season. Average AW in MZ2 was greater than 1 at the beginning of the season (until 45 days after sowing) and then very close to 1 through the end of the growing season. Portions of MZ3 and MZ4 had lower $NDVI$ values than MZ1 and MZ2. In these areas, irrigation was likely excessive. AW was considerably higher than 1 for the entire vegetative growth of maize and during the early reproductive stages. Once irrigation was halted in the northeastern corner of the site (i.e., approximately over the area comprised by MZ3) at 74 day after sowing, the AW in MZ3 gradually decreased until the end of the season, while $NDVI$ in MZ3 remained stable. Halting irrigation in the northeastern corner of the site had little-to-no effect on the spatial extent of MZ3 and the other MZs, as shown in Fig. 4.4c.The analysis of the daily total within-MZ AW variance (S^2) provided further support for the use of $NDVI$ to identify areas with similar AW conditions at the site. In Fig. 4.5e, the calculated total MZ variance is normalized by the daily whole-site AW variance. Especially beyond 45 days after sowing (the beginning of the VT growth stage), the normalized within-MZ variance is much less than 1, showing that a large part of the total AW variance was explained by splitting the site into dynamic MZs which were delineated based on an analysis of $NDVI$. Fraisse et al. (2001) used yield within-zone variance to evaluate soil-derived MZs at the end of the season. Our results suggest that daily AW S^2could also be used for in-season evaluation of management zone designs.

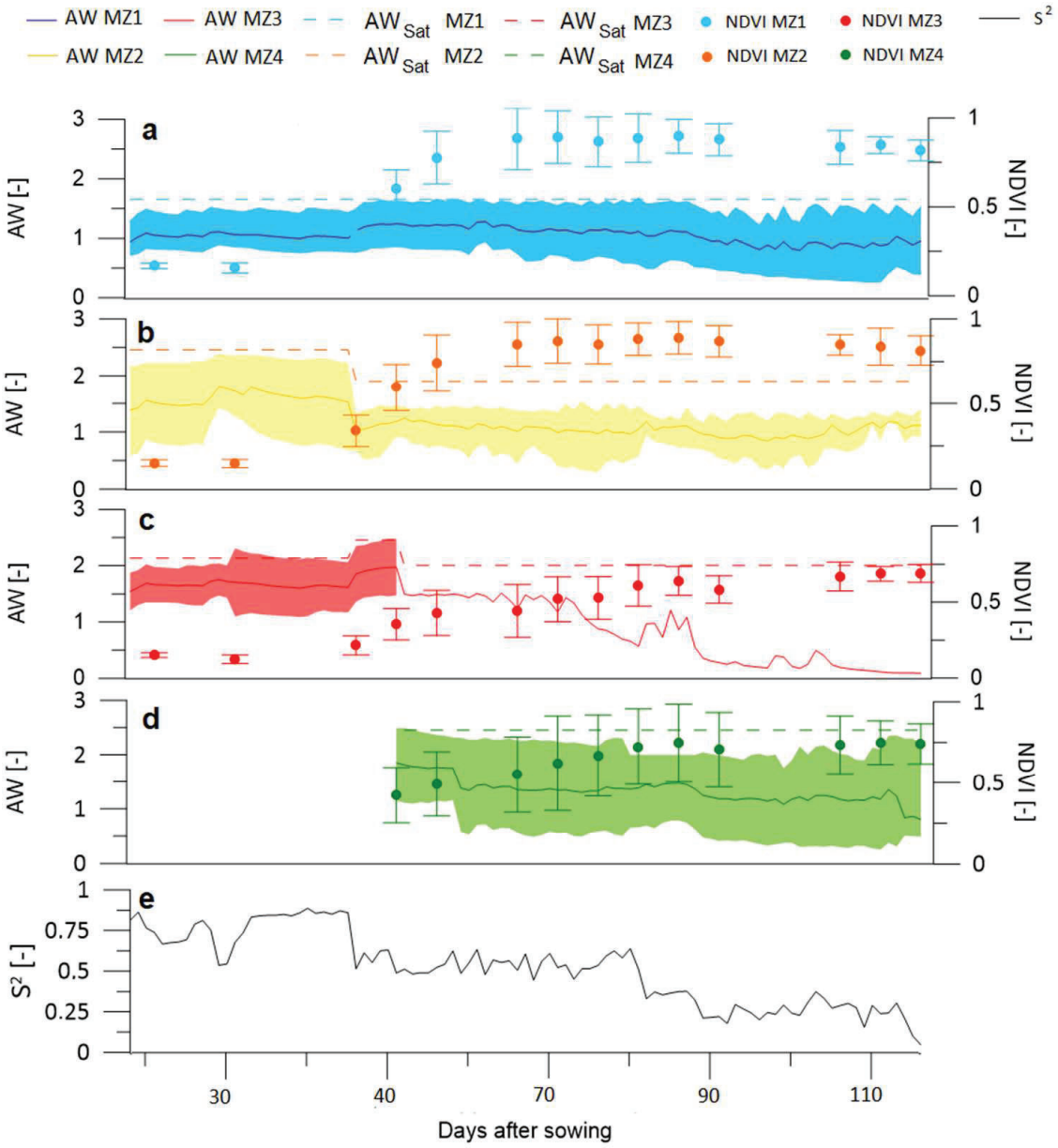

Figure 4.5. Soil profile available water (AW) and NDVI averages for a) MZ1, b) MZ2, c) MZ3, d) MZ4. Shaded areas represents the maximum in minimum AW at each MZ, while dash lines show availabe water saturated (AW_{sat}) (θ) and field capacity point (θ_{fc}). Error bars represents the maximum and minimum NDVI at each MZ. Note that AW = 1 corresponds to a soil water content equal to field capacity. Panel e) shows the daily total within-MZ weighted variance (S^2) of AW as a fraction of the daily field-wide AW variance.

4.4. Discussion

4.4.1. NDVI and irrigation scheduling simulations

The *AW* and *NDVI* time series data show that soil water content was a major factor determining *NDVI* spatiotemporal variability at the site. *NDVI* is an indicator of maize crop health, and several studies have found positive correlations between *NDVI*, *AW*, and crop

growth (Scudiero et al., 2014; West et al., 2018). However, those studies were for water scarce conditions. Crop stress and reductions in growth can occur from too much water in the soil profile as well as too little (Feddes et al., 1978). In the current study, where maize was grown under nearly waterlogged conditions for most of the growing season (Fig. 4), changes in $NDVI$ and AW between consecutive Sentinel 2 scenes were negatively correlated, with Pearson r equal to -0.64 (MZ1), -0.87 (MZ2), -0.79 (MZ3), and -0.83 (MZ4) (all significant at $p<0.05$). Thus, as has been noted elsewhere (Long et al., 2015; Quebrajo et al., 2018; Scudiero et al., 2018; Shanahan et al., 2008), $NDVI$ data alone should not be used to make irrigation management decisions; $NDVI$ (and/or other plant canopy information) should be integrated with soil information to properly understand plant processes at a site.

With respect to within-season management decisions, one way to make the connection between $NDVI$-based dynamic management zone delineation and soil conditions would be to use a simulation model to make within-season forecasts of soil and crop conditions for different management options. Here, we determined optimal irrigation scheduling for each growing stage using the simulation/optimization approach exposed in chapter 3 and Hydrus-1D model (Šimůnek et al., 2016). First, we simulated the field experiment using hydraulic properties measured at each monitoring station and the recorded irrigation schedule and ET_c as boundary conditions. In demonstrating agreement between measured AW and simulated available water (SAW), as well as showing a correspondence between simulated transpiration (ST_a) rates and $NDVI$, we show that (i.) the $NDVI$-based zoning was consistent with a physically based model representation of the study site, and (ii.) the model was adequately parameterized and calibrated to permit further investigation of what-if scenarios. Second, we calculated an irrigation scheduling table for each dynamic MZ that would allow growers to optimize transpiration, water applied throughout the growing season.

4.4.2. Hydrus 1-D available water and transpiration simulations

The well-known Hydrus-1d model solves the Richards Equation numerically to simulate variably saturated water flow and root water uptake in soils. The model inputs and parameterizations used in our simulations are detailed in the supplementary material (Hydrus 1D Simulations section). Simulations of the experiment for differing monitoring locations all used the same inputs and parameters except for (i.) the soil hydraulic properties, which were measured at each station during the field campaign (Table 4.2), and (ii.) the irrigation boundary condition, which differed only for stations P10 and P11 because irrigation was stopped during the experiment.

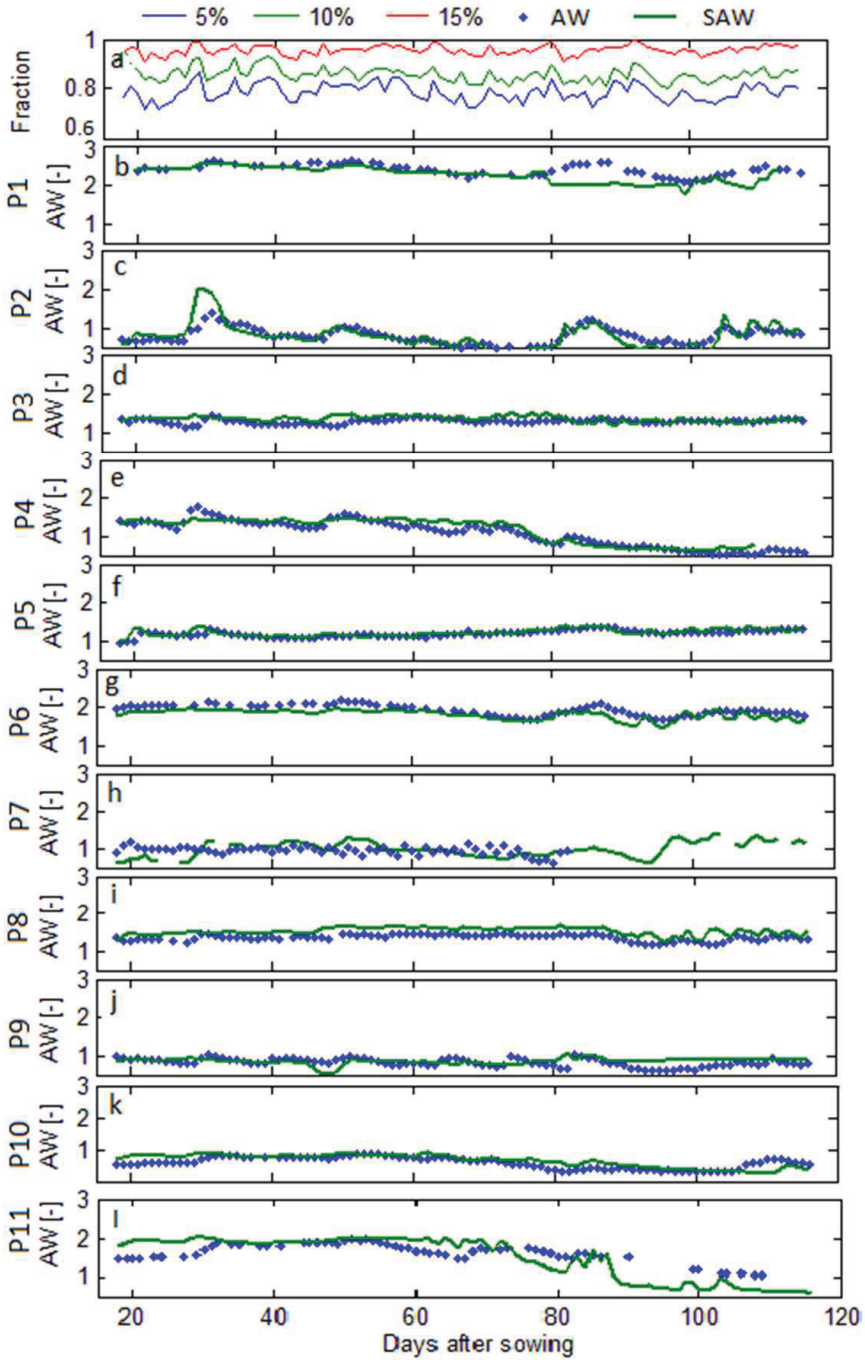

Figure 4.6. a) Evaluation of profile Available Water (AW) simulations showings the fraction of error greater than 5, 10, and 15%. From b) to l) Comparison between measured Available water (AW) and simulated Available Water (SAW) at each station (P1 - P11).

In Fig. 4.6, daily observed *AW* for each station is compared with daily *SAW*. Generally good agreement between *AW* and *SAW* existed for all stations, although it is noted that the *AW* time courses were relatively non-dynamic. Still, the simulations were done using independently measured hydraulic properties and without any parameter fitting, so the agreement is quite good. Missing data towards the end of the season in P7 was due to

rodents chewing on the sensor cables. Sensor loss due to rodents is a common problem in many agricultural regions. Enough sensors should be ideally set out so that each MZ includes more than one sensor, so that within zone spatial variability is accounted for and as a fail-safe in case of sensor loss.

Figure 4.7 shows the weekly ST_a at each MZ and the potential transpiration (T_p) at the site. At MZ1 and MZ2, ST_a weekly averages were always equal or slightly smaller than potential transpiration through the entire growing season. At MZ3 and MZ4, ST_a weekly values were remarkably lower than weekly potential transpiration. There was good correspondence between ST_a and $NDVI$ at each MZ, with a Pearson r of 0.6 (MZ1), 0.51 (MZ2), 0.69 (MZ3), and 0.82 (MZ4). In agreement with the results discussed for $NDVI$ and AW data (section 4.*3.2. Remote Sensing and Dynamic Management Zones Delineation*), low ST_a values at MZ3 and MZ4 were due to waterlogging. Stations in MZ3 and MZ4 (see Table 4.3) had AW and SAW over 1 for most of the growing season (Fig. 4.5).

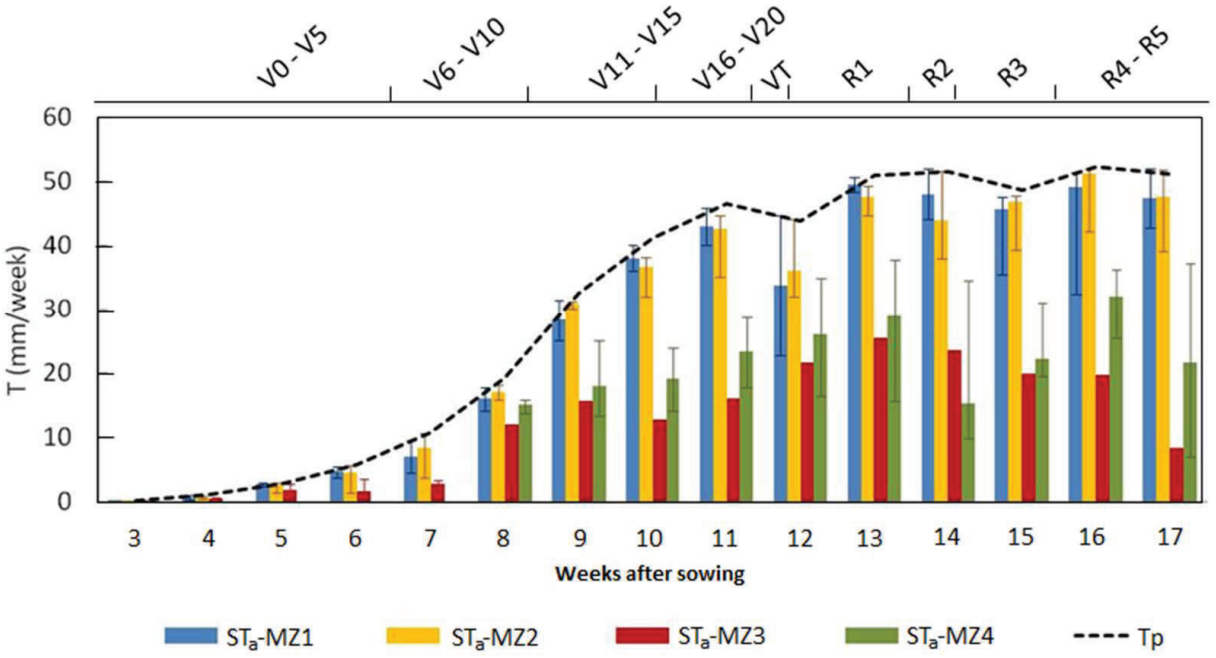

Figure 4.7. Simulated weekly transpiration at each MZ with the growing stages. Error bars represent the maximum and minimum and the dash line shows the weekly potential transpiration.

4.4.3. Irrigation scheduling for within-season decision making

We used the methodology exposed in chapter 3 to investigate an optimal irrigation scheduling strategy based on dynamics MZs delineation. The main goal of the optimization was to improve irrigation scheduling and to guarantee optimal crop conditions. This methodology is capable of generating the optimal combination of two different irrigation

parameters, which are (i) the limit threshold or soil pressure head where irrigation is triggered (h^*); and (ii) the irrigation duration (τ). As output of these simulations it is possible to obtain optimal actual transpiration (OpT_a) and the water necessary to cover transpiration demand, which is optimal water applied ($OpWA$).

The methodology employed optimizes irrigation scheduling solving a simulation/optimization problem (see chapter 3). However, considering the existence of different MZs, and the variability within them, it is difficult for an agriculture to follow irrigation scheduling recommendations resulting from this methodology. Thus, it would be difficult to take within-season management decisions. In order to solve this necessity, simulations have been repeated but considering different, new and lower pressure heads thresholds (h_{th}) than the optimal one ($h_{th} \leq h^*$). Thus, the irrigation required ($\Delta\theta$) to bring soil-water status back to the optimal one might be increase. In this case, irrigation rate (I_{rate}) is constant and cannot be modified, therefore, τ is modified increasing their values. The model inputs are summarized in the supporting information (Irrigation scheduling section).

A dynamic-MZ irrigation approach is presented in Tables 4.4 (MZ1), 4.5 (MZ2), 4.6 (MZ3) and 4.7 (MZ4). They represent an irrigation scheduling calendar that could have been used at the site based on simulated soil-water balance at different growth stages. This calendar was developed with the objectives of (i) propose an optimal irrigation scheduling allowing agricultures to take within-season irrigation management decisions, (ii) guaranteeing optimal crop growth (i.e., maximizing crop transpiration) (iii) if it is possible save water at the end of the season.

Optimal irrigation strategies are represented in Tables 4.4 – 4.7, in bold. Below them, are reported all irrigation strategies alternatives in order to allow agriculture to readjust irrigation in case that some parts of the field do not follow the optimal irrigation recommendation. In case that $h^* \geq h_{th}$; as a general term, and following the tendency of this work, there are two main groups; (i) MZ1 with τ=1.1 – 2.6 h·d^{-1} and h^*=-23.3 - -30 kPa; MZ2 with τ=1.9 – 2.0 h·d^{-1} and h^*=-18.4 - -30 kPa. These parameters represent medium frequent and short irrigations. (ii) MZ3 with τ=2 h·d^{-1} and h^*=-10 - -20 kPa; MZ4 with τ=2 – 2.3 h·d^{-1} and h^*=-10 - -16.7 kPa. They represent very frequent and short irrigations. The other situation that can be in the site is when $h^* \leq h_{th}$; note that in this case τ increase because water consumed might be supplied until similar values as the optimal irrigation scheduling.

Table 4.8 shows a summary of transpiration and water applied at the end of the season in case that optimal irrigation scheduling is applied in the field. The transpiration and water

applied from the other irrigation alternatives are not reported because it has been seen that irrigation scheduling is dynamic during the growing season, therefore, it was not possible to represent these results in a table. However, it is assumed that transpiration is lower than results reported in Table 4.8, because they do not represent optimal irrigation scheduling. Note that in even though in MZ1 and MZ2 any soil water content problem has been observed during this work, transpiration increases from 4.8 to 8 %. But the most transpiration improvement is represented by MZ3 and MZ4, where it increases a 23.9 and 52.6 %, respectively. Considering water applied, the optimal strategies apply less water in all cases than the experiment simulations. Water saving in MZ1 and MZ2 is quite similar, -11 and -12.8 %, while in MZ3 and MZ4, optimal irrigation applies a -28.5 and -16.6 % of water.

Considering all data presented and discussed in this work, it has been seen that even though $NDVI$ is not an appropriate variable to determine irrigation scheduling, when it is integrated with sensors and ground measurements, it helps us to understand if there is some problem regarding on irrigation scheduling. In this case, we have seen that in two different MZs of the filed, waterlogging, crop genetics and soil tillage could decrease crop transpiration, showing low $NDVI$ values. In addition, Hydrus 1-D simulations have simulated the field experiment to allow us to simulate what-if scenarios in order to propose a different irrigation scheduling strategy. In this case, strategies proposed are capable of increasing transpiration with less water, verifying that water clogging could be the main problem in this field.

Table 4.4. Irrigation scheduling calendar in MZ1 based on growing stages and MZs distribution. h_{th}, is the possible pressure head threshold; h^* is the optimal pressure head threshold; $\Delta\theta$, is the irrigation required; τ, is the irrigation duration; Z_{tr}, is the trigger soil depth. Optimal irrigation scheduling are represented in bold.

		V0-V5			**V6-V10**			**V11-V15**			**VT**			**R1-R6**		
		Z_{tr} (cm) = 10			**Z_{tr} (cm) = 20**			**Z_{tr} (cm) = 20**			**Z_{tr} (cm) = 40**			**Z_{tr} (cm) = 40**		
	h_{th} (kPa)	**h^* (kPa)**	**$\Delta\theta$ (mm)**	**τ (h/d)**	**h^* (kPa)**	**$\Delta\theta$ (mm)**	**τ (h/d)**	**h^* (kPa)**	**$\Delta\theta$ (mm)**	**τ (h/d)**	**h^* (kPa)**	**$\Delta\theta$ (mm)**	**τ (h/d)**	**h^* (kPa)**	**$\Delta\theta$ (mm)**	**τ (h/d)**
	0	-	-	-	-	-	-	-	-	-	-	-	-	-	-	-
	-10	-	-	-	-	-	-	-	-	-	-	-	-	-	-	-
	-20	-	-	-	-	-	-	-	-	-	-	-	-	-	-	-
	-30	**-26.7**	**13.1**	**2.0**	**-23.3**	**1.9**	**1.1**	**-30.0**	**19.0**	**2.9**	**-30.0**	**15.0**	**2.3**	**-30.0**	**17.0**	**2.6**
MZ1	**-40**	-26.7	15.1	2.3	-23.3	2.2	1.1	-30.0	21.0	3.2	-30.0	17.0	2.6	-30.0	21.0	3.2
	-50	-26.7	15.1	2.3	-23.3	2.5	1.2	-30.0	23.0	3.5	-30.0	21.0	3.2	-30.0	25.0	3.8
	-60	-26.7	16.1	2.5	-23.3	2.8	1.2	-30.0	25.0	3.8	-30.0	23.0	3.5	-30.0	29.0	4.5
	-70	-26.7	16.1	2.5	-23.3	2.8	1.2	-30.0	25.0	3.8	-30.0	25.0	3.8	-30.0	33.0	5.1
	-80	-26.7	16.1	2.5	-23.3	2.8	1.2	-30.0	25.0	3.8	-30.0	29.0	4.5	-30.0	37.0	5.7
	-90	-26.7	16.1	2.5	-23.3	3.2	1.2	-30.0	27.0	4.2	-30.0	33.0	5.1	-30.0	41.0	6.3
	-100	-26.7	17.1	2.6	-23.3	3.5	1.2	-30.0	29.0	4.5	-30.0	33.0	5.1	-30.0	45.0	6.9

Table 4.5. Irrigation scheduling calendar in MZ2 based on growing stages and MZs distribution. h_{th}, is the possible pressure head threshold; h^* is the optimal pressure head threshold; $\Delta\theta$, is the irrigation required; τ, is the irrigation duration; Z_{tr}, is the trigger soil depth. Optimal irrigation scheduling are represented in bold.

		V0-V5			**V6-V10**			**V11-V15**			**VT**			**R1-R6**		
		Z_{tr} (cm) = 10			**Z_{tr} (cm) = 20**			**Z_{tr} (cm) = 20**			**Z_{tr} (cm) = 40**			**Z_{tr} (cm) = 40**		
	h_{th} (kPa)	**h^* (kPa)**	**$\Delta\theta$ (mm)**	**τ (h/d)**	**h^* (kPa)**	**$\Delta\theta$ (mm)**	**τ (h/d)**	**h^* (kPa)**	**$\Delta\theta$ (mm)**	**τ (h/d)**	**h^* (kPa)**	**$\Delta\theta$ (mm)**	**τ (h/d)**	**h^* (kPa)**	**$\Delta\theta$ (mm)**	**τ (h/d)**
MZ2	**0**	-	-	-	-	-	-	-	-	-	-	-	-	-	-	-
	-10	-	-	-	-	-	-	-	-	-	-	-	-	-	-	-
	-20	**-18.3**	**12.4**	**1.9**	**-24.0**	**15.3**	**2.4**	-	-	-	-	-	-	-	-	-
	-30	-18.3	13.9	2.1	-24.0	18.3	2.8	**-30.0**	**13.0**	**2.0**	**-30.0**	**13.0**	**2.0**	**-30.0**	**13.0**	**2.0**
	-40	-18.3	14.4	2.2	-24.0	19.3	3.0	-30.0	18.0	2.8	-30.0	23.0	3.5	-30.0	23.0	3.5
	-50	-18.3	15.9	2.4	-24.0	22.3	3.4	-30.0	21.0	3.2	-30.0	29.0	4.5	-30.0	29.0	4.5
	-60	-18.3	16.9	2.6	-24.0	24.3	3.7	-30.0	23.0	3.5	-30.0	33.0	5.1	-30.0	33.0	5.1
	-70	-18.3	17.9	2.8	-24.0	26.3	4.0	-30.0	25.0	3.8	-30.0	37.0	5.7	-30.0	37.0	5.7
	-80	-18.3	17.9	2.8	-24.0	26.3	4.0	-30.0	25.0	3.8	-30.0	37.0	5.7	-30.0	37.0	5.7
	-90	-18.3	19.9	3.1	-24.0	30.3	4.7	-30.0	29.0	4.5	-30.0	45.0	6.9	-30.0	45.0	6.9
	-100	-18.3	19.9	3.1	-24.0	30.3	4.7	-30.0	29.0	4.5	-30.0	45.0	6.9	-30.0	45.0	6.9

Table 4.6. Irrigation scheduling calendar in MZ3 based on growing stages and MZs distribution. h_{th}, is the possible pressure head threshold; h^* is the optimal pressure head threshold; $\Delta\theta$, is the irrigation required; τ, is the irrigation duration; Z_{tr}, is the trigger soil depth. Optimal irrigation scheduling are represented in bold.

		V0-V5			**V6-V10**			**V11-V15**			**VT**			**R1-R6**		
		Z_{tr} (cm) = 10			**Z_{tr} (cm) = 20**			**Z_{tr} (cm) = 20**			**Z_{tr} (cm) = 40**			**Z_{tr} (cm) = 40**		
	h_{th} (kPa)	**h^* (kPa)**	**$\Delta\theta$ (mm)**	**τ (h/d)**	**h^* (kPa)**	**$\Delta\theta$ (mm)**	**τ (h/d)**	**h^* (kPa)**	**$\Delta\theta$ (mm)**	**τ (h/d)**	**h^* (kPa)**	**$\Delta\theta$ (mm)**	**τ (h/d)**	**h^* (kPa)**	**$\Delta\theta$ (mm)**	**τ (h/d)**
MZ3	**0**	-	-	-	-	-	-	-	-	-	-	-	-	-	-	-
	-10	-	-	-	**-10.0**	**13.0**	**2.0**	**-10.0**	**13.0**	**2.0**	**-10.0**	**13.0**	**2.0**	**-10.0**	**13.0**	**2.0**
	-20	**-20.0**	**13.0**	**2.0**	-10.0	17.0	2.6	-10.0	17.0	2.6	-10.0	21.0	3.2	-10.0	21.0	3.2
	-30	-20.0	15.0	2.3	-10.0	21.0	3.2	-10.0	21.0	3.2	-10.0	29.0	4.5	-10.0	29.0	4.5
	-40	-20.0	16.0	2.5	-10.0	23.0	3.5	-10.0	23.0	3.5	-10.0	33.0	5.1	-10.0	33.0	5.1
	-50	-20.0	17.0	2.6	-10.0	25.0	3.8	-10.0	25.0	3.8	-10.0	37.0	5.7	-10.0	37.0	5.7
	-60	-20.0	18.0	2.8	-10.0	27.0	4.2	-10.0	27.0	4.2	-10.0	41.0	6.3	-10.0	41.0	6.3
	-70	-20.0	18.5	2.8	-10.0	24.0	3.7	-10.0	24.0	3.7	-10.0	35.0	5.4	-10.0	35.0	5.4
	-80	-20.0	18.0	2.8	-10.0	25.0	3.8	-10.0	25.0	3.8	-10.0	37.0	5.7	-10.0	37.0	5.7
	-90	-20.0	20.0	3.1	-10.0	27.0	4.2	-10.0	27.0	4.2	-10.0	41.0	6.3	-10.0	41.0	6.3
	-100	-20.0	20.5	3.2	-10.0	28.0	4.3	-10.0	28.0	4.3	-10.0	43.0	6.6	-10.0	43.0	6.6

Table 4.7. Irrigation scheduling calendar in MZ4 based on growing stages and MZs distribution. h_{th}, is the possible pressure head threshold; h^* is the optimal pressure head threshold; $\Delta\theta$, is the irrigation required; τ, is the irrigation duration; Z_{tr}, is the trigger soil depth. Optimal irrigation scheduling are represented in bold.

		V0-V5			**V6-V10**			**V11-V15**			**VT**			**R1-R6**		
		Z_{tr} (cm) = 10			**Z_{tr} (cm) = 20**			**Z_{tr} (cm) = 20**			**Z_{tr} (cm) = 40**			**Z_{tr} (cm) = 40**		
	h_{th} (kPa)	**h^* (kPa)**	**$\Delta\theta$ (mm)**	**τ (h/d)**	**h^* (kPa)**	**$\Delta\theta$ (mm)**	**τ (h/d)**	**h^* (kPa)**	**$\Delta\theta$ (mm)**	**τ (h/d)**	**h^* (kPa)**	**$\Delta\theta$ (mm)**	**τ (h/d)**	**h^* (kPa)**	**$\Delta\theta$ (mm)**	**τ (h/d)**
MZ4	**0**							-	-	-	-	-	-	-	-	-
	-10							-	-	-	**-10.0**	**13.0**	**2.0**	**-10.0**	**13.0**	**2.0**
	-20							**-16.7**	**15.0**	**2.3**	-10.0	17.0	2.6	-10.0	17.0	2.6
	-30							-16.7	19.0	2.9	-10.0	25.0	3.8	-10.0	25.0	3.8
	-40							-16.7	21.0	3.2	-10.0	29.0	4.5	-10.0	29.0	4.5
	-50							-16.7	23.0	3.5	-10.0	33.0	5.1	-10.0	33.0	5.1
	-60							-16.7	23.0	3.5	-10.0	33.0	5.1	-10.0	33.0	5.1
	-70							-16.7	25.0	3.8	-10.0	37.0	5.7	-10.0	37.0	5.7
	-80							-16.7	27.0	4.2	-10.0	41.0	6.3	-10.0	41.0	6.3
	-90							-16.7	27.0	4.2	-10.0	41.0	6.3	-10.0	41.0	6.3
	-100							-16.7	29.0	4.5	-10.0	45.0	6.9	-10.0	45.0	6.9

Table 4.8. Optimal actual transpiration (OpT_a) and optimal water applied ($OpWA$) results compared with simulated actual transpiration (ST_a) and simulated water applied (SAW).

	OpT_a (mm)	OpT_a/ST_a (%)	$OpWA$ (mm)	$OpWA/SAW$ (%)
MZ1	405.6	8.0	525.5	-11.0
MZ2	405.6	4.8	517.8	-12.8
MZ3	107.5	23.9	217.5	-28.5
MZ4	271.7	52.6	350.2	-16.6

4.5. Conclusions

Spatial variability depends on different variables and parameters that complicate irrigation scheduling decisions. In addition, no single methodology for defining irrigation scheduling exists, nor one that is able to provide an overview of the whole system. In this work, we have improved irrigation scheduling in a maize field site where four different maize varieties were sown and where irrigation was applied with unifrom criteria. The improvement is based on MZ delineation with unsupervised $NDVI$ clustering. It is proved that this is the most optimal way to divide the field into different zones rather than by maize varieties. In this case, therefore, crop variety is not the only variable to consider when MZs are delineated; for instance, soil properties, soil tillage and crop genetics should also be taken into account. Furthermore, it is shown that MZs have a dynamic pattern, changing their extension and number during the growing season. In this case, the maximum number of MZs were 4; MZ1 and MZ2, where $NDVI$ values represent a normal crop performance, while MZ3 and MZ4 present anomalous low $NDVI$ measurements, which can be related with maize growth problems.

AW measurements are employed to demostrate that soil water conditions in MZ3 and MZ4 are different than those in MZ1 and MZ2. In the former case, it is shown that soil hydraulic properties represent a soil with higher water retention, and thus uniform and excessive irrigation (10.2 % more than the ET_c) lead to waterlogging. Furthermore, it is demostrated that a relationship exists between AW and $NDVI$ at each MZ, revealing that irrigation scheduling was not appropiate in MZ3 and MZ4. These measurements are also used to validate MZ delineation. In this case, S^2 results show that there is a gain in terms of uniformity when the field is divided into different MZs. Thus, water content sensors are able to validate and complement information provided by MZ delineation.

Hydrus 1-D has been employed in order to propose an appropiate irrigation scheduling for each MZ as well as to simulate “what if” scenarios,. The field experiment was first simulated

in order to validate the its own representation. The results show that a good agreement exists between AW and SAW, thereby showing that Hydrus 1-D provides a reasonable reproduction of the field experiment. With regard to the optimal irrigation results, we wish to stress that optimal irrigation strategies are also dynamic with MZ patterns. In all cases, optimal irrigation scheduling strategies are able to increase transpiration and save water when compared with experimental simulations. Moreover, there is a remarkable improvement in MZ3 and MZ4, where a 28.5 and 16.6 % volume of water is saved, while transpiration increases by 23.9 and 52.6 %, respectively. Simulation models therefore enable us to confirm that one of the issues in this field was the water logging occurring in MZ3 and MZ4, produced by the unifrom irrigation scheduling applied.

This work reports that irrigation scheduling can be improved by the correct combination of different methdologies that provide direct or indirect irrigation scheduling information. All of these methodologies are employed for different purposes and each one needs to be complemented by the others, thereby providing a full overview of the system as a whole.

.

Acknowledgements to project Low Input Sustainable Agriculture (LISA)
funded by RIS3CAT

Chapter 5

Conclusions

In this thesis irrigation scheduling has been improved by combining kinds of measurements from several methodologies and tools. Each of them has been used with the main goal to be employed for specific purposes and objectives. That is why that in this thesis concludes with:

- In our conditions and scenarios water content sensors were a more useful and accurate tool to monitor water content in an irrigated field than the remote sensing algorithm tested.
    - The DISPATCH algorithm provides poor spatial-temporal resolution. Furthermore, water content provided by DISPATCH algorithm represents the first 5 cm depth and not the water content in the root zone which is necessary to accurate schedule irrigation.
- When a simulation model has predictive capability, it is a powerful tool to optimize irrigation scheduling.
    - The methodology presented in chapter 3 optimizes irrigation and maximizes economic net margin. In addition, this methodology increases net margin resulting from traditional irrigation scheduling method.
    - Optimal irrigation scheduling depends on soil hydraulic properties of each field, because they modify water movement and how water is distributed through the root zone.
- In contrast to algorithms which measures water content using remote sensing data, in our field site, the crop cover remote sensing data provided powerful information for irrigation scheduling, specifically to determine field spatial variability and to delineate management zones in the agriculture field.
    - In our field site, management zones have a dynamic pattern during the growing season. This dynamics pattern has been validated with water content sensors, showing that when field is divided into different zones, available water spatial variability decreases rather than when the field is considered as a single zone.
    - The fact of existence of different management zones shows that irrigation scheduling must be readjusted to consider specific features of each management zone. In addition, irrigation scheduling might be dynamic. In

our field site, optimal irrigation scheduling strategy saves water and increases transpiration.

- Soil water status and the irrigation scheduling strategy conducted in the field site, directly affected crop status and its development. Thus, an optimal irrigation strategy and a correct soil water content monitoring is crucial to guarantee crop yield.

Finally, the authors of this thesis wants to conclude remarking that if irrigation scheduling should be improved, all methodologies employed in this thesis must be used together. Each one provides different kind of information but at the same time, all of them need the other to be complemented. Thus, irrigation scheduling cannot be improved using a single methodology because the point of view ultimate result is incompleted.

To conclude and considering FAO predictions, the significant projected increase in world population and the climate change scenario, the potential implication of this thesis is to determine how irrigation scheduling can become more sustainable, by increasing crop productivity, but at the same time saving water.

References

Abdi, H., Williams, L.J., 2013. Principal components analysis. Methods Mol. Biol. 930, 527–547. https://doi.org/10.1007/978-1-62703-059-5_22

Albergel, C., Rosnay, P. De, Gruhier, C., Muñoz-sabater, J., Hasenauer, S., Isaksen, L., Kerr, Y., Wagner, W., 2011. in Situ Observations.

Alberola, C., Lichtfouse, E., Navarrete, M., Debaeke, P., Souchère, V., 2008. Agronomy for sustainable development. Ital. J. Agron. 3, 77–78. https://doi.org/10.1051/agro

Allen, R.G., Pereira, L.S., Raes, D., Smith, M., Ab, W., 1998. Allen_FAO1998 1–15. https://doi.org/10.1016/j.eja.2010.12.001

Arbat, G., Olivé, F., Roselló, A., 2009. Distribución Del Agua En El Suelo En Riego Por Surcos Alternos Y No Alternos En El Cultivo De Maíz. Congreso.Cimne.Com IX, 1–8.

Arbat, G., Puig-Bargués, J., Barragán, J., Bonany, J., Ramírez de Cartagena, F., 2008. Monitoring soil water status for micro-irrigation management versus modelling approach. Biosyst. Eng. 100, 286–296. https://doi.org/10.1016/j.biosystemseng.2008.02.008

Arslan, S., Colvin, T.S., 2002. Grain Yield Mapping: Yield Sensing, Yield Reconstruction, and Errors. Precis. Agric. 135–154. https://doi.org/10.1023/A

Atkinson, P., Curran, P., 1997. Choosing an appropriate spatial resolution for remote sensing investigations. Photogramm. Eng. Remote Sens. 63, 1345–1351.

Bauer-Marschallinger, B., Freeman, V., Cao, S., Paulik, C., Schaufler, S., Stachl, T., Modanesi, S., Massari, C., Ciabatta, L., Brocca, L., Wagner, W., 2018. Toward Global Soil Moisture Monitoring With Sentinel-1: Harnessing Assets and Overcoming Obstacles. IEEE Trans. Geosci. Remote Sens. PP, 1–20. https://doi.org/10.1109/TGRS.2018.2858004

Bellvert, J., Zarco-Tejada, P.J., Girona, J., Fereres, E., 2014. Mapping crop water stress index in a 'Pinot-noir' vineyard: Comparing ground measurements with thermal remote sensing imagery from an unmanned aerial vehicle. Precis. Agric. 15, 361–376. https://doi.org/10.1007/s11119-013-9334-5

Biswas, A., 2014. Landscape characteristics influence the spatial pattern of soil water storage: Similarity over times and at depths. Catena 116, 68–77. https://doi.org/10.1016/j.catena.2013.12.004

Biswas, A., Si, B.C., 2011. Application of continuous wavelet transform in examining soil spatial variation: A review. Math. Geosci. 43, 379–396. https://doi.org/10.1007/s11004-011-9318-9

Bitar, A. Al, Leroux, D., Kerr, Y.H., Member, S., Merlin, O., Richaume, P., Sahoo, A., Wood, E.F., 2012. Evaluation of SMOS Soil Moisture Products Over Continental U . S . Using the SCAN / SNOTEL Network. IEEE Trans. Geosci. Remote Sens. 50, 1572–1586. https://doi.org/10.1109/TGRS.2012.2186581

Blonquist, J.M., Jones, S.B., Robinson, D.A., 2006. Precise irrigation scheduling for turfgrass using a subsurface electromagnetic soil moisture sensor. Agric. Water Manag. 84, 153–165. https://doi.org/10.1016/j.agwat.2006.01.014

Bogena, H.R., Huisman, J.A., Oberdörster, C., Vereecken, H., 2007. Evaluation of a low-cost soil water content sensor for wireless network applications. J. Hydrol. 344, 32–42. https://doi.org/10.1016/j.jhydrol.2007.06.032

Bosch, D.D., Lakshmi, V., Jackson, T.J., Choi, M., Jacobs, J.M., 2006. Large scale measurements of soil moisture for validation of remotely sensed data: Georgia soil moisture experiment of 2003. J. Hydrol. 323, 120–137. https://doi.org/10.1016/j.jhydrol.2005.08.024

Brocca, L., Tarpanelli, A., Filippucci, P., Dorigo, W., Zaussinger, F., Gruber, A., Fernández-prieto, D., 2018. Int J Appl Earth Obs Geoinformation How much water is used for irrigation ? A new approach exploiting coarse resolution satellite soil moisture products. Int J Appl Earth Obs Geoinf. 73, 752–766. https://doi.org/10.1016/j.jag.2018.08.023

Buckley, T.N., 2017. Modeling Stomatal Conductance. Plant Physiol. 174, 572–582. https://doi.org/10.1104/pp.16.01772

Budds, J., Hinojosa, L., 2012. Restructuring and rescaling water governance in mining contexts: The co-production of waterscapes in Peru. Water Altern. 5, 119–137.

Budyko, M.I., 1961. The Heat Balance of the Earth's Surface. Sov. Geogr. 2, 3–13. https://doi.org/10.1080/00385417.1961.10770761

Burt, C.M., Training, I., Obispo, S.L., 1996. Modern Water Control and Management Practices in Irrigation : Methodology and Criteria for Evaluating Table of Contents.

Burt, T.P., Butcher, D.P., 1985. Topographic controls of soil moisture distributions. J. Soil Sci. 36, 469–486. https://doi.org/10.1111/j.1365-2389.1985.tb00351.x

Campbell, C.S., Devices, D., 1986. Calibrating ECH 2 O Soil Moisture Probes 2–4.

Campbell, G., 1982. campbell 1986.pdf. Academic Press, New York.

Carlson, T., 2007. An overview of the "triangle method" for estimating surface evapotranspiration and soil moisture from satellite imagery. Sensors 7, 1612–1629. https://doi.org/10.3390/s7081612

Chauhan, N.S., Miller, S., Ardanuy, P., 2003. Spaceborne soil moisture estimation at high resolution: A microwave-optical/IR synergistic approach. Int. J. Remote Sens. 24, 4599–4622. https://doi.org/10.1080/0143116031000156837

Clarke Topp, G., Reynolds, W.D., 1998. Time domain reflectometry: A seminal technique for measuring mass and energy in soil. Soil Tillage Res. 47, 125–132. https://doi.org/10.1016/S0167-1987(98)00083-X

Clothier, B.E., Green, S.R., 1994. Rootzone processes and the efficient use of irrigation water. Agric. Water Manag. 25, 1–12. https://doi.org/10.1016/0378-

3774(94)90048-5

Colman, E.A., 1947. A Laboratory Procdure for Determining the Field Capacity of Soils. Soil Sci. https://doi.org/10.1097/00010694-194704000-00003

Cosh, M.H., Jackson, T.J., Bindlish, R., Prueger, J.H., 2004. Watershed scale temporal and spatial stability of soil moisture and its role in validating satellite estimates. Remote Sens. Environ. 92, 427–435. https://doi.org/10.1016/j.rse.2004.02.016

Cosh, M.H., Jackson, T.J., Starks, P., Heathman, G., 2006. Temporal stability of surface soil moisture in the Little Washita River watershed and its applications in satellite soil moisture product validation. J. Hydrol. 323, 168–177. https://doi.org/10.1016/j.jhydrol.2005.08.020

Curran, P.J., 1988. The semivariogram in remote sensing: An introduction. Remote Sens. Environ. 24, 493–507. https://doi.org/10.1016/0034-4257(88)90021-1

Dabach, S., Lazarovitch, N., Šimůnek, J., Shani, U., 2013. Numerical investigation of irrigation scheduling based on soil water status. Irrig. Sci. 31, 27–36. https://doi.org/10.1007/s00271-011-0289-x

Das, N.N., Mohanty, B.P., 2006. Root Zone Soil Moisture Assessment Using Remote Sensing and Vadose Zone Modeling. Vadose Zo. J. 5, 296. https://doi.org/10.2136/vzj2005.0033

de Lima, R.S.N., de Assis Figueiredo, F.A.M.M., Martins, A.O., de Deus, B.C. da S., Ferraz, T.M., Gomes, M. de M. de A., de Sousa, E.F., Glenn, D.M., Campostrini, E., 2015. Partial rootzone drying (PRD) and regulated deficit irrigation (RDI) effects on stomatal conductance, growth, photosynthetic capacity, and water-use efficiency of papaya. Sci. Hortic. (Amsterdam). 183, 13–22. https://doi.org/10.1016/j.scienta.2014.12.005

de Oliveira, R.A., Ramos, M.M., de Aquino, L.A., 2015. Irrigation management, Sugarcane: Agricultural Production, Bioenergy and Ethanol. Elsevier Inc. https://doi.org/10.1016/B978-0-12-802239-9.00008-6

Dean, T.J., Bell, J.P., Baty, A.J.B., 1987. Soil moisture measurement by an improved capacitance technique, Part I. Sensor design and performance. J. Hydrol. 93, 67–78. https://doi.org/10.1016/0022-1694(87)90194-6

DeJonge, K.C., Taghvaeian, S., Trout, T.J., Comas, L.H., 2015. Comparison of canopy temperature-based water stress indices for maize. Agric. Water Manag. 156, 51–62. https://doi.org/10.1016/j.agwat.2015.03.023

Delwart, S., Bouzinac, C., Wursteisen, P., Berger, M., Drinkwater, M., Martín-Neira, M., Kerr, Y.H., 2008. SMOS validation and the COSMOS campaigns. IEEE Trans. Geosci. Remote Sens. 46, 695–703. https://doi.org/10.1109/TGRS.2007.914811

Denmead, O.T., Shaw, R.H., 1962. Availability of Soil Water to Plants as Affected by Soil Moisture Content and Meteorological Conditions1. Agron. J. 54, 385. https://doi.org/10.2134/agronj1962.00021962005400050005x

Dillon, M.E., Collini, E.A., Ferreira, L.J., 2016. Sensitivity of WRF short-term forecasts to different soil moisture initializations from the GLDAS database over South America in March 2009. Atmos. Res. 167, 196–207. https://doi.org/10.1016/j.atmosres.2015.07.022

Döll, P., 2002. Impact of climate change and variability on irrigation requirements: a global prespective. Clim. Change 54, 269–293.

Doorenbos, J., Pruitt, W.O., 1975. Guidelines for Predicting Crop Water Requirements. Irrig. Drain. Pap. No. 24, FAO.

Dudley, N.J., Howell, D.T., Musgrave, W.F., 1971. Optimal Intraseasonal Irrigation Water Allocation. Water Resour. Res. 7, 770–788. https://doi.org/10.1029/WR007i004p00770

Escorihuela, M.J., Quintana-Seguí, P., 2016. Comparison of remote sensing and simulated soil moisture datasets in Mediterranean landscapes. Remote Sens. Environ. 180, 99–114. https://doi.org/10.1016/j.rse.2016.02.046

Evans, R.G., LaRue, J., Stone, K.C., King, B.A., 2013. Adoption of site-specific variable rate sprinkler irrigation systems. Irrig. Sci. 31, 871–887. https://doi.org/10.1007/s00271-012-0365-x

Fares, A., Polyakov, V., 2006. Advances in Crop Water Management Using Capacitive Water Sensors. Adv. Agron. 90, 43–77. https://doi.org/10.1016/S0065-2113(06)90002-9

Feddes, R.A., Bresler, E., Neuman, S., 1974. Field test of a modified numerical model for water uptake by roots systems. Water Resour. 10.

Feddes, R.A., Kowalik, P.J., Zaradny, H., 1978. Simulation of Field Water Use and Crop Yield. Simulation Monograph 308.

Ferrarezi, R.S., Dove, S.K., Van Iersel, M.W., 2015. An automated system for monitoring soil moisture and controlling irrigation using low-cost open-source microcontrollers. Horttechnology 25, 110–118.

Flexas, J., Bota, J., Cifre, J., Escalona, J.M., Galmés, J., Gulías, J., Lefi, E.K., Martínez-Cañellas, S.F., Moreno, M.T., Ribas-Carbó, M., Riera, D., Sampol, B., Medrano, H., 2004. Understanding down-regulation of photosynthesis under water stress: Future prospects and searching for physiological tools for irrigation management. Ann. Appl. Biol. 144, 273–283. https://doi.org/10.1111/j.1744-7348.2004.tb00343.x

Fontanet, M., Fernàndez-garcia, D., Ferrer, F., 2018a. The value of satellite remote sensing soil moisture data and the DISPATCH algorithm in irrigation fields. Hydrol. Earth Syst. Sci. https://doi.org/https://doi.org/10.5194/hess-2018-94

Fontanet, M., D. Fernàndez-Garcia, G. Rodrigo, F. Ferrer, J.M. Villar. Combined simulation and optimization framework for irrigation scheduling in agriculture fields. (Vadose Zone Journal submitted).

Fraisse, C.W., Sudduth, K.A., Kitchen, N.R., 2001. Delineation of Site-Specific management Zones by Unsupervised Classification of Topographic Atributes and Soil Electrical

Conductivity. Am. Soc. Agric. Eng. 155 44, 155–166. https://doi.org/10.1117/12.840574

Fu, B. and H.G., 1994. Land evaluations in an areaof severe erosion: the loess plateau of China. L. Degrad. Rehabil.l. Degrad. Rehabil. 5:33-40, 33–40.

Gardner, W. H.: Water content, in: Methods of Soil Analyses, edited by: Klute, A., Agronomy Monograph 9, ASA, Madison, WI, 493–541, 1986.

Gardener, W.R., 1960. Dynamic aspects of water availability to plants. Soil Sci. 89, 63–73.

Garkusha, I.N., Hnatushenko, V. V., Vasyliev, V. V., 2017. Using Sentinel-1 data for monitoring of soil moisture. 2017 IEEE Int. Geosci. Remote Sens. Symp. 1656–1659. https://doi.org/10.1109/IGARSS.2017.8127291

Gee, G.W. and Bauder, J.W. (1986) Particle-Size Analysis. In: Klute, A., Ed., Methods of Soil Analysis, Part 1. Physical and Mineralogical Methods, Agronomy Monograph No. 9, 2nd Edition, American Society of Agronomy/Soil Science Society of America, Madison, WI, 383-411.

Georgi, C., Spengler, D., Itzerott, S., Kleinschmit, B., 2018. Automatic delineation algorithm for site-specific management zones based on satellite remote sensing data. Precis. Agric. 19, 684–707. https://doi.org/10.1007/s11119-017-9549-y

Girona, J., Mata, M., Del Campo, J., Arbonés, A., Bartra, E., Marsal, J., 2006. The use of midday leaf water potential for scheduling deficit irrigation in vineyards. Irrig. Sci. 24, 115–127. https://doi.org/10.1007/s00271-005-0015-7

Gonçalves, J.M., Pereira, L.S., Fang, S.X., Dong, B., 2007. Modelling and multicriteria analysis of water saving scenarios for an irrigation district in the upper Yellow River Basin. Agric. Water Manag. 94, 93–108. https://doi.org/10.1016/j.agwat.2007.08.011

Haghverdi, A., Leib, B.G., Washington-Allen, R.A., Ayers, P.D., Buschermohle, M.J., 2015. Perspectives on delineating management zones for variable rate irrigation. Comput. Electron. Agric. 117, 154–167. https://doi.org/10.1016/j.compag.2015.06.019

Hall, A.W., 1999. Priorities for irrigated agriculture. Agric. Water Manag. 40, 25–29. https://doi.org/10.1016/S0378-3774(98)00099-7

Hanjra, M.A., Blackwell, J., Carr, G., Zhang, F., Jackson, T.M., 2012. Wastewater irrigation and environmental health: Implications for water governance and public policy. Int. J. Hyg. Environ. Health 215, 255–269. https://doi.org/10.1016/j.ijheh.2011.10.003

Hanson, B.R., Orloff, S., Peters, D., 1977. Monitorina soil moisture hebs refine irriaation manaaement 54.

Harabasz, J., Scroll, P., For, D., 1974. Communications in Statistics A dendrite method for cluster analysis. Commun. Stat. 1, 37–41. https://doi.org/10.1080/03610927408827101

Hawley, 1983. Journal of Hydrology, 62 (1983) 179--200. J. Hydrol. 62, 179–200. https://doi.org/10.1016/0022-1694(83)90102-6

Holzman, M.E., Rivas, R., Piccolo, M.C., 2014. International Journal of Applied Earth Observation and Geoinformation Estimating soil moisture and the relationship with crop yield using surface temperature and vegetation index 28, 181–192.

Hoppula, K.I., Salo, T.J., 2007. Tensiometer-based irrigation scheduling in perennial strawberry cultivation. Irrig. Sci. 25, 401–409. https://doi.org/10.1007/s00271-006-0055-7

Hornacek, M., Wagner, W., Sabel, D., Truong, H.-L., Snoeij, P., Hahmann, T., Diedrich, E., Doubkova, M., 2012. Potential for High Resolution Systematic Global Surface Soil Moisture Retrieval via Change Detection Using Sentinel-1. IEEE J. Sel. Top. Appl. Earth Obs. Remote Sens. 5, 1303–1311. https://doi.org/10.1109/JSTARS.2012.2190136

Huang, J., Hartemink, A.E., Arriaga, F., Chaney, N.W., 2019. Unraveling location-specific and time-dependent interactions between soil water content and environmental factors in cropped sandy soils using Sentinel-1 and moisture probes. J. Hydrol. 575, 780–793. https://doi.org/10.1016/j.jhydrol.2019.05.075

Huber, B., 1928. Weitere quantitative Untersuchungen über das Wasserleitungssystem der Pflanzen.

Inman, D., Khosla, R., Reich, R., Westfall, D.G., 2008. Normalized difference vegetation index and soil color-based management zones in irrigated maize. Agron. J. 100, 60–66. https://doi.org/10.2134/agronj2007.0020

Irmak, S., Haman, D.Z., Bastug, R., 2000. Determination of crop water stress index for irrigation timing and yield estimation of corn. Agron. J. 92, 1221–1227. https://doi.org/10.2134/agronj2000.9261221x

Jackson, T.J., Cosh, M.H., Bindlish, R., Starks, P.J., Bosch, D.D., Seyfried, M., Goodrich, D.C., Moran, M.S., Du, J., 2010. Validation of advanced microwave scanning radiometer soil moisture products. IEEE Trans. Geosci. Remote Sens. 48, 4256–4272. https://doi.org/10.1109/TGRS.2010.2051035

Jackson, T.J., Schugge, J., Engman, E.T., 1996. Remote sensing applications to hydrology: soil moisture. Hydrol. Sci. J. 41, 517–530. https://doi.org/10.1080/02626669609491523

Jones, H.G., 2004. Irrigation scheduling: Advantages and pitfalls of plant-based methods. J. Exp. Bot. 55, 2427–2436. https://doi.org/10.1093/jxb/erh213

Jones, H.G., 1999. Use of infrared thermometry for estimation of stomatal conductance as a possible aid to irrigation scheduling. Agric. For. Meteorol. 95, 139–149. https://doi.org/10.1016/S0168-1923(99)00030-1

Kassie, B.T., Kimball, B.A., Jamieson, P.D., Bowden, J.W., Sayre, K.D., Groot, J.J.R., Pinter, P.J., Lamorte, R.L., Hunsaker, D.J., Wall, G.W., Leavitt, S.W., 2018. Field experimental data for crop modeling of wheat growth response to nitrogen fertilizer , elevated CO 2 , water stress , and high temperature 4, 9–15.

Kerr, Y.H., Waldteufel, P., Richaume, P., Wigneron, J.P., Ferrazzoli, P., Mahmoodi, A., Bitar, A. Al, Cabot, F., Gruhier, C., Juglea, S.E., Leroux, D., Mialon, A., Delwart, S., 2012. The SMOS Soil Moisture Retrieval Algorithm. Geosci. Remote Sens. 50, 1384–1403. https://doi.org/10.1109/TGRS.2012.2184548

Kerr, Y.H., Waldteufel, P., Wigneron, J., Delwart, S., Cabot, F., Font, J., Reul, N., Boutin, J., Gruhier, C., Juglea, S.E., Drinkwater, M.R., Mecklenburg, S., Hahne, A., Martı, M., 2010. The SMOS Mission : New Tool for Monitoring Key Elements of the Global Water Cycle 98.

Kerr, Y.H., Waldteufel, P., Wigneron, J.P., Martinuzzi, J.M., Font, J., Berger, M., 2001. Soil moisture retrieval from space: The Soil Moisture and Ocean Salinity (SMOS) mission. IEEE Trans. Geosci. Remote Sens. 39, 1729–1735. https://doi.org/10.1109/36.942551

Koestel, J.K., Norgaard, T., Luong, N.M., Vendelboe, A.L., Moldrup, P., Jarvis, N.J., Lamandé, M., Iversen, B. V., Wollesen De Jonge, L., 2013. Links between soil properties and steady-state solute transport through cultivated topsoil at the field scale. Water Resour. Res. 49, 790–807. https://doi.org/10.1002/wrcr.20079

Koriche, S.A., Rientjes, T.H.M., 2016. Application of satellite products and hydrological modelling for flood early warning. Phys. Chem. Earth 93, 12–23. https://doi.org/10.1016/j.pce.2016.03.007

Koster, R.D., Suarez, M.J., 2001. Soil Moisture Memory in Climate Models. J. Hydrometeorol. 2, 558–570. https://doi.org/10.1175/1525-7541(2001)002<0558:SMMICM>2.0.CO;2

Kruskal, W.H., Wallis, W.A., 1952. Use of Ranks in One-Criterion Variance Analysis Author (s): William H . Kruskal and W . Allen Wallis Published by : Taylor & Francis , Ltd . on behalf of the American Statistical Association Stable URL : http://www.jstor.org/stable/2280779 Accessed : 02. M J. Am. Stat. Assoc. 47, 583–621. https://doi.org/10.1002/med

Le Roux, X., Bariac, T., Mariotti, a, 1995. Spatial partitioning of the soil water resoucre between grasses and shrub compnents in a west African humid savanna. Oecologia 104, 145–155. https://doi.org/10.1007/BF00328579

Lehmann, P., Assouline, S., Or, D., 2008. Characteristic lengths affecting evaporative drying of porous media. Phys. Rev. E - Stat. Nonlinear, Soft Matter Phys. 77, 1–16. https://doi.org/10.1103/PhysRevE.77.056309

Liang, X., Liakos, V., Wendroth, O., Vellidis, G., 2016. Scheduling irrigation using an approach based on the van Genuchten model. Agric. Water Manag. 176, 170–179. https://doi.org/10.1016/j.agwat.2016.05.030

Lievens, H., Tomer, S.K., Al Bitar, A., De Lannoy, G.J.M., Drusch, M., Dumedah, G., Hendricks Franssen, H.J., Kerr, Y.H., Martens, B., Pan, M., Roundy, J.K., Vereecken, H., Walker, J.P., Wood, E.F., Verhoest, N.E.C., Pauwels, V.R.N., 2015. SMOS soil moisture assimilation for improved hydrologic simulation in the Murray Darling Basin, Australia. Remote Sens. Environ. 168, 146–162. https://doi.org/10.1016/j.rse.2015.06.025

Linker, R., Ioslovich, I., Sylaios, G., Plauborg, F., Battilani, A., 2016. Optimal model-based deficit irrigation scheduling using AquaCrop: A simulation study with cotton, potato and tomato. Agric. Water Manag. 163, 236–243. https://doi.org/10.1016/j.agwat.2015.09.011

Liu, H., Whiting, M.L., Ustin, S.L., Zarco-Tejada, P.J., Huffman, T., Zhang, X., 2018. Maximizing the relationship of yield to site-specific management zones with object-oriented segmentation of hyperspectral images. Precis. Agric. 19, 348–364. https://doi.org/10.1007/s11119-017-9521-x

Long, D.S., Whitmus, J.D., Engel, R.E., Brester, G.W., 2015. Net returns from terrain-based variable-rate nitrogen management on dryland spring wheat in Northern Montana. Agron. J. 107, 1055–1067. https://doi.org/10.2134/agronj14.0331

Ma, Y., Feng, S., Song, X., 2015. Evaluation of optimal irrigation scheduling and groundwater recharge at representative sites in the North China Plain with SWAP model and field experiments. Comput. Electron. Agric. 116, 125–136. https://doi.org/10.1016/j.compag.2015.06.015

Maas, E.V., Hoffman, G.., 1977. Crop salt tolerance—current assessment. J. Irrig. Drain. 103, 115–134.

Mailhol, J.C., Ruelle, P., Walser, S., Schütze, N., Dejean, C., 2011. Analysis of AET and yield predictions under surface and buried drip irrigation systems using the Crop Model PILOTE and Hydrus-2D. Agric. Water Manag. 98, 1033–1044. https://doi.org/10.1016/j.agwat.2011.01.014

Malbéteau, Y., Merlin, O., Molero, B., Rüdiger, C., Bacon, S., 2015. DisPATCh as a tool to evaluate coarse-scale remotely sensed soil moisture using localized in situ measurements: Application to SMOS and AMSR-E data in Southeastern Australia. Int. J. Appl. Earth Obs. Geoinf. 45, 221–234. https://doi.org/10.1016/j.jag.2015.10.002

Martínez-Casasnovas, J., Escolà, A., Arnó, J., 2018. Use of Farmer Knowledge in the Delineation of Potential Management Zones in Precision Agriculture: A Case Study in Maize (Zea mays L.). Agriculture 8, 84. https://doi.org/10.3390/agriculture8060084

Martínez-Romero, A., Martínez-Navarro, A., Pardo, J.J., Montoya, F., Domínguez, A., 2017. Real farm management depending on the available volume of irrigation water (part II): Analysis of crop parameters and harvest quality. Agric. Water Manag. 192, 58–70. https://doi.org/10.1016/j.agwat.2017.06.021

Martini, E., Wollschläger, U., Musolff, A., Werban, U., Zacharias, S., 2017. Principal component analysis of the spatiotemporal pattern of soil moisture and apparent electrical conductivity. Vadose Zo. J. 16. https://doi.org/10.2136/vzj2016.12.0129

Mattia, F., Satalino, G., Balenzano, A., Rinaldi, M., Steduto, P., Moreno, J., 2015. SENTINEL-1 FOR WHEAT MAPPING AND SOIL MOISTURE RETRIEVAL. IGARSS 2, 2832–2835.

Merlin, O., Chehbouni, G., Walker, J.P., Panciera, R., Kerr, Y.H., Merlin, O., Chehbouni, G., Walker, J.P., Panciera, R., Kerr, Y.H.A., 2008. A simple methods for downscaling passive microwave based soil moisture Passive microwave soil moisture

downscaling using evaporative fraction Olivier Merlin Abdelghani Chehbouni Jeffrey P . Walker Rocco Panciera Yann Kerr Centre d ' Etudes Spatiales de la. IEEE Geosci. Remote Sens. Lett. 46, 786–769.

Merlin, O., Jacob, F., Wigneron, J.P., Walker, J., Chehbouni, G., 2012. Multidimensional disaggregation of land surface temperature using high-resolution red, near-infrared, shortwave-infrared, and microwave-L bands. IEEE Trans. Geosci. Remote Sens. 50, 1864–1880. https://doi.org/10.1109/TGRS.2011.2169802

Merlin, O., Malbéteau, Y., Notfi, Y., Bacon, S., Er-raki, S., 2015. Performance Metrics for Soil Moisture Downscaling Methods : Application to DISPATCH Data in Central Morocco 3783–3807. https://doi.org/10.3390/rs70403783

Merlin, O., Stefan, V., Malbéteau, Y., Escorihuela, M.-J., Rüdiger, C., Jarlan, L., 2013. Data disaggregation and evapotranspiration modeling: a synergism between multi-spectral/multi-resolution remote sensing data. Am. Geophys. Union.

Molero, B., Merlin, O., Malbéteau, Y., Al Bitar, A., Cabot, F., Stefan, V., Kerr, Y., Bacon, S., Cosh, M.H., Bindlish, R., Jackson, T.J., 2016. SMOS disaggregated soil moisture product at 1 km resolution: Processor overview and first validation results. Remote Sens. Environ. 180, 361–376. https://doi.org/10.1016/j.rse.2016.02.045

Moran, M.S., T.R., C., Inoue, Y., Vidal, A., 1994. Estimating crop water defficiency using the relation between surface minus air temperature and spectral vegetation index. Remote Sens. Environ. 49, 246–263. https://doi.org/10.1016/0034-4257(94)90020-5

Narayan, U., Lakshmi, V., and Jackson, T. J.: High resolution estimation of soil moisture using L-band radiometer and radar observations made during trhe SMEX02 experiments, IEEE T. Geosci. Remote, 44, 1545–1554, 2006.

Nelson, D.W and Sommers, L.E. (1996). Methods of Soil Analysis. Part 3. Chemical Methods. Soil Science Society of America Book Series no.5, pp. 961-1010.

Neuman, S., Feddes, Bresler, E., 1974. Finite element simulation of flow in saturated-unsaturated soils considering water uptake by plants, Third Annual Report, Project No A10-SWC-77. Hydraul. Eng. Lab. 231–237.

Nielsen, P.J.G.Y.K.S.D.R., 1985. (1985) Spatial Variability of Field-measured Soil-water Characteristics 49, 215–260.

Nobel, P.S., 1983. Biophysical Plant Physiology and Ecology.

Noory, H., Liaghat, A.M., Parsinejad, M., Haddad, O.B., 2011. Optimizing Irrigation Water Allocation and Multicrop Planning Using Discrete PSO Algorithm. J. Irrig. Drain. Eng. 138, 437–444. https://doi.org/10.1061/(asce)ir.1943-4774.0000426

Ochsner, et al., 2013. State of the art in large-scale soil moisture monitoring. Soil Sci. Soc. Am. Journal, Soil Sci. Soc. Am.

Odeh, I.O.A., McBratney, A.B., Chittleborough, D.J., 2010. Soil Pattern Recognition with Fuzzy-c-means: Application to Classification and Soil-Landform Interrelationships.

Soil Sci. Soc. Am. J. 56, NP. https://doi.org/10.2136/sssaj1992.03615995005600020050x

Ortega, J.F., De Juan, J.A., Tarjuelo, J.M., 2004. Evaluation of the water cost effect on water resource management: Application to typical crops in a semiarid region. Agric. Water Manag. 66, 125–144. https://doi.org/10.1016/j.agwat.2003.10.005

Paloscia, S., Pettinato, S., Santi, E., Notarnicola, C., Pasolli, L., Reppucci, A., 2013. Soil moisture mapping using Sentinel-1 images: Algorithm and preliminary validation. Remote Sens. Environ. 134, 234–248. https://doi.org/10.1016/j.rse.2013.02.027

Pereira, L.S., Gonçalves, J.M., Dong, B., Mao, Z., Fang, S.X., 2007. Assessing basin irrigation and scheduling strategies for saving irrigation water and controlling salinity in the upper Yellow River Basin, China. Agric. Water Manag. 93, 109–122. https://doi.org/10.1016/j.agwat.2007.07.004

Pereira, L.S., Oweis, T., Zairi, A., Santos, L., 2002. Irrigation management under water scarcity. Agric. Water Manag. 57, 175–206. https://doi.org/10.1016/S0378-3774(02)00075-6

Pereira, L.S., Paredes, P., Sholpankulov, E.D., Inchenkova, O.P., Teodoro, P.R., Horst, M.G., 2009. Irrigation scheduling strategies for cotton to cope with water scarcity in the Fergana Valley, Central Asia. Agric. Water Manag. 96, 723–735. https://doi.org/10.1016/j.agwat.2008.10.013

Perry, C., 2011. Accounting for water use: Terminology and implications for saving water and increasing production. Agric. Water Manag. 98, 1840–1846. https://doi.org/10.1016/j.agwat.2010.10.002

Phene, C.J., Howell, T.A., 1984. of High-Frequency Irrigation Systems.

Philip, J.R., 1966. Plant Water Relations: Some Physical Aspects. Annu. Rev. Plant Physiol. 17, 245–268. https://doi.org/10.1146/annurev.pp.17.060166.001333

Philip, J.R., 1956. Evaporation, and soil moisture and heat fields in the soil. J. Meteorol. 14, 354–366.

Pitts, D., Peterson, K., Gilbert, G., Fastenau, R., 1996. Field assessment of irrigation system performance. Appl. Eng. Agric. 12, 307–313.

Playán, E., Faci, J.., Bensaci, A., Slatni, A., 2000. A case study for irrigation modernisation. Agric. Water Manag. 42, 313–334. https://doi.org/10.1016/s0378-3774(99)00045-1

Pyrcz, M., Deutsch, C., 2003. The whole story on the hole effect. Geostatistical Assoc. Australas. Newsl. 18 18, 18.

Quebrajo, L., Perez-Ruiz, M., Pérez-Urrestarazu, L., Martínez, G., Egea, G., 2018. Linking thermal imaging and soil remote sensing to enhance irrigation management of sugar beet. Biosyst. Eng. 165, 77–87. https://doi.org/10.1016/j.biosystemseng.2017.08.013

Radcliffe, D., Simunek, J., 2010. Soil Physics with Hydrus. Modelling and Application.

Raes, D., Steduto, P., Hsiao, T.C., Fereres, E., 2010. AquaCrop - Reference Manual, Version 3.1.

Reca, J., Roldán, J., Alcaide, M., 2001. Optimisation model for water allocation in deficit irrigation systems: I. Description of the model. Agric. water … 48, 103–116.

Reyes, J., Wendroth, O., Matocha, C., Zhu, J., 2019. Delineating Site-Specific Management Zones and Evaluating Soil Water Temporal Dynamics in a Farmer's Field in Kentucky. Vadose Zo. J. 18, 0. https://doi.org/10.2136/vzj2018.07.0143

Ribas-carbo, M., Flexas, J., Bota, J., Galme, J., 2006. or. Physiol. Plant. 127, 343–352. https://doi.org/10.1111/j.1399-3054.2005.00621.x

Richards, L.A., 1944. Moisture Retention by Some Irrigated Soils as Related to Soil-Moisture Tension. J. Agric. Res. 69, 215–235.

Richards, L.A., 1931. Capillary conduction of liquids through porous mediums. J. Appl. Phys. 1, 318–333. https://doi.org/10.1063/1.1745010

Ritchie, J.T., 1972. Model for Predicting Evaporation from a Row Crop with Incomplete Cover. Water Resour. Res. 8, 1204–1213.

Ritchie, S.W., Hanway, J.J., Benson, G.O., 1997. How a corn plant develops.; Spec. Publ. 48.

Robock, A., Vinnikov, K.Y., Srinivasan, G., Entin, J.K., Hollinger, S.E., Speranskaya, N.A., Liu, S., Namkhai, A., 2000. The Global Soil Moisture Data Bank. Bull. Am. Meteorol. Soc. 81, 1281–1299. https://doi.org/10.1175/1520-0477(2000)081<1281:TGSMDB>2.3.CO;2

Romanyà, J., Rovira, P., 2011. An appraisal of soil organic C content in Mediterranean agricultural soils. Soil Use Manag. 27, 321–332. https://doi.org/10.1111/j.1475-2743.2011.00346.x

Rouse, R.W.H., Haas, J.A.W., Deering, D.W., 1974. Monitoring Vegetation Systems in the Great Plains with ERTS. Third Earth Resour. Technol. Satell. Symp. Vol. I Tech. Present. NASA SP-351 309–317.

Sakthivadivel, R., Merrey, D.J., Fernando, N., 1993. Cumulative relative water supply: A methodology for assessing irrigation system performance. Irrig. Drain. Syst. 7, 43–67. https://doi.org/10.1007/BF00880908

Saxton, K.E., Rawls, W.J., 2006. Soil Water Characteristic Estimates by Texture and Organic Matter for Hydrologic Solutions. Soil Sci. Soc. Am. J. 70, 1569. https://doi.org/10.2136/sssaj2005.0117

Schaap, M.G., Leij, F.J., Van Genuchten, M.T., 2001. Rosetta: A computer program for estimating soil hydraulic parameters with hierarchical pedotransfer functions. J. Hydrol. 251, 163–176. https://doi.org/10.1016/S0022-1694(01)00466-8

Schaap, M.G., Robinson, D. a., Friedman, S.P., Lazar, a., 2003. Measurement and Modeling

of the TDR Signal Propagation through Layered Dielectric Media. Soil Sci. Soc. Am. J. 67, 1113. https://doi.org/10.2136/sssaj2003.1113

Schelle, H., Heise, L., Jänicke, K., Durner, W., 2013. Water retention characteristics of soils over the whole moisture range: A comparison of laboratory methods. Eur. J. Soil Sci. 64, 814–821. https://doi.org/10.1111/ejss.12108

Schenatto, K., Souza, E.G., Bazzi, C.L., Beneduzzi, H.M., 2015. Management Zones with NDVI Data through Corn and Soybean Yield. First Conf. Prox. Sens. Support. Precis. Agric. https://doi.org/10.3997/2214-4609.201413856

Schepers, A.R., Shanahan, J.F., Liebig, M.A., Schepers, J.S., Johnson, S.H., Luchiari, A., 2004. Appropriateness of Management Zones for Characterizing Spatial Variability of Soil Properties and Irrigated Corn Yields across Years. Agron. J. 96, 195–203.

Scudiero, E., Teatini, P., Corwin, D.L., Dal Ferro, N., Simonetti, G., Morari, F., 2014. Spatiotemporal response of maize yield to edaphic and meteorological conditions in a saline farmland. Agron. J. 106, 2163–2174. https://doi.org/10.2134/agronj14.0102

Scudiero, E., Teatini, P., Corwin, D.L., Deiana, R., Berti, A., Morari, F., 2013. Delineation of site-specific management units in a saline region at the Venice Lagoon margin, Italy, using soil reflectance and apparent electrical conductivity. Comput. Electron. Agric. 99, 54–64. https://doi.org/10.1016/j.compag.2013.08.023

Scudiero, E., Teatini, P., Manoli, G., Braga, F., Skaggs, T., Morari, F., 2018. Workflow to Establish Time-Specific Zones in Precision Agriculture by Spatiotemporal Integration of Plant and Soil Sensing Data. Agronomy 8, 253. https://doi.org/10.3390/agronomy8110253

Segovia-Cardozo, D.A., Rodríguez-Sinobas, L., Zubelzu, S., 2019. Water use efficiency of corn among the irrigation districts across the Duero river basin (Spain): Estimation of local crop coefficients by satellite images. Agric. Water Manag. 212, 241–251. https://doi.org/10.1016/j.agwat.2018.08.042

Shanahan, J.F., Kitchen, N.R., Raun, W.R., Schepers, J.S., 2008. Responsive in-season nitrogen management for cereals. Comput. Electron. Agric. 61, 51–62. https://doi.org/10.1016/j.compag.2007.06.006

Simunek, J., Sejna, M., 2014. HYDRUS User manual, Version 2.

Šimůnek, J., van Genuchten, M.T., Šejna, M., 2016. Recent Developments and Applications of the HYDRUS Computer Software Packages. Vadose Zo. J. 15, 0. https://doi.org/10.2136/vzj2016.04.0033

Šimůnek, J., van Genuchten, M.T., Šejna, M., 2008. Development and Applications of the HYDRUS and STANMOD Software Packages and Related Codes. Vadose Zo. J. 7, 587. https://doi.org/10.2136/vzj2007.0077

Singh, R., Jhorar, R.K., van Dam, J.C., Feddes, R.A., 2006. Distributed ecohydrological modelling to evaluate irrigation system performance in Sirsa district, India II: Impact

of viable water management scenarios. J. Hydrol. 329, 714–723. https://doi.org/10.1016/j.jhydrol.2006.03.016

Siyal, A.A., Skaggs, T.H., 2009. Measured and simulated soil wetting patterns under porous clay pipe sub-surface irrigation. Agric. Water Manag. 96, 893–904. https://doi.org/10.1016/j.agwat.2008.11.013

Skaggs, T.H., Trout, T.J., Rothfuss, Y., 2010. Drip Irrigation Water Distribution Patterns: Effects of Emitter Rate, Pulsing, and Antecedent Water. Soil Sci. Soc. Am. J. 74, 1886. https://doi.org/10.2136/sssaj2009.0341

Soentoro, E.A., Perwira, E., Suryadi, Y., 2018. Optimization of irrigation water use to increase the benefit of agricultural products 01026, 1–6.

Starr, J. L. and Paltineanu, I. C.: Methods for Measurement of Soil Water Content: Capacitance Devices, in: Dane, J. H. and Topp, G. C., Methods of Soil Analysis: Part 4 Physical Methods, Soil Science Society of America, Inc., Soil Science Society of America, Inc., 463–474, 2002.

Stewart, J.I., Hagan, R.M., Pruitt, W.O., Hanks, R.J., Riley, P., J., Danielson, R.E., Franklin, W.T., Jackson, E.B., 1977. Optimising crop production through control Report, of water and salinity levels in the soil.

Sun, H.Y., Liu, C.M., Zhang, X.Y., Shen, Y.J., Zhang, Y.Q., 2006. Effects of irrigation on water balance, yield and WUE of winter wheat in the North China Plain. Agric. Water Manag. 85, 211–218. https://doi.org/10.1016/j.agwat.2006.04.008

Thompson, R.B., Gallardo, M., Valdez, L.C., Fernández, M.D., 2007. Using plant water status to define threshold values for irrigation management of vegetable crops using soil moisture sensors. Agric. Water Manag. 88, 147–158. https://doi.org/10.1016/j.agwat.2006.10.007

Topp, G.C., Davis, J.L., Annan, A.P., 1980. Electromagnetic Determination of Soil Water Content: Measruements in Coaxial Transmission Lines. Water Resour. Res. 16, 574–582. https://doi.org/10.1029/WR016i003p00574

Toureiro, C., Serralheiro, R., Shahidian, S., Sousa, A., 2017. Irrigation management with remote sensing: Evaluating irrigation requirement for maize under Mediterranean climate condition. Agric. Water Manag. 184, 211–220. https://doi.org/10.1016/j.agwat.2016.02.010

Turner, N.C., 1990. Plant water relations and irrigation management. Agric. Water Manag. 17, 59–73. https://doi.org/10.1016/0378-3774(90)90056-5

Twarakavi, N.K.C., Sakai, M., Šimůnek, J., 2009a. An objective analysis of the dynamic nature of field capacity. Water Resour. Res. 45, 1–9. https://doi.org/10.1029/2009WR007944

Twarakavi, N.K.C., Sakai, M., Šimůnek, J., 2009b. An objective analysis of the dynamic nature of field capacity. Water Resour. Res. 45, 1–9. https://doi.org/10.1029/2009WR007944

Van den Honert, T.H.., 1948. Water transport in plants as a catenary process. Discuss. Faraday Soc. 3, 146–153. https://doi.org/10.1039/df9480300146

van Genuchten, M.T., 1987. A numerical model for water and solute movement in and below the root zone. Res. Report, U.S. Salin. Lab. USDA, ARS, Riverside, CA.

van Genuchten, M.T., 1980. A Closed-form Equation for Prediccting Hydraulic Conductivity of Unsaturated Soils. Soil Sci. Soc. Am. J. https://doi.org/doi:10.2136/sssaj1980.03615995004400050002x

van Genuchten MTh, Leij FJ, Y.S., 1991. The RETC code for quantifying the hydraulic functions of unsaturated soils. US Environ. Prot. Agency R. S. Kerr Environ. Res. Lab. Off. Res. Dev. Ada, OK.

van Lier, Q., Wendroth, O., 2016. Reexamination of the Field Capacity Concept in a Brazilian Oxisol. Soil Sci. Soc. Am. J. 80, 264. https://doi.org/10.2136/sssaj2015.01.0035

Vellidis, G., Liakos, V., Perry, C., Porter, W.M., Tucker, M.A., 2016. Irrigation Scheduling for Cotton Using Soil Moisture Sensors, Smartphone Apps, and Traditional Methods 772–780.

Vellidis, G., Tucker, M., Perry, C., Kvien, C., Bednarz, C., 2008. A real-time wireless smart sensor array for scheduling irrigation. Comput. Electron. Agric. 61, 44–50. https://doi.org/10.1016/j.compag.2007.05.009

Vidal, A., Manager, T., Comeau, A., Plusquellec, H., Gadelle, F., 2001. Case studies on water conservation in the Mediterranean region.

Viña, A., Gitelson, D.C., Rundquist, G., Keydan, B., Leavitt, Schepers, J.S., 2004. Monitoring Maize (Zea mays L.) Phenology with Remote Sensing. Agron. J. 96, 1139–1147. https://doi.org/10.1007/978-1-4614-3103-9

Wagner, W., Sabel, D., Doubkova, M., Bartsch, A., Pathe, C., 2010. The Potential of Sentinel-1 for Monitoring Soil Moisture with a high Spatial Resolution at Global Scale. ESA Spec. Publ. SP-674 5.

Walker, S.H., 1999. More from less - Better water management: Issues and future policy. Agric. Water Manag. 40, 135–138. https://doi.org/10.1016/S0378-3774(98)00094-8

Wallace, J.S., 2000. Increasing agricultural water use efficiency to meet future food production. Water 82, 105–119.

Wanders, N., Karssenberg, D., De Roo, A., De Jong, S.M., Bierkens, M.F.P., 2014. The suitability of remotely sensed soil moisture for improving operational flood forecasting. Hydrol. Earth Syst. Sci. 18, 2343–2357. https://doi.org/10.5194/hess-18-2343-2014

Wang, L., Qu, J.J., 2009. Satellite remote sensing applications for surface soil moisture monitoring: A review. Front. Earth Sci. China 3, 237–247. https://doi.org/10.1007/s11707-009-0023-7

Wendroth, O., Pohl, W., Koszinski, S., Rogasik, H., Ritsema, C.J., Nielsen, D.R., 1999. Spatio-temporal patterns and covariance structures of soil water status in two Northeast-German field sites. J. Hydrol. 215, 38–58. https://doi.org/10.1016/S0022-1694(98)00260-1

West, H., Quinn, N., Horswell, M., White, P., 2018. Assessing vegetation response to soil moisture fluctuation under extreme drought using sentinel-2. Water (Switzerland) 10, 1–22. https://doi.org/10.3390/w10070838

Western, A.W., Blöschl, G., Grayson, R.B., 1998. Geostatistical characterisation of soil moisture patterns in the Tarrawarra catchment. J. Hydrol. 205, 20–37. https://doi.org/10.1016/S0022-1694(97)00142-X

Woodcock, C.E., Strahler, A.H., 1987. the Factor of Scale in Remote-Sensing. Remote Sens. Environ. 21, 311–332. https://doi.org/10.1016/0034-4257(87)90015-0

Wright, J.L., Jensen, M.E., 1978. Development and Evaluation of Evapotranspiration Models for Irrigation Scheduling. Trans. ASAE 21, 88–91, 96.

Yang, Y., Wendroth, O., Walton, R.J., 2016. Temporal Dynamics and Stability of Spatial Soil Matric Potential in Two Land Use Systems. Vadose Zo. J. 15, 0. https://doi.org/10.2136/vzj2015.12.0157

Zaussinger, F., Dorigo, W., Gruber, A., Tarpanelli, A., Filippucci, P., Brocca, L., 2018. Estimating irrigation water use over the contiguous United States by combining satellite and reanalysis soil moisture data 1–42.

Zhang, N., Wang, M., Wang, N., 2002. Precision agriculture*a worldwide overview Naiqian. Comput. Electron. Agric. 36, 113–132. https://doi.org/10.1111/j.1751-1097.1990.tb01731.x

Zhang, S., Zhu, X., Zhou, S., Shang, H., Luo, J., Tsang, D.C.W., 2018. Hydrothermal Carbonization for Hydrochar Production and Its Application, Biochar from Biomass and Waste. Elsevier Inc. https://doi.org/10.1016/b978-0-12-811729-3.00015-7

Zotarelli, L., Dukes, M.D., Morgan, K.T., 2010. Interpretation of Soil Moisture Content to Determine Soil Field Capacity and Avoid Over-Irrigating Sandy Soils Using Soil Moisture Sensors. Univ. Florida Coop. Ext. Serv. AE 460. http//edis.ifas.ufl.edu/ae460. 1–4.

Zurweller, B.A., Rowland, D.L., Mulvaney, M.J., Tillman, B.L., Migliaccio, K., Wright, D., Erickson, J., Payton, P., Vellidis, G., 2019. Optimizing cotton irrigation and nitrogen management using a soil water balance model and in-season nitrogen applications. Agric. Water Manag. 216, 306–314. https://doi.org/10.1016/j.agwat.2019.01.011

Supporting information

This section comprises supporting information for Chapters 4.

Appendix A. Supplementary material of Chapter 4: Dynamics management zone to improve irrigation scheduling

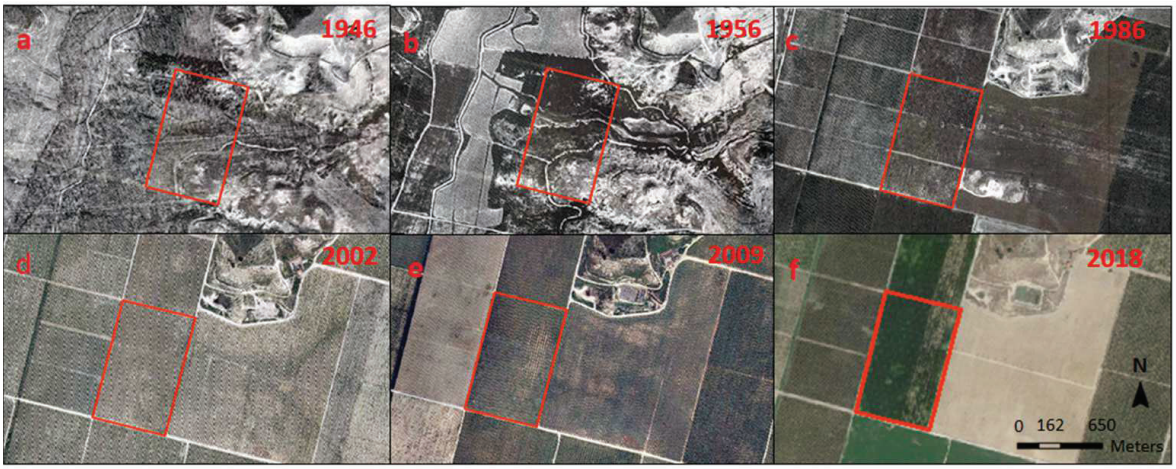

Figure S1. Historical land use and topography modifications at the study site.

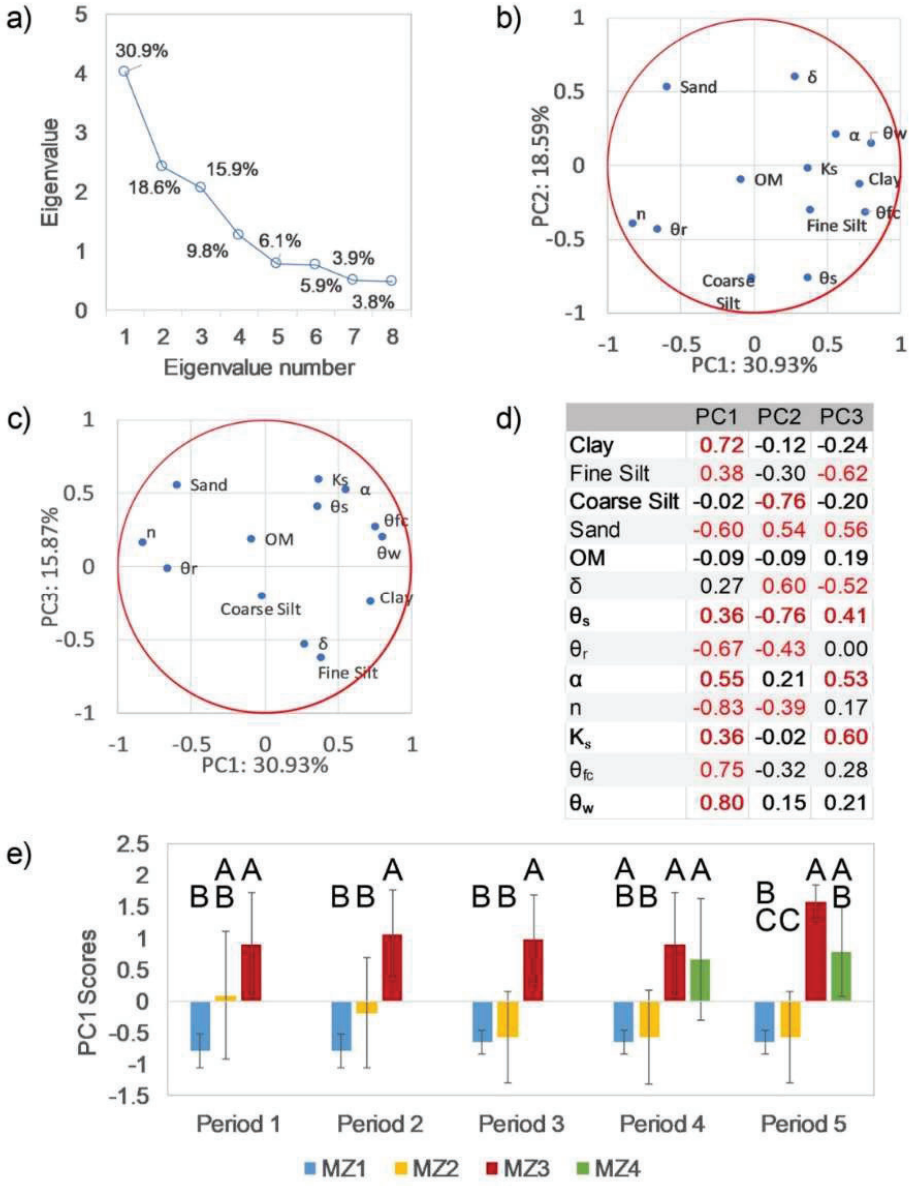

	PC1	PC2	PC3
Clay	0.72	-0.12	-0.24
Fine Silt	0.38	-0.30	-0.62
Coarse Silt	-0.02	-0.76	-0.20
Sand	-0.60	0.54	0.56
OM	-0.09	-0.09	0.19
δ	0.27	0.60	-0.52
θ_s	0.36	-0.76	0.41
θ_r	-0.67	-0.43	0.00
α	0.55	0.21	0.53
n	-0.83	-0.39	0.17
K_s	0.36	-0.02	0.60
θ_{fc}	0.75	-0.32	0.28
θ_w	0.80	0.15	0.21

Figure S2. a) Eigenvalue and percent of variance explained by the first eight components of the principal component (PC) analysis; b) bi-plot of select soil properties (clay. fine silt. coarse silt. sand. and organic matter (OM) content; bulk density (ρb); water content at saturation (θs); residual water content (θr); water content at field capacity (θfc); water content at wilting point (θwp); saturated hydraulic conductivity (Ks); and shape parameters α and n) for PC1 and PC2; c) same for PC1 and PC3; d) Pearson correlation matrix for the first three PCs and selected soil properties (significant ($p<0.05$) correlations highlighted in red); and e) averages (bars) and standard deviations (lines) ofPC1 for the four management zones (MZs) through the growing season. Capital letters indicate significant ($p<0.05$) differences within MZs according to the Kruskal-Wallis test.

Hydurs-1D Simulations

Hydrus-1d (Šimůnek et al., 2008, 2016) was used to simulated soil moisture dynamics and water balance components at each monitoring station. Each simulation spanned 105 days, from the 18th to the 123rd day after sowing. The 60 cm soil profile consisted of three layers/materials, as specified in Table 2. Soil hydraulic properties were specified using the van Genuchten-Mualem model (van Genuchten, 1980) Eq. (S1-S2).)

$$\theta(h) = \begin{cases} \theta_r + \dfrac{\theta_s - \theta_r}{(1 + |\alpha h|^n)^m} & h < 0 \\ \theta_s & h \geq 0 \end{cases}. \tag{S1}$$

$$K(h) = K_s S_e^{1/2} \left[1 - \left(1 - S_e^{1/m}\right)^m\right]^2 \tag{S2}$$

where θ ($cm^3 \cdot cm^{-3}$) is the volumetric water content; h is the soil water pressure head (cm); θ_s ($cm^3 \cdot cm^{-3}$) is saturated water content; θ_r ($cm^3 \cdot cm^{-3}$) is residual water content; K_s ($cm \cdot d^{-1}$) is saturated hydraulic conductivity; n and α are dimensionless shape parameters; $S_e = \frac{\theta - \theta_r}{\theta_s - \theta_r}$; and $m = 1 - 1/n$.

The potential evaporation and transpiration values needed in the root water uptake model, equations (9) and (11), were calculated by partitioning ET_c into potential evaporation E_p and transpiration T_p based on the Canopy Cover (Raes et al., 2010), which determines that $ET_c = \alpha E_p + (1 - \alpha) T_p$, being α the soil cover fraction. Atmospheric boundary condition was imposed at the surface and a free drainage condition was used at the bottom.

In Hydrus, root water uptake is simulated using a sink term S Eq. (S3) which has three parts, the potential transpiration rate (T_p) ($cm \cdot d^{-1}$), the root density distribution (β) (cm^{-1}), and the dimensionless water stress function ($\alpha(h)$),

$$S(h, z, t) = \alpha(h, z, t) \beta(z, t) T_p(t) \tag{S3}$$

The actual transpiration rate (T_a) ($cm \cdot d^{-1}$) Eq. (S4) is calculated by integrating Eq.(S3) over the root zone L_R.

$$T_a = \int_{L_R} S(h.z.t) dz = T_p \int_{L_R} \alpha(h, z, t) \beta(z, t) dz, \tag{S4}$$

Roots were measured twice a month during the field campaign excavating a plant and measuring root depth. This information is used in the model to consider root growth and to make realistic simulations in terms of root water uptake through the soil profile. Water stress ($\alpha(h)$) function model employed in these simulation is Feddes et al. (1978) Eq. (S5) model.

$$\alpha(h) = \begin{cases} \dfrac{h - h_4}{h_3 - h_4} & h_3 > h > h_4 \\ 1 & h_2 \geq h \geq h_3 \\ \dfrac{h - h_1}{h_2 - h_1} & h_1 > h > h_2 \\ 0 & h \leq h_4 \; or \; h \geq h_1 \end{cases} \quad \text{(S5)}$$

Parameterized by four critical values of pressure head. this function prescribes that uptake is maximal ($\alpha = 1$) when the soil water pressure head is between $h_2 \geq h \geq h_3$. drops off linearly above or below that range ($h_3 > h > h_4$ or $h_1 > h > h_2$), and becomes zero whenever $h \leq h_4 \; or \; h \geq h_1$. According to the database in Hydrus-1D, the parameter values for maize are h_1 = -1.5, h_2 = -3.0, h_3 = -60. and h_4 = -800. kPa, respectively. The value of h_3 was allowed to vary as a function of evaporative demand as modeled by Hyrdurs-1D.

Three observation nodes were inserted in the domain at the same depths as the soil moisture sensors, 15, 35 and 50 cm. Soil moisture values simulated at the observation nodes were used to determine the simulated available water (SAW), using the same procedure as with the field data.

Simulated actual transpiration (ST_a) and simulated water applied (SWA) results from each station were extracted. ST_a and SWA were calculated averaging stations results considering dynamics MZ.

Irrigation Scheduling

In order to apply Fontanet methodology Hydrus 1D is also employed. All soil, environmental and crop inputs are the same as in previous Hydrus 1D simulations. Irrigation parameters have been constrained into h^*= -10. -20. -30. .... -100 kPa and τ = 1. 2. .... 4 h·d^{-1}. In this case irrigation rate (I_{rate}) is constant (6.5 l·h^{-1}·m^{-2}). The triggered depth (Z_{tr}) changes during the growing season and it is located through the soil profile depending on root growth measurements. New h_{th}considered to simulate alternative irrigation scheduling and dryer conditions are defined from 0 to -100 kPa.

Irrigation parameters have been defined at each station and also at different crop growing stages (V0-V5, V6-V10, V11-V15, VT, R1-R6). The optimal irrigation at each grow stage period and MZ have been defined averaging these irrigation parameters.

Finally, Optimal actual transpiration (OpT_a) and optimal water applied ($OpWA$) at the end of the season in each MZ are also computed averaging results from each station.